



This is a repository copy of *Measurements of the suppression and correlations of dijets in Pb+Pb collisions at $\sqrt{s_{NN}}=5.02$ TeV*.

White Rose Research Online URL for this paper:

<https://eprints.whiterose.ac.uk/205921/>

Version: Published Version

Article:

Aad, G. orcid.org/0000-0002-6665-4934, Abbott, B. orcid.org/0000-0002-5888-2734,
Abbott, D.C. orcid.org/0000-0002-7248-3203 et al. (2896 more authors) (2023)
Measurements of the suppression and correlations of dijets in Pb+Pb collisions at
 $\sqrt{s_{NN}}=5.02$ TeV. Physical Review C, 107 (5). 054908. ISSN 2469-9985

<https://doi.org/10.1103/physrevc.107.054908>

Reuse

This article is distributed under the terms of the Creative Commons Attribution (CC BY) licence. This licence allows you to distribute, remix, tweak, and build upon the work, even commercially, as long as you credit the authors for the original work. More information and the full terms of the licence here:
<https://creativecommons.org/licenses/>

Takedown

If you consider content in White Rose Research Online to be in breach of UK law, please notify us by emailing eprints@whiterose.ac.uk including the URL of the record and the reason for the withdrawal request.



eprints@whiterose.ac.uk
<https://eprints.whiterose.ac.uk/>

Measurements of the suppression and correlations of dijets in Pb+Pb collisions at $\sqrt{s_{NN}} = 5.02$ TeV

G. Aad *et al.**
(ATLAS Collaboration)



(Received 3 May 2022; accepted 6 July 2022; published 11 May 2023)

Studies of the correlations of the two highest transverse momentum (leading) jets in individual Pb+Pb collision events can provide information about the mechanism of jet quenching by the hot and dense matter created in such collisions. In Pb+Pb and pp collisions at $\sqrt{s_{NN}} = 5.02$ TeV, measurements of the leading dijet transverse momentum (p_T) correlations are presented. Additionally, measurements in Pb+Pb collisions of the dijet pair nuclear modification factors projected along leading and subleading jet p_T are made. The measurements are performed using the ATLAS detector at the LHC with 260 pb^{-1} of pp data collected in 2017 and 2.2 nb^{-1} of Pb+Pb data collected in 2015 and 2018. An unfolding procedure is applied to the two-dimensional leading and subleading jet p_T distributions to account for experimental effects in the measurement of both jets. Results are provided for dijets with leading jet p_T greater than 100 GeV. Measurements of the dijet-yield-normalized x_J distributions in Pb+Pb collisions show an increased fraction of imbalanced jets compared to pp collisions; these measurements are in agreement with previous measurements of the same quantity at 2.76 TeV in the overlapping kinematic range. Measurements of the absolutely normalized dijet rate in Pb+Pb and pp collisions are also presented, and show that balanced dijets are significantly more suppressed than imbalanced dijets in Pb+Pb collisions. It is observed in the measurements of the pair nuclear modification factors that the subleading jets are significantly suppressed relative to leading jets with p_T between 100 and 316 GeV for all centralities in Pb+Pb collisions.

DOI: [10.1103/PhysRevC.107.054908](https://doi.org/10.1103/PhysRevC.107.054908)

I. INTRODUCTION

The principal physics aim of the heavy-ion program at the Large Hadron Collider (LHC) is to produce and measure the properties of the quark-gluon plasma (QGP). In quantum chromodynamics (QCD), the QGP is a high-temperature state of matter in which quarks and gluons are no longer confined in color-neutral hadrons such as protons and neutrons (for a recent review, see Ref. [1]). In order to understand the properties of the QGP at short distances, high transverse momenta (p_T) probes such as jets of correlated particles are used.

The overall rate of jets in a given centrality¹ interval in Pb+Pb collisions at a given p_T is characterized by the nuclear modification factor,

$$R_{AA} = \frac{1}{N_{\text{evt}}} \frac{dN_{\text{jet}}}{dp_T} \Bigg/ \left(\langle T_{AA} \rangle \frac{d\sigma_{pp}}{dp_T} \right), \quad (1)$$

where N_{jet} and σ_{pp} are the jet yield in Pb+Pb collisions and the jet cross section in pp collisions, respectively, measured as a function of the jet p_T , and where N_{evt} is the total number of Pb+Pb events within the chosen centrality interval. Additionally, $\langle T_{AA} \rangle$ is the mean nuclear thickness function [2] for the centrality interval. The R_{AA} value is 1 in the absence of nuclear effects; however, in the most central Pb+Pb collisions, R_{AA} is observed to be about a factor of 2 lower than that in pp collisions scaled by $\langle T_{AA} \rangle$, up to a p_T of approximately 1 TeV [3–5]. This suppression, referred to as *jet quenching*, is generally explained by the interplay of radiative and collisional energy loss in reducing the jet p_T by moving energy associated with the initial parton to wider angles, with some of it being outside the jet cone. Given the steeply falling jet p_T spectrum, this leads to fewer jets being measured at a given jet p_T , giving rise to R_{AA} values below 1. For recent reviews, see Refs. [6,7].

Jets are mostly produced in pairs in $2 \rightarrow 2$ scattering processes. The QCD evolution of the initial partons gives rise to back-to-back jets, referred to here as “dijets.” Compared to single-jet suppression, dijets in Pb+Pb collisions provide a cleaner probe for studying jet quenching. The two jets are expected to experience asymmetric energy loss due to traversing unequal path lengths in the QGP [8], driven by the geometry of the overlapping nuclei and the relative orientation of the jet trajectories through the evolving medium. Measurements of the azimuthal anisotropy of jets [9] have already shown that the geometry of the overlapping nuclei affects the relative rates of jets measured in Pb+Pb collisions. Additionally,

*Full author list given at the end of the article.

¹Centrality characterizes the degree to which the nuclei overlap. The most central collisions have full overlap and the highest multiplicities, while the most peripheral collisions have only minimal overlap and have multiplicity closer to that in pp collisions at the same nucleon-nucleon collision energy.

jets are expected to experience jet-by-jet fluctuations in the energy-loss process [10]. The measurement of the p_T balance of dijets provides a way to constrain the relative importance of fluctuations and geometry in jet quenching.

In order to compare the final transverse momenta of the two jets which define a dijet, the leading dijet momentum balance

$$x_J \equiv p_{T,2}/p_{T,1} \quad (2)$$

is measured. Here, the leading dijet is constructed using the highest two p_T jets out of the set of jets in an event; $p_{T,1}$ is the transverse momentum of the highest- p_T (leading) jet and $p_{T,2}$ is the transverse momentum of the second-highest- p_T (subleading) jet.

In pp collisions, the showering process in vacuum (in the absence of a significant QGP), as well as higher-order scattering processes, can lead to imbalanced dijet transverse momenta. However, the most probable situation is that the jets are nearly balanced in p_T [11]. Previous dijet measurements in Pb+Pb collisions have observed that jets are more likely to have a larger momentum imbalance in Pb+Pb collisions than in pp collisions [11–13].

Previous publications reported only the dijet imbalance normalized by the measured dijet yields, in order to study the changes in the shape of the x_J distribution as a function of the heavy-ion collision centrality. Past studies did not address the absolute rate at which dijets are produced in Pb+Pb collisions, which could assess whether leading dijets are suppressed at levels similar to those for “inclusive jets” (all jets in the event which meet p_T and rapidity selections) [3]. This paper thus presents both types of measurements with leading dijets in Pb+Pb and pp collisions at $\sqrt{s_{NN}} = 5.02$ TeV. These measurements use 2.2 nb^{-1} of Pb+Pb collisions collected in 2015 and 2018 as well as 260 pb^{-1} of pp data collected in 2017 with the ATLAS detector [14] at the LHC.

Jets are reconstructed using the anti- k_t algorithm [15] with radius parameter $R = 0.4$. Leading dijets are constructed from the two highest- p_T jets in the event and are required to have the two jets nearly back-to-back in azimuth with $\Delta\phi \equiv |\phi_1 - \phi_2| \geq 7\pi/8$ and $|y| < 2.1$.² The measurement is performed in logarithmic p_T bins from 100 to 562 GeV for leading jets and above 32 GeV for subleading jets. Events whose two highest- p_T jets do not meet the selection criteria are discarded.

The primary observable for this measurement is the two-dimensional yield of leading dijets (N_{pair}) meeting the

²ATLAS uses a right-handed coordinate system with its origin at the nominal interaction point (IP) in the center of the detector, and the z axis along the beam pipe. The x axis points from the IP to the center of the LHC ring, and the y axis points upward. Cylindrical coordinates (r, ϕ) are used in the transverse plane, ϕ being the azimuthal angle around the z axis. The pseudorapidity is defined in terms of the polar angle θ as $\eta = -\ln \tan(\theta/2)$. The rapidity is defined as $y = 0.5 \ln[(E + p_z)/(E - p_z)]$, where E and p_z are the energy and z component of the momentum along the beam direction, respectively. Transverse momentum and transverse energy are defined as $p_T = p \sin \theta$ and $E_T = E \sin \theta$, respectively. The angular distance between two objects with relative differences $\Delta\eta$ in pseudorapidity and $\Delta\phi$ in azimuth is given by $\Delta R = \sqrt{(\Delta\eta)^2 + (\Delta\phi)^2}$.

selection criteria:

$$\frac{d^2N_{\text{pair}}}{dp_{T,1}dp_{T,2}}. \quad (3)$$

Projections of the two-dimensional distribution in expression (3) can be used to construct x_J distributions as a function of $p_{T,1}$ and $p_{T,2}$. The x_J values, as defined in Eq. (2), are reported for $0.32 < x_J < 1.0$ for selections in $p_{T,1}$. The minimum x_J value is chosen to be consistent with previous measurements [11]. The x_J distributions are presented with two normalizations. The first uses the dijet yield normalization to extract the *dijet-yield-normalized* x_J distributions:

$$\frac{1}{N_{\text{pair}}} \frac{dN_{\text{pair}}}{dx_J}. \quad (4)$$

This normalization, expression (4), has been used in previous dijet measurements by ATLAS and CMS [11–13]. The second normalization provides *absolutely normalized* x_J distributions:

$$\frac{1}{\langle T_{AA} \rangle N_{\text{evt}}^{\text{AA}}} \frac{dN_{\text{pair}}^{\text{AA}}}{dx_J} \quad (5)$$

in Pb+Pb collisions and

$$\frac{1}{L_{pp}} \frac{dN_{\text{pair}}^{pp}}{dx_J} \quad (6)$$

in pp collisions. Here $\langle T_{AA} \rangle$ [2] is the mean nuclear thickness function for the events under consideration, $N_{\text{evt}}^{\text{AA}}$ is the number of minimum-bias events, and L_{pp} is the integrated luminosity of the pp collisions [16]. The absolutely normalized x_J distributions allow a direct comparison between the dijet rates measured in Pb+Pb and pp collisions. Additionally, the absolutely normalized x_J distributions can be integrated over the measurement range of $0.32 < x_J < 1.0$ to construct the pair nuclear modification factors for dijets as a function of the leading and subleading jet p_T . These quantities are defined analogously to the nuclear modification factor for inclusive jets, Eq. (1), as

$$R_{\text{AA}}^{\text{pair}}(p_{T,1}) = \frac{\frac{1}{\langle T_{AA} \rangle N_{\text{evt}}^{\text{AA}}} \int_{0.32 \times p_{T,1}}^{p_{T,1}} \frac{d^2N_{\text{pair}}^{\text{AA}}}{dp_{T,1}dp_{T,2}} dp_{T,2}}{\frac{1}{L_{pp}} \int_{0.32 \times p_{T,1}}^{p_{T,1}} \frac{d^2N_{\text{pair}}^{pp}}{dp_{T,1}dp_{T,2}} dp_{T,2}} \quad (7)$$

and

$$R_{\text{AA}}^{\text{pair}}(p_{T,2}) = \frac{\frac{1}{\langle T_{AA} \rangle N_{\text{evt}}^{\text{AA}}} \int_{p_{T,2}}^{p_{T,2}/0.32} \frac{d^2N_{\text{pair}}^{\text{AA}}}{dp_{T,1}dp_{T,2}} dp_{T,1}}{\frac{1}{L_{pp}} \int_{p_{T,2}}^{p_{T,2}/0.32} \frac{d^2N_{\text{pair}}^{pp}}{dp_{T,1}dp_{T,2}} dp_{T,1}}. \quad (8)$$

By integrating over $p_{T,2}$ ($p_{T,1}$), one can access information from $R_{\text{AA}}^{\text{pair}}(p_{T,1})$ [$R_{\text{AA}}^{\text{pair}}(p_{T,2})$] about the differential rate of dijet production in leading (subleading) jet p_T bins. Comparison of these two quantities at a fixed jet p_T provides information about the relative suppression of leading and subleading jets.

II. ATLAS DETECTOR

The ATLAS detector [14] at the LHC covers nearly the full solid angle around the nominal interaction point. It contains an inner tracking detector surrounded by a thin superconducting solenoid, electromagnetic and hadronic calorimeters,

a zero-degree calorimeter, and a muon spectrometer which incorporates three large superconducting toroidal magnets. The inner-detector system is immersed in a 2 T axial magnetic field and provides charged-particle tracking within $|\eta| < 2.5$.

The ATLAS calorimeter system covers the pseudorapidity range $|\eta| < 4.9$. Within the region $|\eta| < 3.2$, electromagnetic calorimetry is provided by barrel and endcap high-granularity lead/liquid-argon (LAr) calorimeters, with an additional thin LAr presampler covering $|\eta| < 1.8$ to allow corrections for energy lost in material upstream of the calorimeters. Hadronic calorimetry is provided by a steel/scintillator-tile calorimeter which is segmented into three barrel structures within $|\eta| < 1.7$, as well as two copper/LAr hadronic endcap calorimeters. To complete the solid angle coverage, forward copper/LAr and tungsten/LAr calorimeter modules (FCal) are used, optimized for electromagnetic and hadronic measurements respectively.

The zero-degree calorimeters (ZDCs) are located symmetrically at $z = \pm 140$ m and cover $|\eta| > 8.3$. They are constructed using tungsten absorber plates with quartz fibers to transmit the Cherenkov light. In Pb+Pb collisions the ZDCs primarily observe “spectator” neutrons, which do not interact during the primary collision.

A two-level trigger system is used within ATLAS to select events of interest [17]. The first-level trigger is implemented in hardware and uses a subset of the detector information to reduce the event rate to at most 100 kHz. This is followed by the software-based high-level trigger, which further reduces the event rate to several kHz of triggered events that are recorded to permanent storage.

An extensive software suite [18] is used in the reconstruction and analysis of real and simulated data, in detector operations, and in the trigger and data acquisition systems of the experiment.

III. DATA AND MONTE CARLO SELECTION

The Pb+Pb data used to perform these measurements were collected in 2015 and 2018, and the pp data used were collected in 2017 with the average number of inelastic interactions per bunch crossing ranging from 1.4 to 4.4. The events were triggered using a series of various p_T -threshold single-jet triggers with the leading jets in the analysis being in a region where the trigger is fully efficient. Although only a small fraction of the Pb+Pb events ($< 0.5\%$) contain multiple collisions, these were suppressed utilizing the observed anticorrelation, expected from the nuclear geometry, between the total transverse energy deposited in both of the forward calorimeters, ΣE_T^{FCal} , and the energy in the ZDC, which is proportional to the number of observed spectator neutrons. Pileup collisions are not rejected in pp collisions.

The overlap area of the two colliding nuclei in Pb+Pb collisions is characterized by the event centrality, which is estimated from the total transverse energy deposited in the FCal [19]. This measurement considers five centrality intervals as defined according to successive percentiles of the ΣE_T^{FCal} distribution obtained from minimum-bias collisions. The centrality intervals considered in this measurement are 0–10% (largest ΣE_T^{FCal}), 10–20%, 20–40%, 40–60%, and 60–80%.

TABLE I. The $\langle T_{AA} \rangle$ values and uncertainties for the centrality selections used in this measurement. These are the results from TGGLAUBERMC v3.2 modeling of the summed transverse energy in the forward calorimeters, ΣE_T^{FCal} .

Centrality selection	$\langle T_{AA} \rangle \pm \delta \langle T_{AA} \rangle$ (1/mb)
0–10%	23.35 ± 0.20
10–20%	14.33 ± 0.17
20–40%	6.79 ± 0.16
40–60%	1.96 ± 0.09
60–80%	0.39 ± 0.03

(smallest ΣE_T^{FCal}). The values of the mean nuclear thickness function, $\langle T_{AA} \rangle$ [2], are determined using TGGLAUBERMC v3.2 [20]; the uncertainties in $\langle T_{AA} \rangle$ are discussed in Ref. [21]. The $\langle T_{AA} \rangle$ values and their uncertainties are listed in Table I for each centrality selection considered in this measurement.

This analysis uses four Monte Carlo (MC) samples to evaluate the detector performance and correct for detector effects. The pp MC sample used in this analysis includes 3.2×10^7 PYTHIA 8 [22] pp jet events generated at $\sqrt{s} = 5.02$ TeV with parameter values set according to the A14 tune [23] and the NNPDF23LO parton distribution functions (PDFs) [24]. Pileup due to additional inelastic pp interactions is similarly generated using PYTHIA 8 with the same PDFs and utilizing the A3 tune [25], tuned for inclusive QCD processes, matching the number of extra collisions in the pp data. The MC samples for Pb+Pb collisions, one for the 2015 detector conditions and one for the 2018 detector conditions, each use 3.2×10^7 pp PYTHIA 8 events with the same A14 tune and PDFs as used for the generation of the pp jet MC samples. The underlying event contribution to the detector signal is accounted for by overlaying the simulated pp events with dedicated Pb+Pb data events from the 2015 Pb+Pb run and 2018 Pb+Pb run respectively. The data events from Pb+Pb collisions were combined with the signal from the PYTHIA 8 simulation of hard scattering events at the digitization stage, and then reconstructed as a combined event. This procedure enables the “data overlay” sample to accurately reproduce the effects of the underlying event on the jet response. This sample was reweighted on an event-by-event basis to ensure the same centrality distribution as that measured in the jet-triggered data samples. The detector response in all three MC samples was simulated utilizing GEANT4 [26,27]. Finally, pp Herwig++ [28] events using the UEE5 tune [29] and the CTEQ6L1 PDFs [30] are used for uncertainty studies.

IV. JET RECONSTRUCTION AND PERFORMANCE

The jet reconstruction procedures follow those used by ATLAS for previous jet measurements in Pb+Pb collisions [3,9]. Jets are reconstructed using the anti- k_t algorithm [15] implemented in the FastJet software package [31]. In both pp and Pb+Pb collisions, jets with $R = 0.2$ and $R = 0.4$ are formed by clustering calorimetric towers of spatial size $\Delta\eta \times \Delta\phi = 0.1 \times \pi/32$. The energies in the towers are obtained by summing the energies of calorimeter cells at the

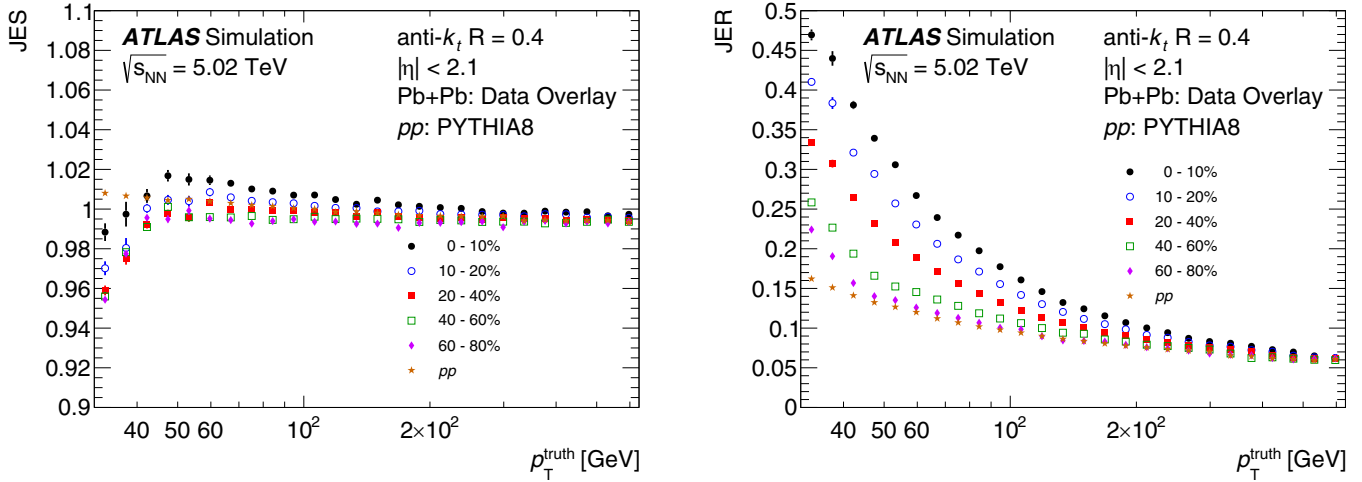


FIG. 1. The jet energy scale, JES (left), and jet energy resolution, JER (right), as a function of p_T^{truth} for centrality selections in Pb+Pb and in pp collisions.

electromagnetic energy scale [32] within the tower boundaries. In Pb+Pb collisions, a background subtraction procedure is applied to estimate, within each event, the underlying event (UE) average transverse energy density, $\rho(\eta, \phi)$, where the ϕ dependence is due to global azimuthal correlations in the particle production from the hydrodynamic flow [33]. The modulation accounts for the contribution to the UE of the second-, third-, and fourth-order azimuthal anisotropy harmonics characterized by values of flow coefficients v_n^{UE} [33]. Additionally, the UE is also corrected for η - and ϕ -dependent nonuniformities of the detector response by correction factors derived in minimum-bias Pb+Pb data. In pp collisions, the same background subtraction procedure is applied to remove the pileup contribution to the jet, but without the ϕ -dependent modulation and without the correction for η - and ϕ -dependent nonuniformities.

An iterative procedure is used to remove the impact of jets on the estimated ρ and v_n^{UE} values. The first estimate of the average transverse energy density of the UE, $\rho(\eta)$, is evaluated in 0.1 intervals of η , excluding towers within $\Delta R = 0.4$ of “seed” jets. In the first subtraction step, the seeds are defined to be a combination of $R = 0.2$ jets and $R = 0.4$ track jets. Track jets are reconstructed by applying the anti- k_t algorithm with $R = 0.4$ to charged particles with $p_T > 4 \text{ GeV}$. The $R = 0.2$ jets must pass a cut on the minimum value of the tower E_T and on a ratio of maximum tower E_T to average tower E_T , while the track jets are required to have $p_T > 7 \text{ GeV}$. The underlying event contribution is then subtracted from each tower constituent and the jet kinematics are recalculated. After the first iteration, the ρ and v_n values are updated by excluding from the UE determination the regions within $\Delta R = 0.4$ of both the track jets and the newly reconstructed $R = 0.2$ jets with $p_T > 25 \text{ GeV}$ (8 GeV) in Pb+Pb (pp) collisions. The updated ρ and v_n^{UE} values are used to update the jet kinematic properties in the second iteration. Jet η - and p_T -dependent correction factors derived in simulations are applied to the measured jet energy to correct for the calorimeter energy response [34,35]. An additional correction based on in situ studies of jets recoiling against photons and jets in other

regions of the calorimeter is applied [36]. This calibration is followed by a “cross-calibration” which relates the jet energy scale (JES) of jets reconstructed by the procedure outlined in this section to the JES in 13 TeV pp collisions [35].

“Truth”-level jets are defined in the MC sample before detector simulation by applying the anti- k_t algorithm with $R = 0.4$ to stable particles with a proper lifetime greater than 30 ps, but excluding muons and neutrinos, which do not leave significant energy deposits in the calorimeter. After the detector simulation the truth jets are matched to the nearest reconstructed jet within $\Delta R < 0.3$. The performance of the jet reconstruction is characterized by the JES and jet energy resolution (JER), which correspond to the mean and variance of the $p_T^{\text{reco}}/p_T^{\text{truth}}$ distribution, where p_T^{reco} is the reconstructed jet p_T and p_T^{truth} is the p_T of the matched truth-level jet. The JES and JER as a function of p_T^{truth} can be seen in Fig. 1. The decrease in the JES for jets with $p_T^{\text{truth}} < 50 \text{ GeV}$ in Pb+Pb collisions stems from jets for which there is an oversubtraction of the underlying event. This is caused by the corresponding region of the detector not containing a “seed” jet above 25 GeV resulting in the jets energy contributing to the UE determination; this is corrected for in the unfolding procedure discussed below. The efficiency of reconstructing a jet with $p_T > 32 \text{ GeV}$, as evaluated from the probability of a truth jet matching to a reconstructed jet with $p_T > 32 \text{ GeV}$ in the MC simulation, can be seen as a function of p_T^{truth} in Fig. 2.

V. DATA ANALYSIS

The analysis and dijet selection used here closely follow those in Ref. [11]. In each data event, the reconstructed leading dijet is constructed from the two highest- p_T^{reco} jets in the event with reconstructed $p_{T,1}^{\text{reco}} > 79 \text{ GeV}$ and $p_{T,2}^{\text{reco}} > 32 \text{ GeV}$, and both jets are required to have $|\eta| < 2.1$. The inclusion of leading jets down to $p_{T,1}^{\text{reco}} > 79 \text{ GeV}$ provides an underflow region for the unfolding to enable inflow and outflow of jets from the measurement region. These dijets are required to be back to back with $|\Delta\phi| > 7\pi/8$. Events in which the leading dijets do not meet these criteria are discarded. For dijets

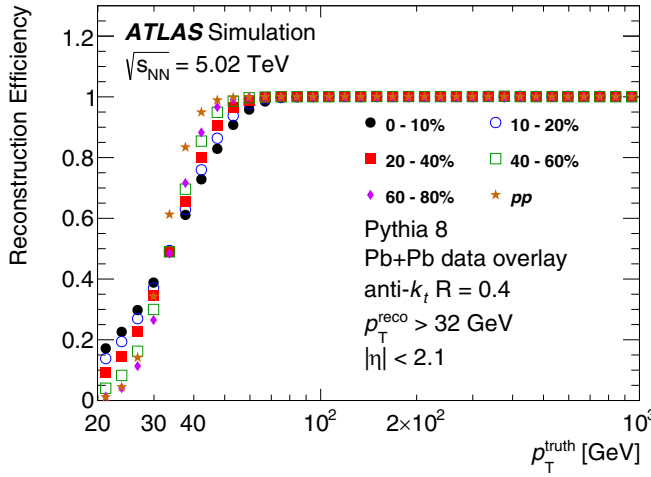
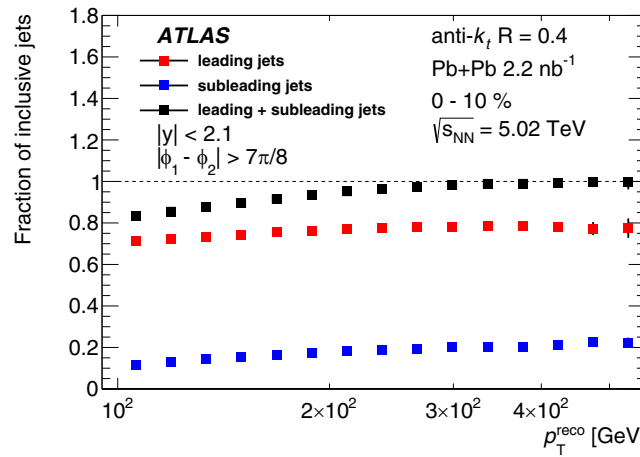


FIG. 2. The efficiency of reconstructing a jet with $p_T^{\text{reco}} > 32$ GeV as a function of p_T^{truth} for centrality selections in Pb+Pb collisions and pp collisions. The statistical uncertainties shown are smaller than the point markers.

matching the selection criteria, two-dimensional ($p_{T,1}^{\text{reco}}, p_{T,2}^{\text{reco}}$) distributions are constructed symmetrically across $p_{T,1}^{\text{reco}} = p_{T,2}^{\text{reco}}$. The distributions are symmetrized to account for the possibility of swapping the leading and subleading jet definition due to the finite JER.

The analysis procedure selects at most one dijet per event and therefore has the potential to produce a biased subsample of the inclusive jets. Figure 3 shows the fraction of the inclusive jets which are also included in the leading dijets used in this analysis. This quantity is shown as a function of p_T^{reco} for both central Pb+Pb and pp collisions. The fraction is 83% (85%) at 100 GeV and rises to more than 95% (95%) at 200 GeV in central Pb+Pb collisions (pp collisions). Due to the steep falloff of the jet yields with increasing p_T and the finite JER, jets reconstructed at a given p_T typically arise from jets at a lower truth p_T , and thus the fractions shown here at



the reconstructed- p_T scale underestimate the true fraction of inclusive jets included at a given p_T . Nevertheless, the large value, and weak p_T dependence, of the fraction of inclusive jets that are part of the leading dijet imply that the dijet selection in this analysis does not produce a particularly biased sample. The fractions are further broken down by leading and subleading jets. The relative fractions of leading and subleading jets at a given p_T are driven largely by the steeply falling p_T spectrum convolved with the shape of the x_J distribution.

The measured ($p_{T,1}^{\text{reco}}, p_{T,2}^{\text{reco}}$) distributions are a combination of the dijet signal and pairs of uncorrelated jets. Since the underlying-event subtraction accounts for azimuthal correlations in the particle production due to hydrodynamic flow, the contribution from uncorrelated dijets is independent of the $\Delta\phi$ of the jets; therefore, a $\Delta\phi$ sideband method is used to remove these pairs as a function of ($p_{T,1}^{\text{reco}}, p_{T,2}^{\text{reco}}$). The symmetrized two-dimensional ($p_{T,1}^{\text{reco}}, p_{T,2}^{\text{reco}}$) distribution of background combinatoric dijets is determined using dijets with $1 < |\Delta\phi| < 1.4$ which, after normalizing to the $\Delta\phi$ window of the signal band, is subtracted from the dijet yields. This effect is strongest for 0–10% centrality Pb+Pb events at low $p_{T,1}^{\text{reco}}$, where combinatoric dijets constitute 13% of the dijets for $79 < p_{T,1}^{\text{reco}} < 100$ GeV, and drops off rapidly both with increasing $p_{T,1}^{\text{reco}}$ and in more peripheral events. Because of how the leading dijet is defined, the presence of residual combinatoric dijets in the sample results in an inefficiency for genuine jet pairs, where one of the jets might be superseded by an uncorrelated third jet. This effect is corrected for using the measured inclusive jet spectrum from minimum-bias events to determine the efficiency loss as a function of the measured jet p_T following the method discussed in Ref. [11]. The resulting combinatoric-subtracted and efficiency-corrected symmetrized two-dimensional ($p_{T,1}^{\text{reco}}, p_{T,2}^{\text{reco}}$) distributions can be seen in Fig. 4 for both central Pb+Pb and pp collisions. The ability to remove uncorrelated jets and extract the truth-level leading-dijet x_J distributions in an unbiased way was confirmed by a closure test performed using the data overlay sample.

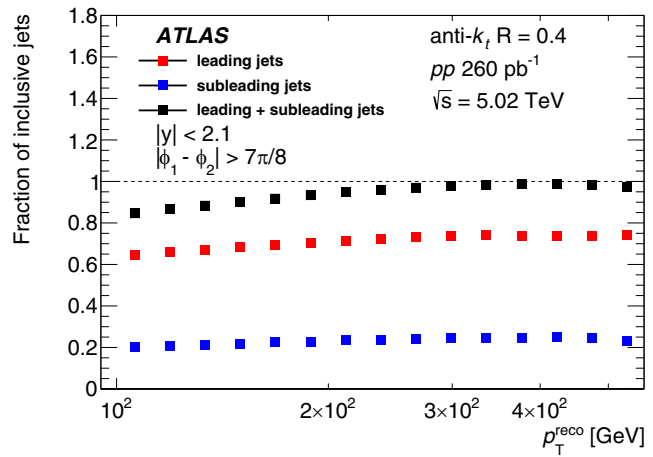


FIG. 3. Measured fractions of the inclusive jets which are part of the leading dijet (black), the leading jet of the dijet (red), or subleading jet of the dijet (blue), all as a function of p_T^{reco} for 0–10% centrality Pb+Pb collisions (left) and pp collisions (right).

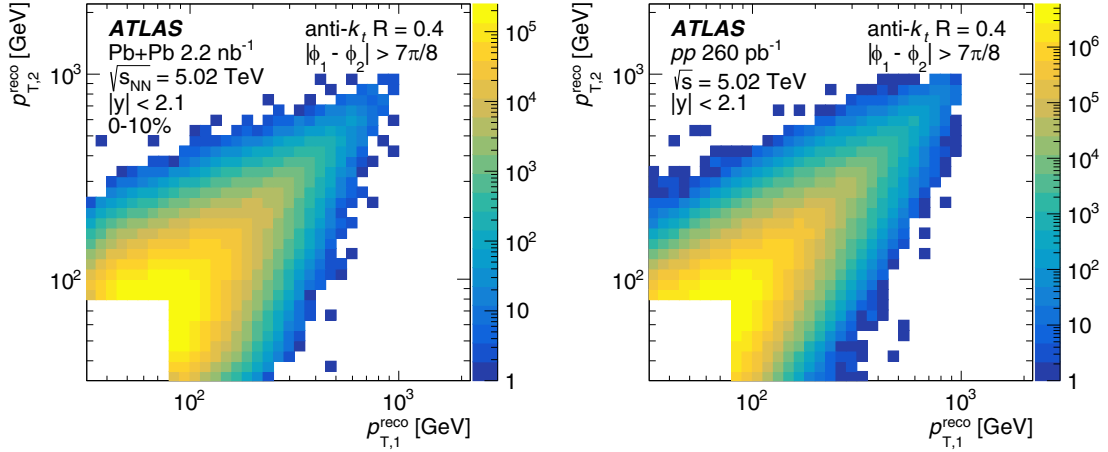


FIG. 4. The background-subtracted and symmetrized ($p_{T,1}^{\text{reco}}, p_{T,2}^{\text{reco}}$) distributions, measured in data, in 0–10% centrality Pb+Pb collisions (left) and pp collisions (right).

In order to correct for the effects of the JES and JER, the measured ($p_{T,1}^{\text{reco}}, p_{T,2}^{\text{reco}}$) distributions are unfolded using the iterative Bayesian unfolding procedure [37] as implemented in the RooUnfold [38] software package. A two-dimensional unfolding is used in order to account for bin migrations of both the leading and the subleading jet p_T , as well as to account for possible swapping of the leading and subleading jets. A separate response matrix is generated for pp collisions as well as for each centrality selection in Pb+Pb collisions. The response matrix used in the unfolding contains the relationship between ($p_{T,1}^{\text{truth}}, p_{T,2}^{\text{truth}}$) and ($p_{T,1}^{\text{reco}}, p_{T,2}^{\text{reco}}$). It is populated by identifying the leading and subleading truth-level jets in the MC sample which are matched to the corresponding reconstructed jets within $\Delta R < 0.3$. In order to account for migration from lower jet p_T^{reco} , the response matrices are populated with truth-level jets down to $p_{T,1}^{\text{truth}}$ of 20 GeV and $p_{T,2}^{\text{truth}}$ of 10 GeV. As with the reconstructed data, truth dijets are required to have $|\Delta\phi^{\text{truth}}| > 7\pi/8$, with each jet being within $|y^{\text{truth}}| < 2.1$. The two selected reconstructed jets from the MC simulations are required to meet the same selection criteria as applied to dijets measured in data. Truth dijets that do not match to a reconstructed dijet meeting the selection criteria are accounted for by using an efficiency correction in the unfolding. Similarly to the construction of the data distributions, the response matrix is populated symmetrically in $p_{T,1}$ and $p_{T,2}$. To construct a Bayesian prior which is similar to the measured distributions, the response matrices are reweighted along the $p_{T,1}^{\text{truth}}$ and $p_{T,2}^{\text{truth}}$ axes by the ratio of the two-dimensional reconstructed yields in data to those from simulation. The number of iterations used in the unfolding is tuned separately for each centrality in Pb+Pb collisions and for pp collisions. The number of iterations in each case was selected to optimize the balance between the accuracy of the final unfolded yield, and the increased statistical uncertainty which results from a larger number of iterations. Six iterations were used for the 0–10% centrality Pb+Pb events, while four iterations were used for all other centralities as well as for pp collisions.

In order to evaluate the statistical uncertainties of the data and the MC simulation, 1000 unfoldings were performed by varying each bin in either the data distribution or the response matrix independently according to its statistical uncertainty while preserving the symmetrization across $p_{T,1} = p_{T,2}$. The rms of the resulting unfolded distributions in each ($p_{T,1}, p_{T,2}$) bin was taken as the contribution to the statistical uncertainty on the corresponding unfolded ($p_{T,1}, p_{T,2}$) bin. The data and response matrix statistical uncertainty components were combined in quadrature in order to obtain the total statistical uncertainty of the unfolded distributions. Due to the large number of bins in the two-dimensional unfolding, in some cases the uncertainties due to the finite MC sample sizes are comparable to those in the data.

To extract measurements of the dijet momentum balance observable, x_J , the unfolded two-dimensional ($p_{T,1}, p_{T,2}$) distributions are first reflected about $p_{T,1} = p_{T,2}$ in order to restore the leading/subleading hierarchy. Then, following the procedure discussed in Ref. [11], the two-dimensional distributions are projected in slices of $p_{T,1}$ into bins of x_J . The upper edge of the i th x_J bin boundary is defined by $[(p_{T,N}/p_{T,0})^{1/N}]^{i-N}$, where N is the number of logarithmic p_T bins (40), and $p_{T,0}$ and $p_{T,N}$ are the minimum (10 GeV) and maximum (1 TeV) bin edges covered by the binning, respectively. This enables the mapping of the logarithmic $p_{T,1}$ and $p_{T,2}$ bins to x_J in such a way that each reported ($p_{T,1}, p_{T,2}$) bin is fully contained within two adjacent x_J bins. In this analysis, half of the yield in each ($p_{T,1}, p_{T,2}$) bin is apportioned to each of the two adjacent x_J bins. Exceptions to this are the bins along the diagonal $p_{T,1} = p_{T,2}$, which contribute solely to the highest x_J bin.

By projecting the resulting distributions over selections of $p_{T,1}$ while normalizing by the number of dijets (N_{pair}) and accounting for the x_J bin widths, measurements of the dijet yield-normalized x_J distributions are extracted. The absolutely normalized x_J distributions are extracted by instead normalizing the x_J distributions by the number of events and either the

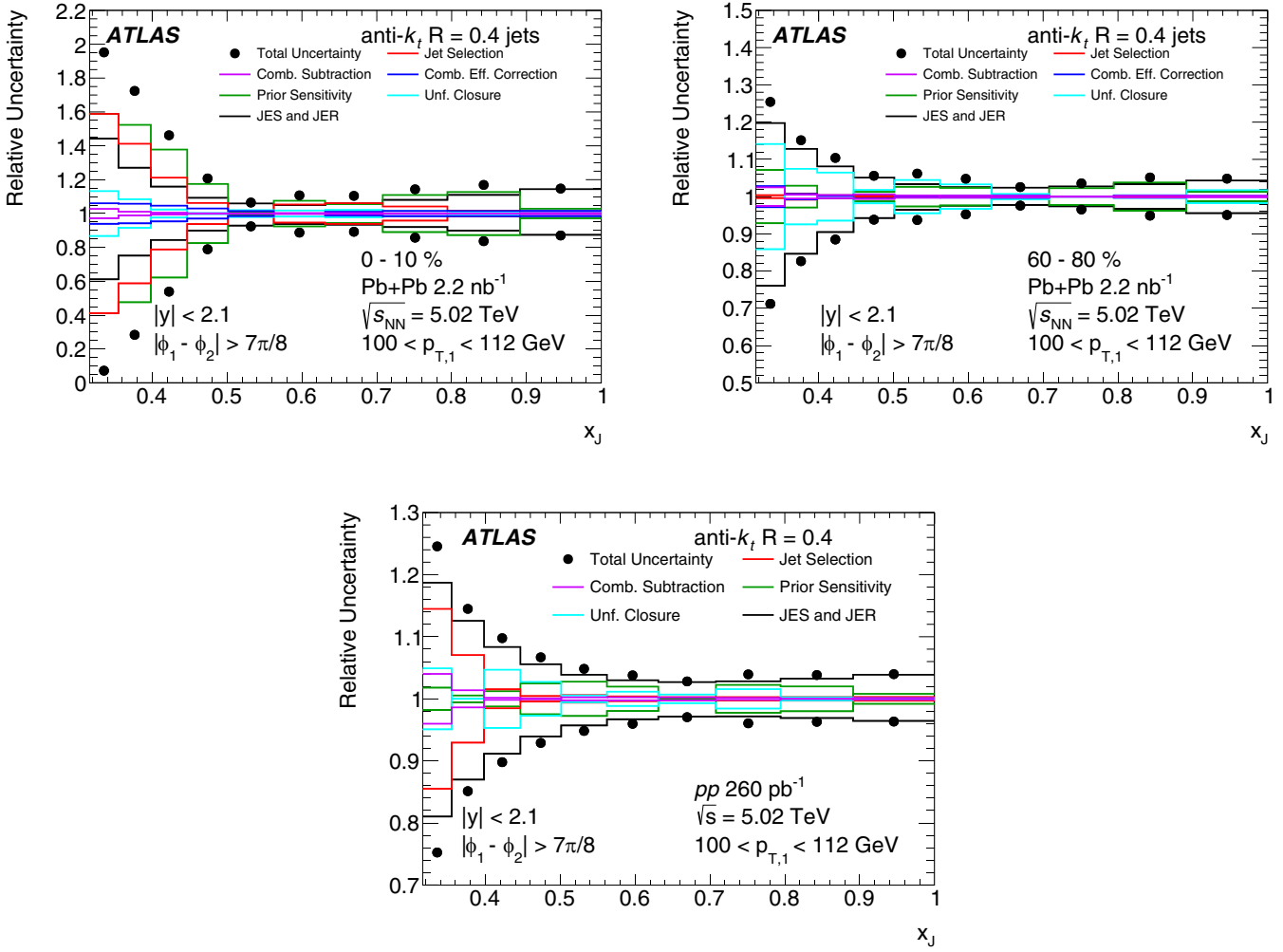


FIG. 5. The systematic uncertainty breakdown of the x_J distributions in central (left) and peripheral (right) Pb+Pb collisions as well as pp collisions (bottom). The panels have different vertical axis ranges.

T_{AA} in Pb+Pb collisions or the integrated luminosity in pp collisions, as described by expression (5).

In order to quantify the energy losses of the leading and subleading jets within a dijet, the nuclear modification factor, R_{AA}^{pair} , is measured for each of these selections. The R_{AA}^{pair} compares the per-event differential yield of jets at a given p_T in Pb+Pb collisions with the cross section in pp collisions scaled by the T_{AA} , as described in Eqs. (7) and (8).

VI. SYSTEMATIC UNCERTAINTIES

Systematic uncertainties for this measurement are attributed to three categories of sources: those which arise from the analysis and unfolding procedure, those which stem from uncertainties in the jet energy resolution (JER) and scale (JES), and those connected with global normalization. For each uncertainty component in the first two categories, the entire analysis procedure, including unfolding, is repeated accounting for the modification to the analysis procedure or the response matrix, and the result is compared with the nominal one. The third category applies to the absolutely normalized x_J distributions, $R_{AA}^{\text{pair}}(p_{T,1})$, and $R_{AA}^{\text{pair}}(p_{T,2})$; it contains the

uncertainty in the determination of the mean nuclear thickness function, $\langle T_{AA} \rangle$, and the pp luminosity. These uncertainties are independent of the jet transverse momentum and are noted on the figures.

The systematic uncertainty in the JES has four parts. First, a centrality-independent baseline component is determined from *in situ* studies of the calorimeter response to jets reconstructed with the procedure used in 13 TeV pp collisions [39]. A second, centrality-independent component accounts for the relative energy scale difference between the jet reconstruction procedures used in this analysis and those in 13 TeV pp collisions. This is evaluated using the cross-calibration procedure described in Ref. [35]. Potential inaccuracies in the PYTHIA 8 MC sample's description of the relative abundances of jets initiated by quarks and gluons and of the calorimetric response to quark and gluon jets are accounted for by the third, centrality independent, component—based on evaluating these same quantities using the Herwig++ MC sample. The fourth, centrality-dependent, component accounts for modifications of the parton shower due to quenching [40], which is not modeled in the simulations. The modifications to the parton shower can impact the detector response to jets in Pb+Pb

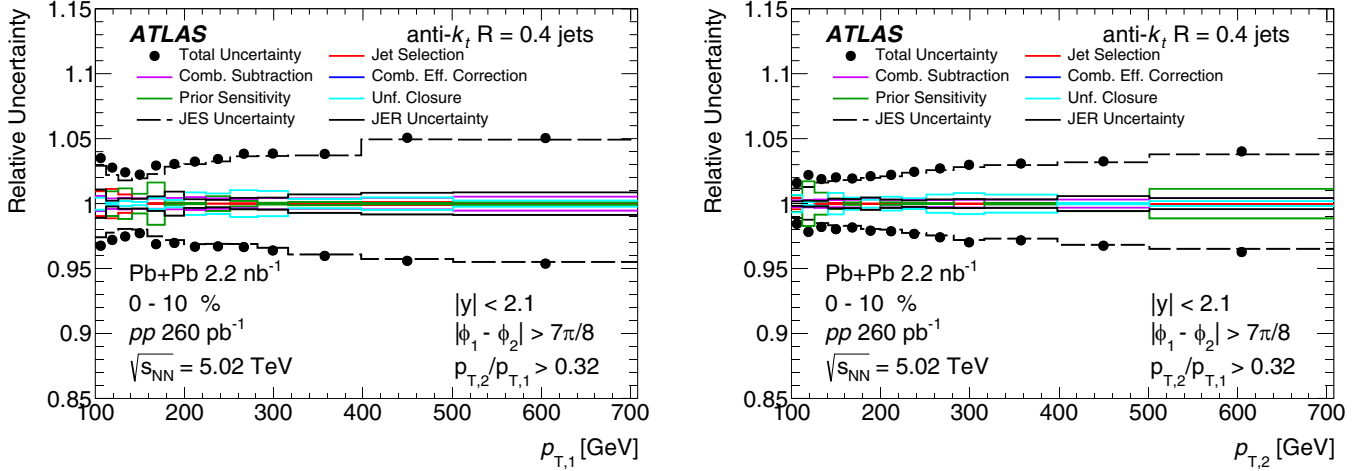


FIG. 6. The systematic uncertainty breakdown of the R_{AA}^{pair} for leading jets (left) and subleading jets (right). Uncertainties on the T_{AA} and pp luminosity are not shown.

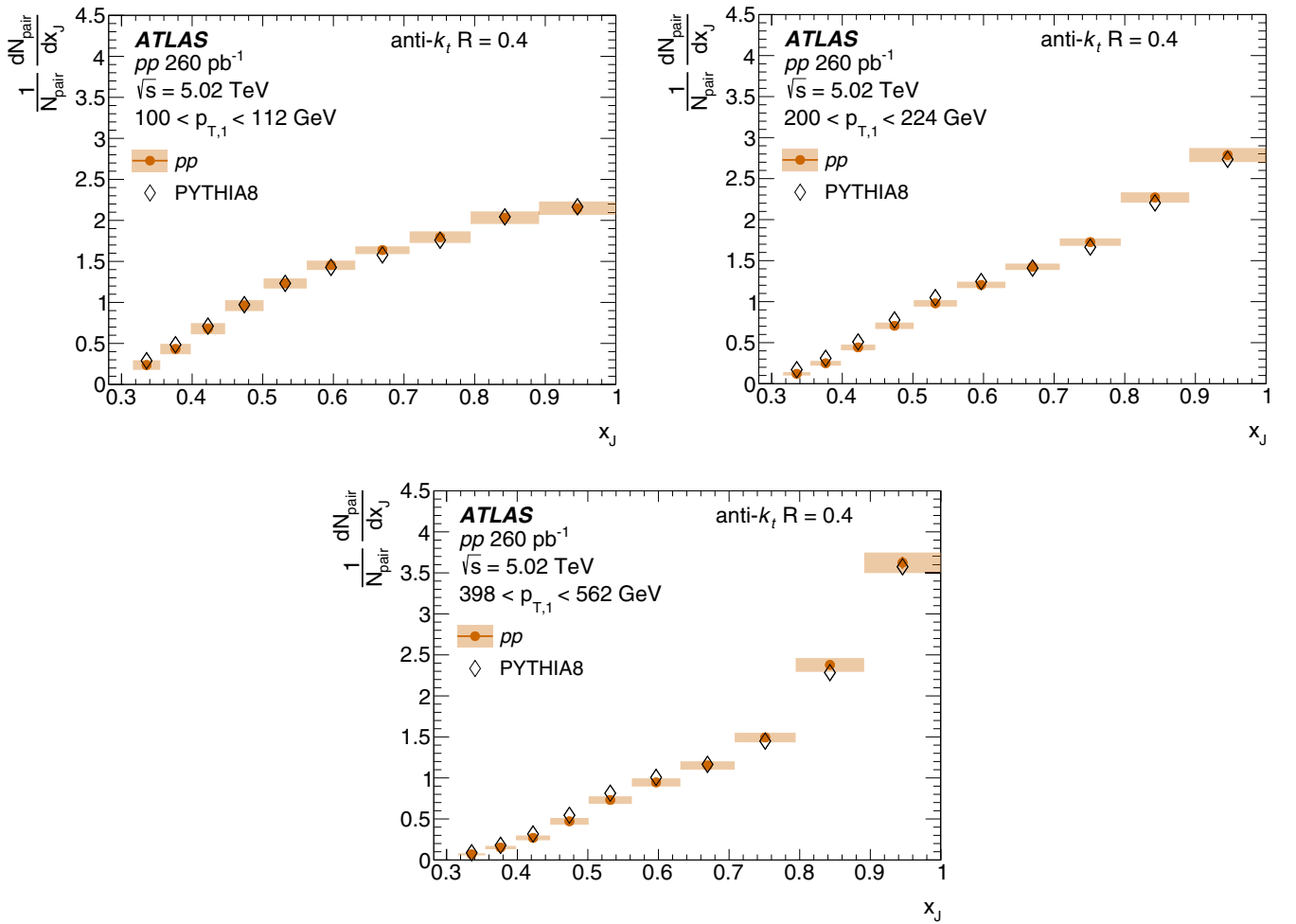


FIG. 7. The dijet-yield-normalized $\frac{1}{N_{\text{pair}}} \frac{dN_{\text{pair}}}{dx_J}$ distributions in pp collisions for three $p_{T,1}$ selections from 100 to 562 GeV overlaid with the corresponding distributions from PYTHIA 8. The statistical uncertainties are shown as error bars (which are smaller than the markers in many cases), and the systematic uncertainties are shown as boxes.

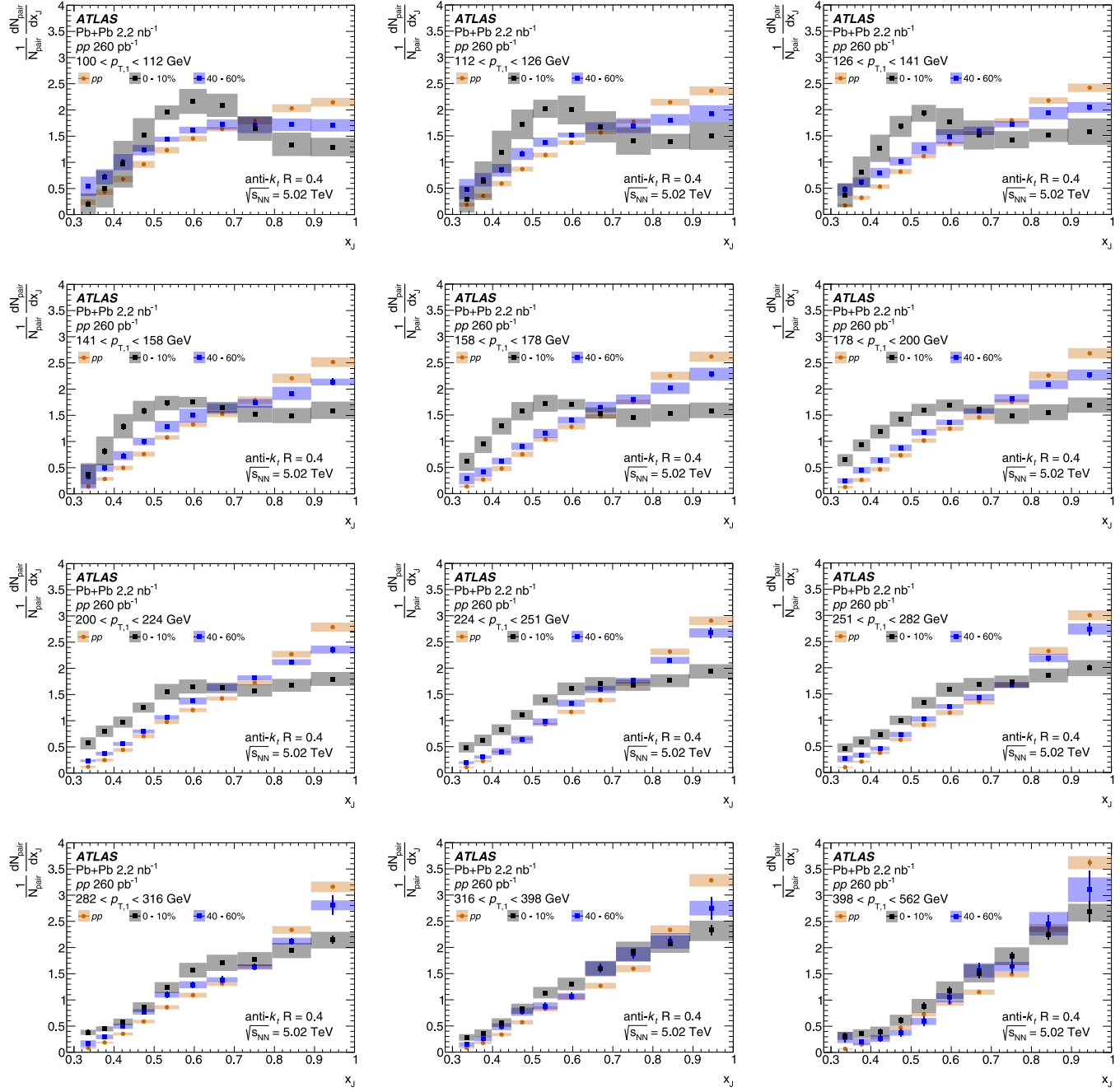


FIG. 8. The dijet-yield-normalized $\frac{1}{N_{\text{pair}}} \frac{dN_{\text{pair}}}{dx_J}$ distributions in 0–10% and 40–60% centrality Pb+Pb collisions and pp collisions for twelve $p_{T,1}$ selections from 100 to 562 GeV. Statistical uncertainties are shown as error bars (which are smaller than the markers in many cases) and systematic uncertainties are shown as boxes.

collisions resulting in a small disagreement in the JES between data and simulations. The extent of this disagreement, and corresponding uncertainty contribution is evaluated by the method used in Ref. [35] for 2015 and 2011 data, which compares the jet p_T measured in the calorimeter with the sum of the transverse momenta of charged particles within the jet, in both the data and MC samples. This uncertainty is determined as a function of event centrality and was found to be independent of jet p_T and η . The selected charged-particle tracks have $p_T > 4$ GeV in order to exclude particles from

the UE. The sum of the charged-particle transverse momenta provides a data-driven estimate of the centrality dependence of the JES arising from the observed centrality-dependent modification of the jet fragmentation due to jet quenching in Pb+Pb collisions [40]. The size of this centrality-dependent uncertainty in the JES reaches 1.2% in the most central collisions and the value is applied independent of x_J . For each individual component, the JES in the MC simulation was modified as a function of p_T and η by one standard deviation, and the response matrix was recomputed.

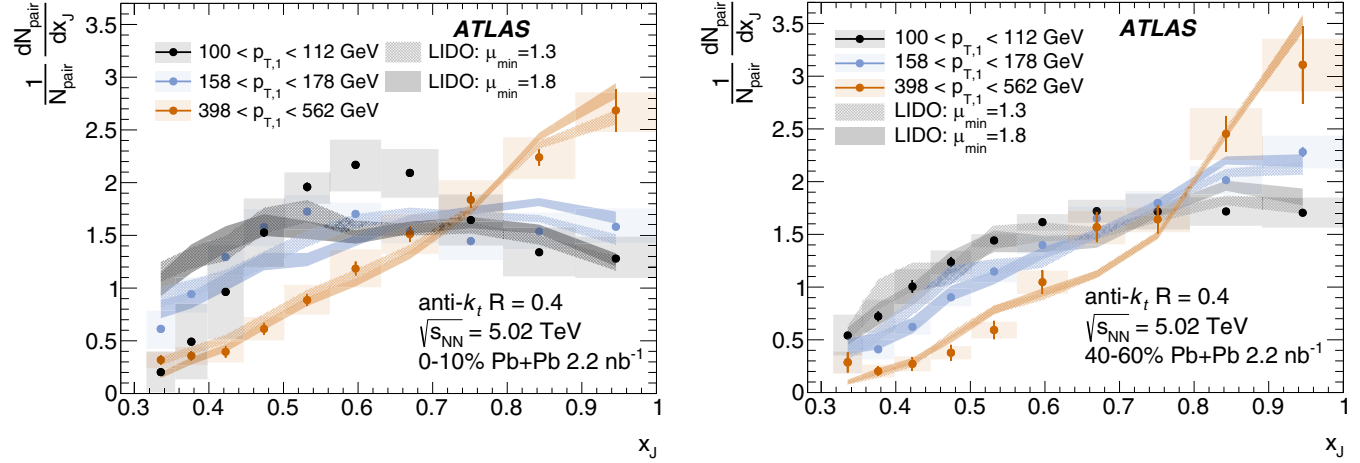


FIG. 9. Comparison of the dijet-yield-normalized x_J distributions in 0–10% (left) and 40–60% (right) centrality Pb+Pb collisions with predictions from LIDO [42] for two values of the jet-medium coupling cutoff parameter, $\mu_{\min} = 1.3$ and $\mu_{\min} = 1.8$. Statistical uncertainties are shown as error bars (which are smaller than the markers in many cases) and systematic uncertainties are shown as boxes.

The uncertainty due to the JER is evaluated by repeating the unfolding procedure with modified response matrices, where an additional contribution is added to the resolution of the reconstructed p_T in the MC sample using a Gaussian smearing procedure. The smearing factor is evaluated using an *in situ* technique in 13 TeV pp data that involves studies of dijet p_T balance [41]. Further, an uncertainty is included to account for differences between the tower-based jet reconstruction and the jet reconstruction used in analyses of 13 TeV pp data, as well as differences in calibration procedures. The modifications to the response are propagated through the unfolding and the resulting uncertainty is symmetrized.

Two sources of systematic uncertainty were included to account for uncertainties in the removal of the combinatoric background. The first contribution stems from the combinatoric subtraction method, and was determined by extracting the two-dimensional ($p_{T,1}, p_{T,2}$) distribution of combinatoric jets from an alternative sideband of $1.1 < |\Delta\phi| < 1.5$ as was done in Ref. [11]. The second contribution stems from the sensitivity of the analysis to the efficiency correction for combinatoric jets, and was evaluated by repeating the analysis without the inclusion of this efficiency correction. The deviation from the nominal result is taken as the uncertainty contribution.

Additional sources of systematic uncertainty which account for the unfolding procedure were considered. The sensitivity to the Bayesian prior was evaluated by modifying the weights applied when producing the response matrix in a centrality-dependent manner in order to enclose the data ($p_{T,1}^{\text{reco}}, p_{T,2}^{\text{reco}}$) distributions between the corresponding MC distributions based on the nominal and alternative priors. There is a sensitivity to the minimum p_T^{jet} in the analysis at small x_J and small $p_{T,1}$ due to the efficiency correction made as part of the unfolding. The sensitivity of the result to this effect is evaluated by varying the minimum reconstructed p_T^{jet} , motivated by the magnitude of the JER, from 32 to 39 GeV for both

data and simulation. This results in a significant contribution to the systematic uncertainties at low x_J in low $p_{T,1}$ bins. For each of these contributions the deviation of the unfolded result from the nominal is symmetrized and taken as a contribution to the systematic uncertainties. A closure test was performed using the MC samples by splitting them into two equal parts and using one part to produce a response matrix and the other in place of the data sample in the unfolding. The deviation between the unfolded result and the underlying truth-level distribution was taken as an estimate of this uncertainty. The uncertainty from each of these contributions is taken independently and symmetrized.

The magnitude of the systematic uncertainties in the dijet-yield-normalized x_J distributions can be seen in Fig. 5 for both central and peripheral Pb+Pb collisions. In the central collisions, the total systematic uncertainties are largely driven by the sensitivity of the unfolding to the choice of prior. In contrast, in peripheral collisions the total uncertainties are largely driven by the uncertainty in the JES and JER. The fractional uncertainties are largest at low x_J in both collision systems; however, the yield in these x_J regions is small.

The systematic uncertainty contributions are similarly propagated to the calculation of the nuclear modification factor. The centrality-independent components of the JES and JER, as well as the sensitivity of the unfolding to the minimum measured p_T^{jet} , are treated as correlated between Pb+Pb and pp collisions. The remainder of the contributions to the systematic uncertainty, including the centrality-dependent component of the JES, are treated as uncorrelated between Pb+Pb and pp . The resulting uncertainties in $R_{AA}^{\text{pair}}(p_{T,1})$ and $R_{AA}^{\text{pair}}(p_{T,2})$ are shown for 0–10% centrality Pb+Pb collisions in Fig. 6; these uncertainties are dominated by the JES uncertainty. In the ratio of $R_{AA}^{\text{pair}}(p_{T,2})$ to $R_{AA}^{\text{pair}}(p_{T,1})$, each source of systematic uncertainty is treated as fully correlated between $R_{AA}^{\text{pair}}(p_{T,2})$ and $R_{AA}^{\text{pair}}(p_{T,1})$, including the global systematic uncertainties.

VII. RESULTS

A. Dijet-yield-normalized x_J distributions

The dijet-yield-normalized x_J distributions in pp collisions are shown for three selections of $p_{T,1}$ from 100 to 562 GeV in Fig. 7. The measured distributions are compared with those from the PYTHIA 8 generator [22] using the A14 tune [23] in combination with the NNPDF23LO PDFs [24]. The PYTHIA 8 sample is able to describe the data over the full x_J range considered.

Figure 8 shows the measured dijet-yield-normalized x_J distributions in pp collisions and as a function of centrality in $Pb+Pb$ collisions for twelve $p_{T,1}$ selections between 100 and 562 GeV. In central collisions, at $100 < p_{T,1} < 112$ GeV a broad maximum is observed in the distributions at x_J around 0.6. With increasing $p_{T,1}$ as well as with decreasing centrality, this feature becomes less pronounced. Significant modification from pp collisions is observed up to $398 < p_{T,1} < 562$ GeV in the full centrality range; the x_J distributions have a reduced fraction of balanced jets and an increased fraction of imbalanced jets.

Figure 9 compares the measured distributions in $Pb+Pb$ collisions with the predictions from the LIDO model [42]. LIDO is a transport model including both elastic jet-medium collisions and medium-induced radiative processes, with event-by-event fluctuations implemented for both processes, as well as a simple model for the response of the medium. LIDO uses PYTHIA 8 [22] with the A14 tune [23] and the CTEQL1 PDF [30] to initialize their energy-loss calculation. The calculations are performed using two high likelihood values for the jet-medium coupling cutoff parameter: $\mu_{\min} = 1.3$ and $\mu_{\min} = 1.8$. This parameter is related to the strength of the coupling between the jet and the medium, where a smaller μ_{\min} value corresponds to a larger coupling, and was constrained using inclusive jet and hadron suppression measurements [42]. Only minimal sensitivity to the jet-medium coupling cutoff parameter is observed in the dijet-yield-normalized x_J distributions, with $\mu_{\min} = 1.3$ and $\mu_{\min} = 1.8$ demonstrating equal ability to reproduce the measured results. The model reproduces the behavior observed at high $p_{T,1}$ and in 40–60% centrality $Pb+Pb$ collisions while not reproducing the relative enhancement of intermediate x_J observed at low $p_{T,1}$ in 0–10% centrality $Pb+Pb$ collisions.

Figure 10 shows a direct comparison between the dijet-yield-normalized x_J distributions in 0–10% centrality $Pb+Pb$ collisions at 5.02 TeV for $100 < p_{T,1} < 200$ GeV and results at 2.76 TeV from Ref. [11] for the same collision centrality and $p_{T,1}$ selections. Although these two measurements are performed at different collision energies, similar levels of quenching are expected, based on measurements of inclusive jets [3,43]. The x_J distributions are observed to be consistent within systematic uncertainties at the two collision energies. For $100 < p_{T,1} < 126$ GeV, a peak is observed at intermediate x_J for both collision energies.

B. Absolutely normalized x_J distributions

The absolutely normalized x_J distributions, as calculated with expressions (5) and (6) for $Pb+Pb$ and pp collisions

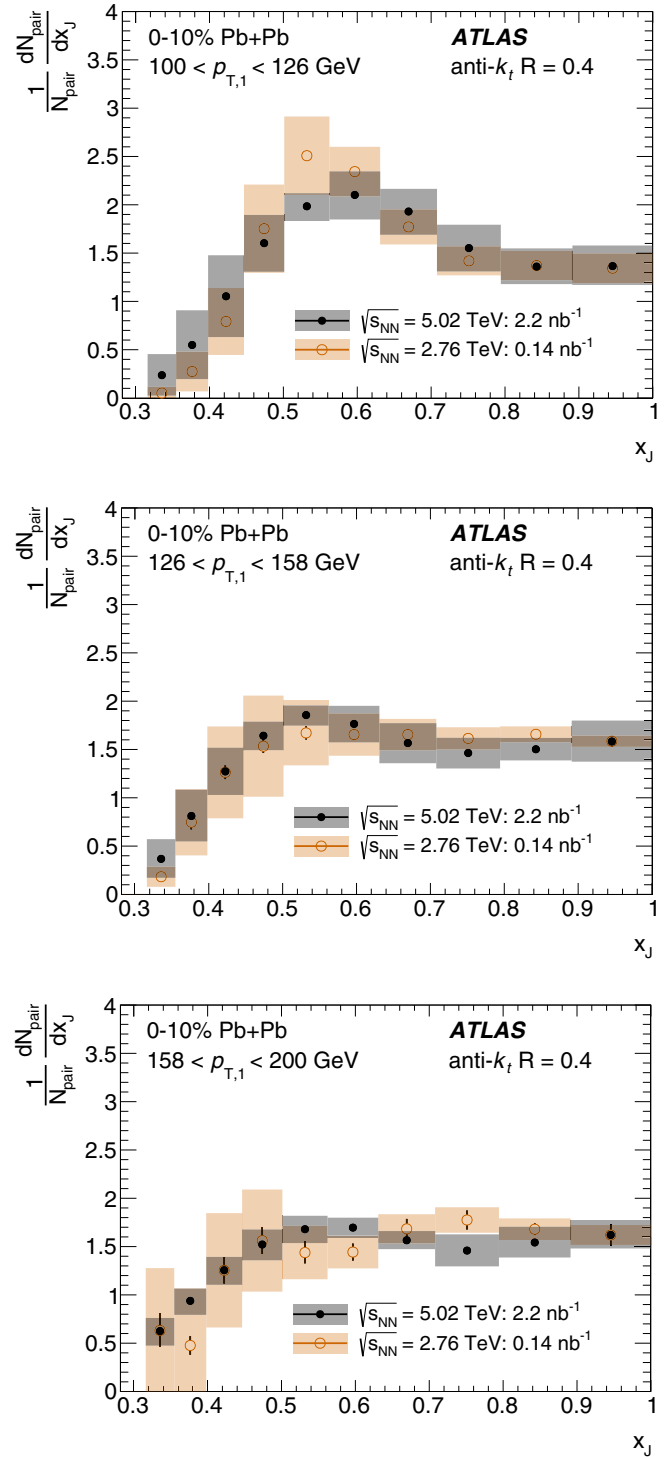


FIG. 10. Comparison of the measured x_J distribution at 5.02 TeV in 0–10% centrality collisions for $100 < p_{T,1} < 126$ GeV (top), $126 < p_{T,1} < 158$ GeV (middle), and $158 < p_{T,1} < 200$ GeV (bottom) with those at 2.76 TeV from Ref. [11]. Statistical uncertainties are shown as error bars (which are smaller than the markers in many cases) and systematic uncertainties are shown as boxes.

respectively, allow a direct comparison of the absolute dijet yields between $Pb+Pb$ and pp collisions as a function of x_J . Figure 11 shows these distributions for pp and $Pb+Pb$

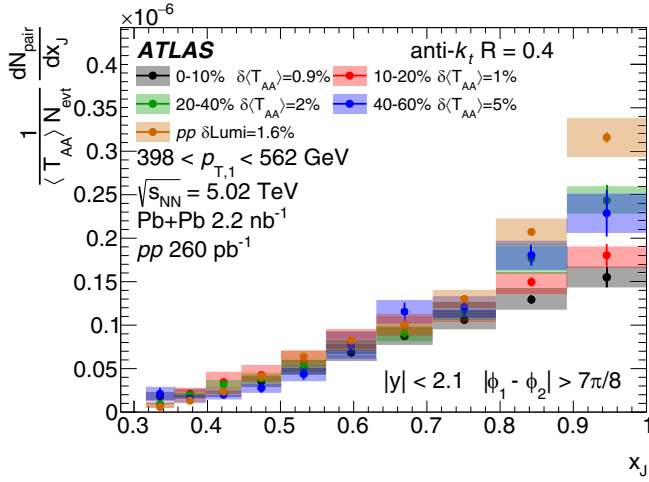
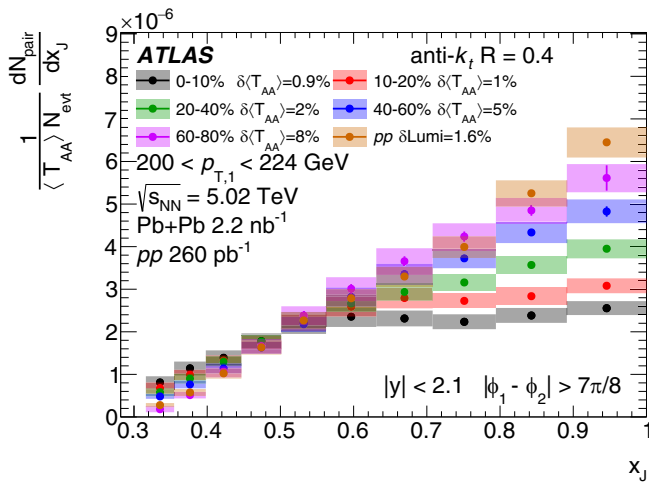
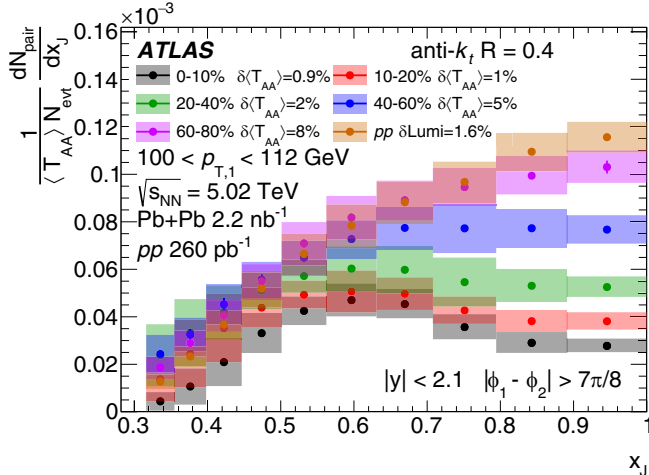


FIG. 11. The absolutely normalized x_J distributions for $100 < p_{T,1} < 112$ GeV (top), $200 < p_{T,1} < 224$ GeV (center), and $398 < p_{T,1} < 562$ GeV (bottom) in pp collisions and for five centrality selections in $Pb+Pb$ collisions. Statistical uncertainties are shown as error bars (which are smaller than the markers in many cases) and systematic uncertainties are shown as boxes. The global normalization uncertainty due to the T_{AA} for each centrality as well as the pp luminosity are listed in the legends.

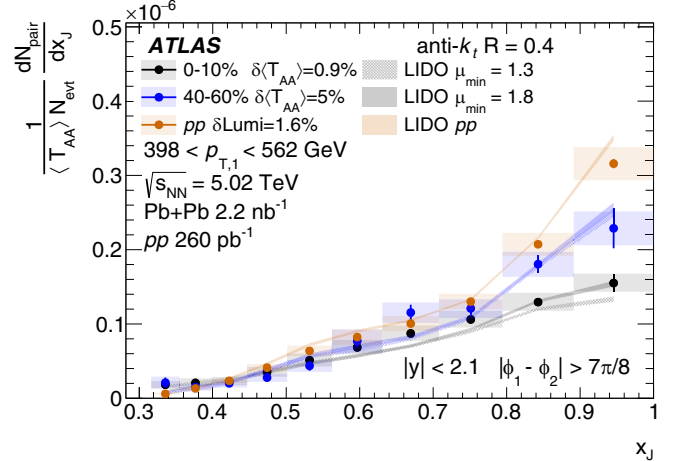
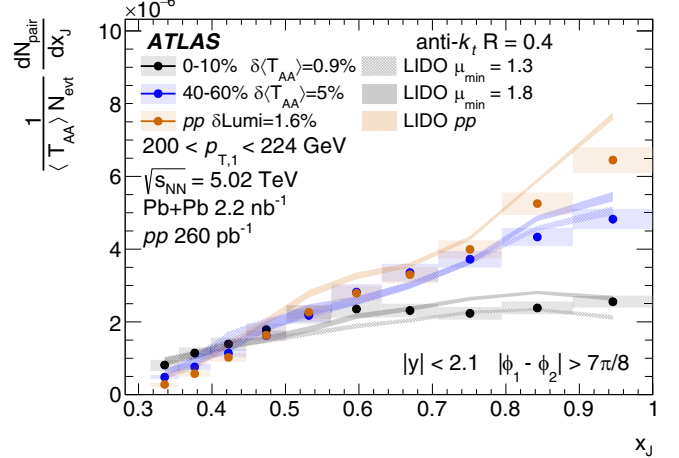
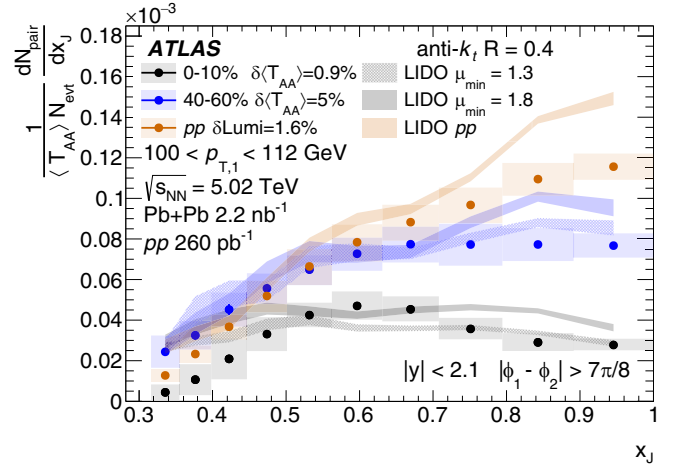


FIG. 12. The absolutely normalized x_J distributions for $100 < p_{T,1} < 112$ GeV (top), $200 < p_{T,1} < 224$ GeV (center), and $398 < p_{T,1} < 562$ GeV (bottom) in pp collisions and for two centrality selections in $Pb+Pb$ collisions. For $Pb+Pb$ collisions, the measurements are compared with predictions from LIDO [42] for two values of the jet-medium coupling cutoff parameter, $\mu_{min} = 1.3$ and $\mu_{min} = 1.8$, and the pp collision measurements are compared with the LIDO pp collision calculation.

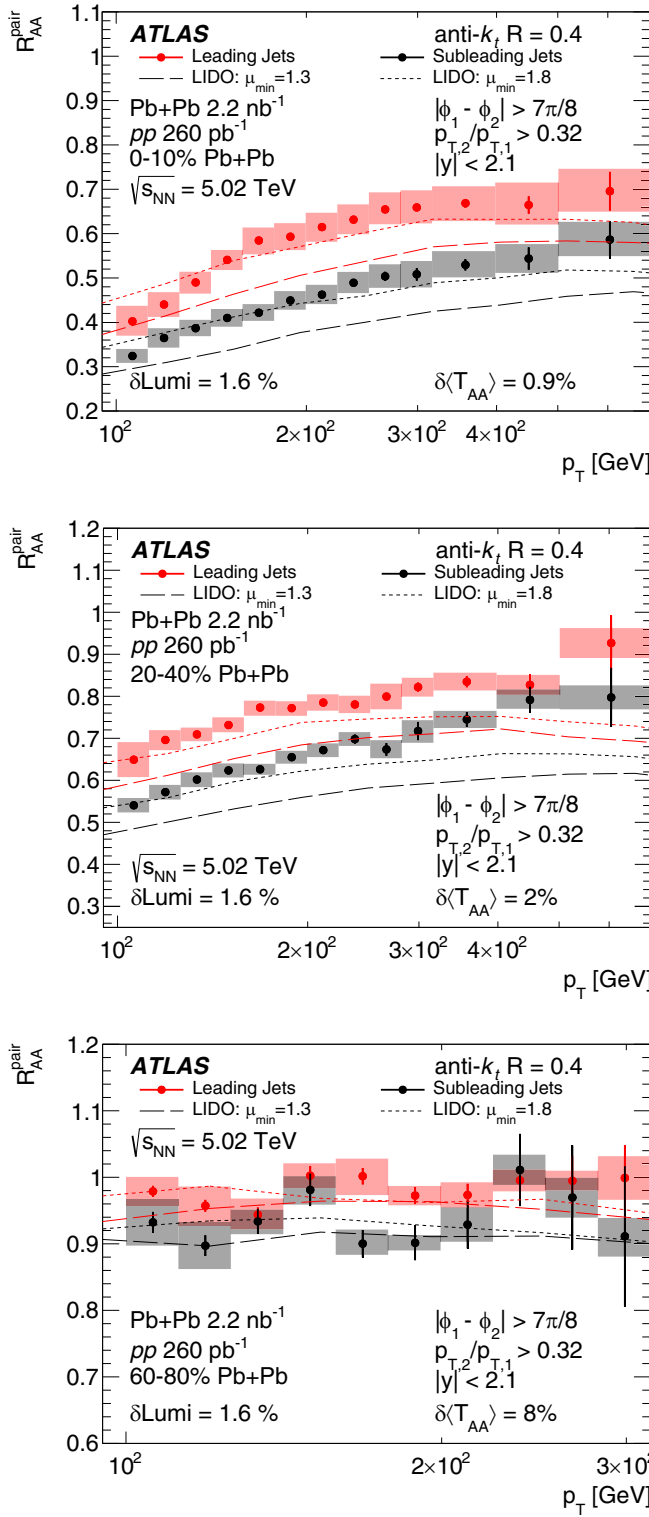


FIG. 13. The leading and subleading jet R_{AA}^{pair} distributions measured for a selection of centrality regions compared with predictions from LIDO [42]. Statistical uncertainties are shown as error bars (which are smaller than the markers in many cases) and systematic uncertainties are shown as boxes.

collisions as a function of centrality for three $p_{T,1}$ selections: 100–112 GeV, 200–224 GeV, and 398–562 GeV. Balanced

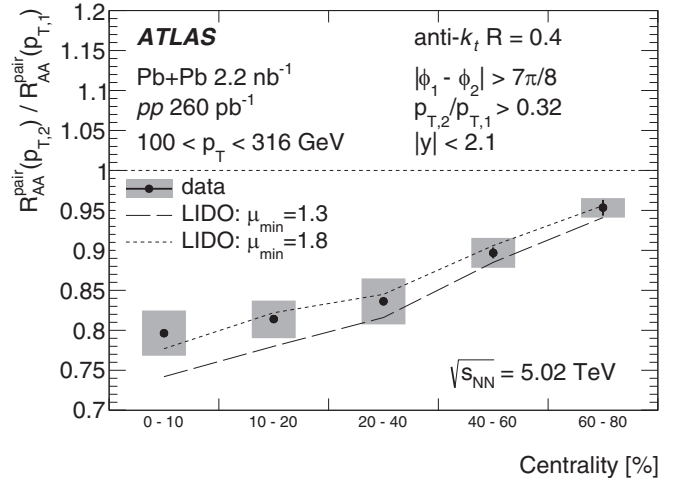


FIG. 14. The ratio of the subleading-jet to leading-jet nuclear modification factors integrated over jet p_T between 100 and 316 GeV. Statistical uncertainties are shown as error bars (which are smaller than the markers in many cases) and systematic uncertainties are shown as boxes.

dijets are suppressed in central Pb+Pb collisions relative to asymmetric dijets, leading to the peak structure observed in the dijet-yield-normalized x_J distributions at low $p_{T,1}$. The depletion of balanced dijets persists over all $p_{T,1}$ and centrality selections measured here, with the magnitude of the depletion decreasing with increasing $p_{T,1}$ and towards more peripheral collisions. When going from central Pb+Pb collisions to pp collisions for $100 < p_{T,1} < 112$ GeV, the suppression of dijets is smaller for $x_J < 0.6$ than for higher x_J . For higher $p_{T,1}$, there is a smaller difference between pp and Pb+Pb collisions at low x_J .

Figure 12 shows the absolutely normalized x_J distributions compared with the same LIDO calculations [42] as in the previous section for three $p_{T,1}$ selections from 100 to 562 GeV. The LIDO pp calculation is also shown. For pp collisions, LIDO uses PYTHIA 8 [22] with the A14 tune [23] and the CTEQL1 PDF [30]. The LIDO model overestimates the pp collision results at large x_J ; the size of the discrepancy between the model and the data decreases with increasing $p_{T,1}$. This trend persists, but with a smaller difference in 40–60% centrality Pb+Pb collisions. In 0–10% centrality Pb+Pb collisions, the LIDO model’s prediction is flatter than the data in the lowest $p_{T,1}$ range, but agrees well at higher $p_{T,1}$.

C. R_{AA}^{pair} of leading and subleading jets

The pair nuclear modification factors projected for leading and subleading jets, as defined in Eqs. (7) and (8), are shown for three centrality selections as a function of the jet p_T in Fig. 13. Both $R_{AA}^{\text{pair}}(p_{T,1})$ and $R_{AA}^{\text{pair}}(p_{T,2})$ show significant modification from a value of one in all but the most peripheral collisions, with a stronger suppression observed at low p_T^{jet} . It is observed that the subleading jets are more suppressed than leading jets, particularly at $p_T > 200$ GeV where nearly all the inclusive jets (within the rapidity range of this analysis) are included in the dijet sample. This behavior is qualitatively

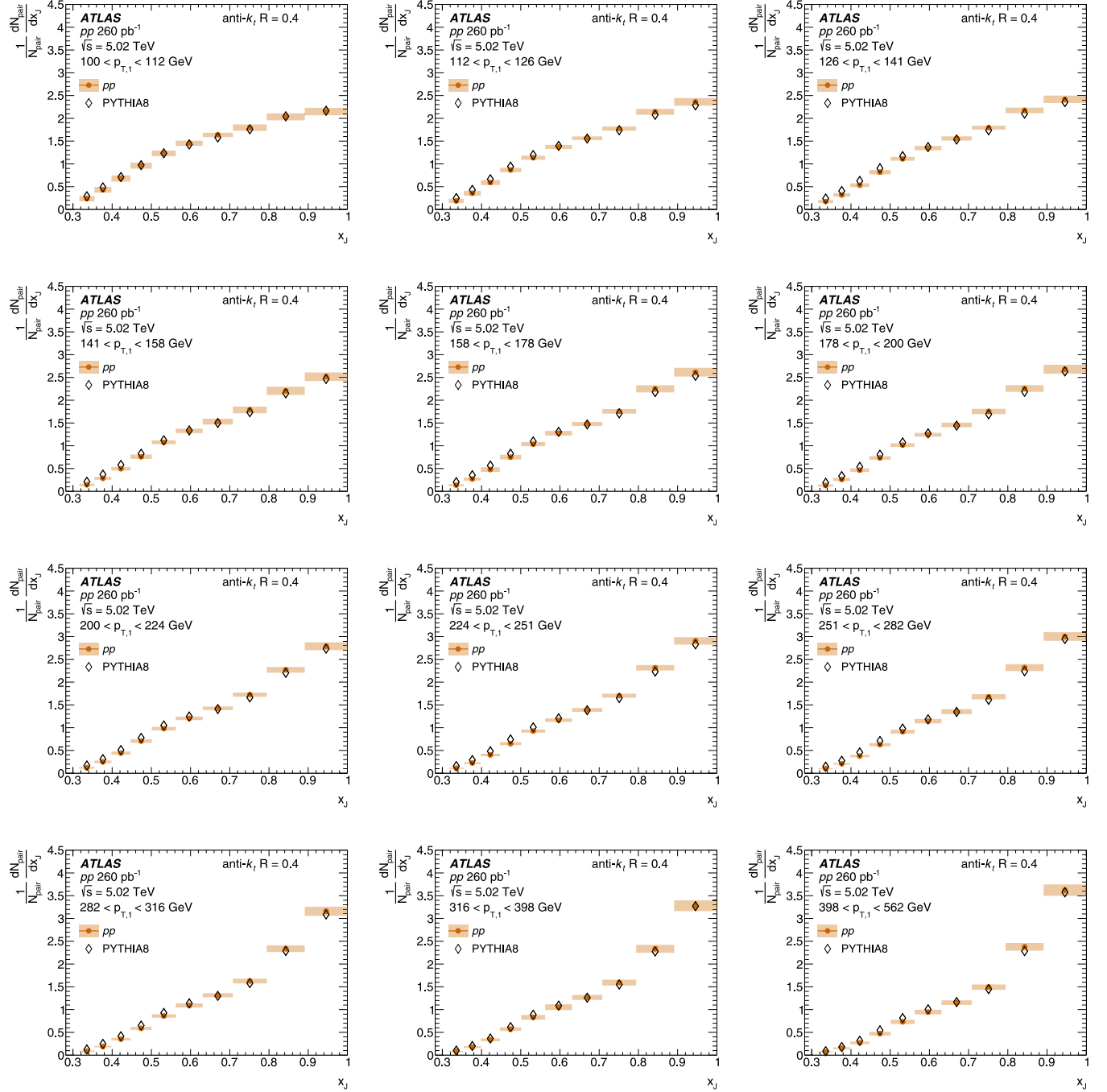


FIG. 15. The dijet-yield-normalized $\frac{1}{N_{\text{pair}}} \frac{dN_{\text{pair}}}{dx_j}$ distributions in pp collisions for twelve $p_{T,1}$ selections from 100 to 562 GeV overlaid with the corresponding distributions from PYTHIA 8. The statistical uncertainties are shown as error bars (which are smaller than the markers in many cases), and the systematic uncertainties are shown as boxes.

reproduced in predictions made by the LIDO [42] model. In the LIDO model, the jet-medium coupling cutoff parameter $\mu_{\min} = 1.3$ clearly predicts a larger suppression for both jets than is observed in the data. The calculation with $\mu_{\min} = 1.8$ is closer to the data but does not describe the trends with p_T and centrality.

The different levels of suppression observed for leading and subleading jets is quantified as a function of centrality

in the ratio $R_{AA}^{\text{pair}}(p_{T,2})/R_{AA}^{\text{pair}}(p_{T,1})$ integrated over p_T^{jet} between 100 and 316 GeV as shown in Fig. 14, where $R_{AA}^{\text{pair}}(p_{T,2})$ is seen to be smaller than $R_{AA}^{\text{pair}}(p_{T,1})$ in all centrality selections. The suppression of subleading jets relative to leading jets is most significant in 0–10% centrality $\text{Pb}+\text{Pb}$ collisions and decreases smoothly towards peripheral $\text{Pb}+\text{Pb}$ collisions. In 0–10% centrality $\text{Pb}+\text{Pb}$ events, subleading jets are approximately 20% more suppressed than leading jets, with 60–80%

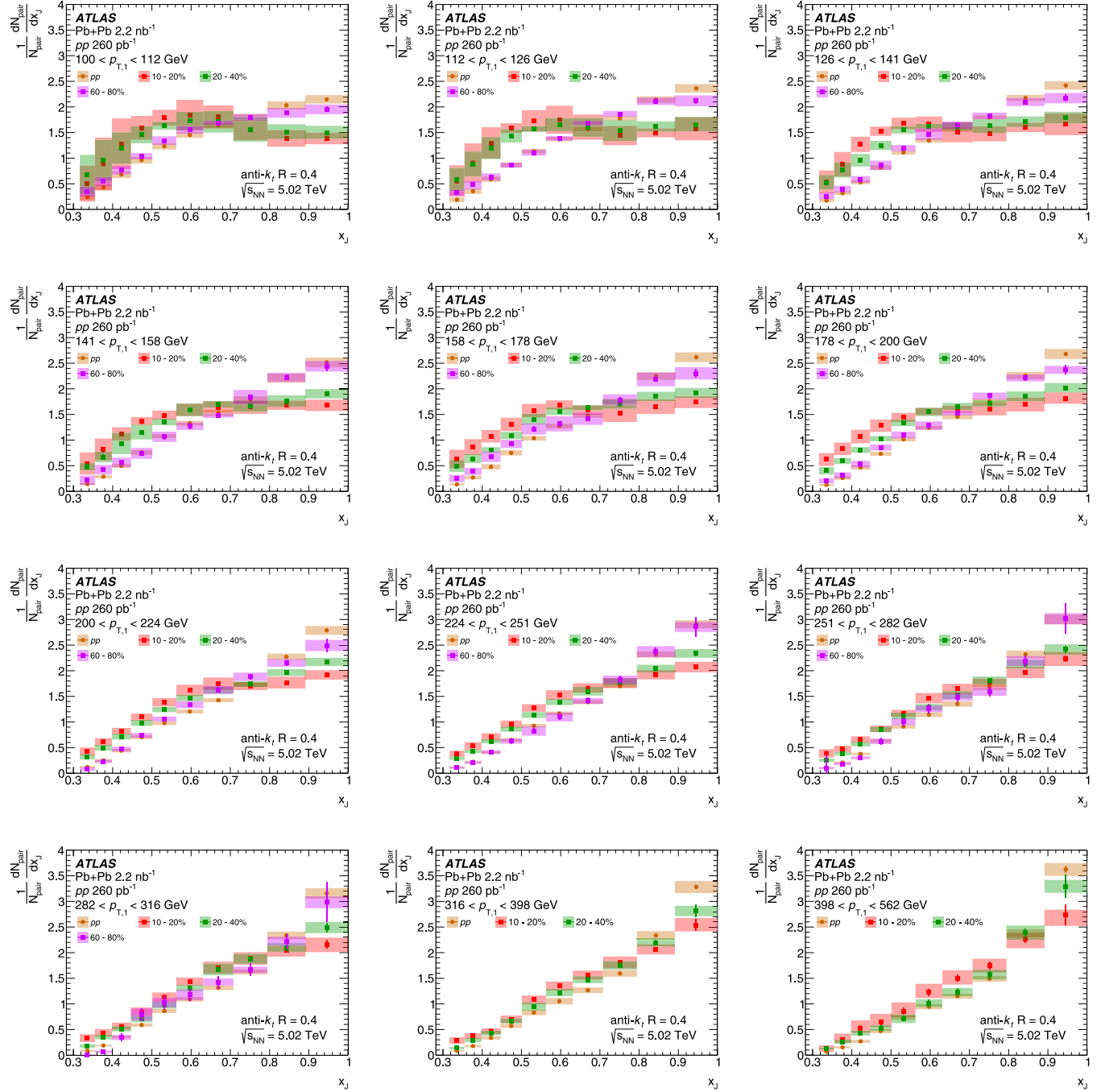


FIG. 16. The unfolded dijet-yield-normalized x_J distributions in both Pb+Pb and pp collisions for twelve $p_{T,\text{leading}}$ selections from 100 to 562 GeV. The results in Pb+Pb collisions are shown in three centrality selections, 10–20%, 20–40%, and 60–80%. Statistical uncertainties are shown as error bars and systematic uncertainties are shown as boxes.

centrality Pb+Pb events seeing only about 5% more suppression for subleading jets than for leading jets. The value of $R_{\text{AA}}^{\text{pair}}(p_{T,2})/R_{\text{AA}}^{\text{pair}}(p_{T,1})$ in 60–80% centrality Pb+Pb events is 3σ away from 1, providing evidence of jet quenching in peripheral Pb+Pb collisions. In contrast, in inclusive jet measurements, due to the larger uncertainties, no significant suppression is observed in this p_T range for the most peripheral Pb+Pb collisions [3]. This is in qualitative agreement with results from CMS [44], which show that, compared to

pp collisions, the subleading jets in dijet events in Pb+Pb collisions have stronger modification to their structure than leading jets.

VIII. CONCLUSION

This paper presents a measurement of the unfolded double-differential yields of leading dijets. The yields are presented as measurements of the dijet x_J distributions and the $R_{\text{AA}}^{\text{pair}}$

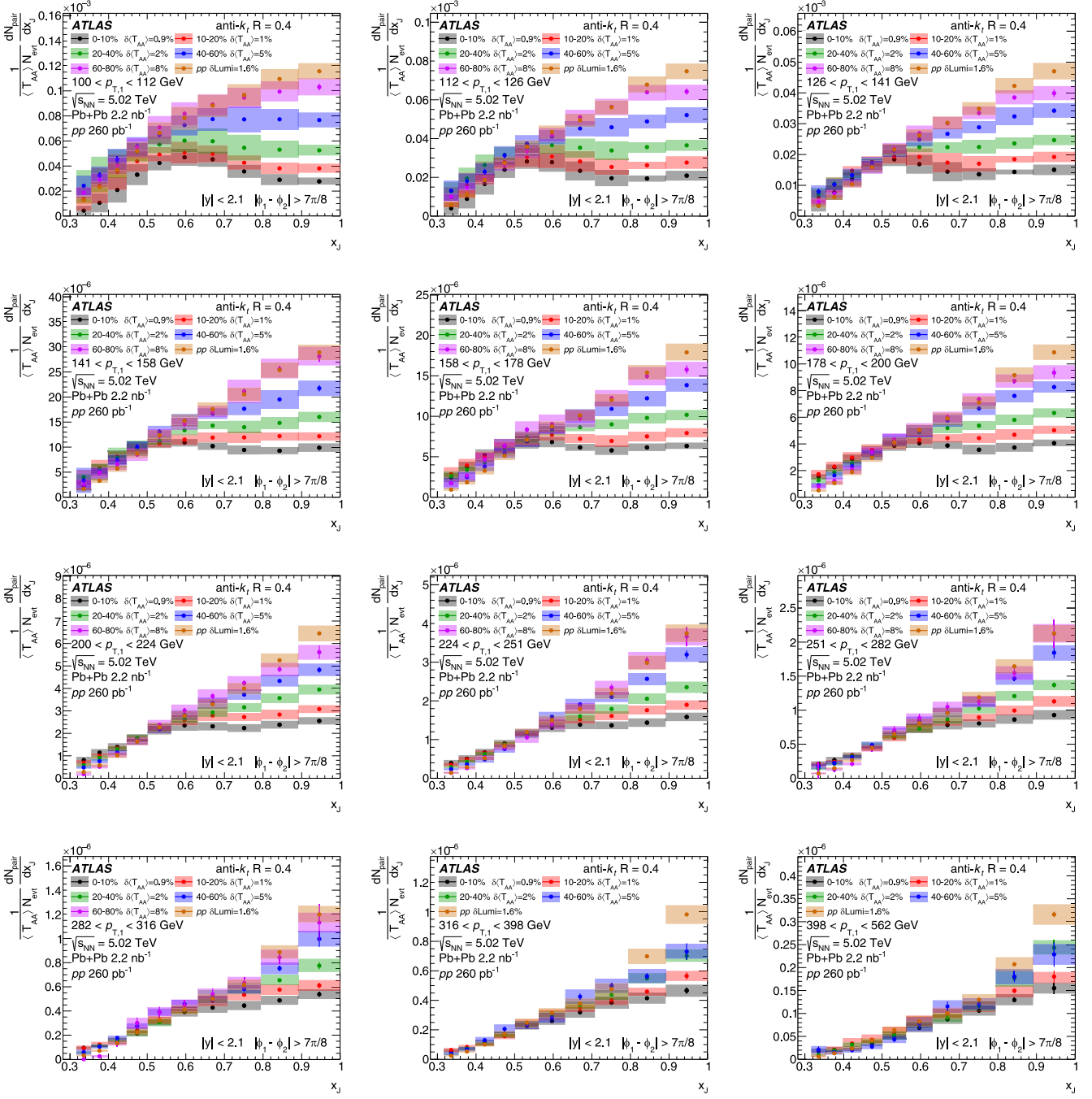


FIG. 17. Comparison of the absolutely normalized x_J distributions in pp collisions and five centrality selections in $Pb+Pb$ collisions.

projected for leading and subleading jets, using 2.2 nb^{-1} of $Pb+Pb$ data and 260 pb^{-1} of pp data collected at $\sqrt{s_{NN}} = 5.02 \text{ TeV}$ by the ATLAS detector at the LHC. The measurement of the x_J distributions is performed differentially in $p_{T,1}$ and centrality, and the R_{AA} of leading and subleading jets is measured differentially in jet p_T and centrality. The presented results are unfolded to correct for detector response and inefficiencies.

The dijet-yield-normalized x_J distributions, across the full $p_{T,1}$ range considered in this analysis, show significant broadening in central $Pb+Pb$ collisions relative to those in pp

collisions. Up to the highest $p_{T,1}$ interval considered in this measurement, $398 < p_{T,1} < 562 \text{ GeV}$, significant modification from the distributions in pp collisions is observed for central $Pb+Pb$ collisions. With decreasing $p_{T,1}$ the modifications from the distributions in pp collisions become larger, with significant modifications observed for all centralities at $100 < p_{T,1} < 112 \text{ GeV}$. In 0–10% centrality $Pb+Pb$ collisions, between 100 and 112 GeV, the distribution is peaked around x_J of 0.6, indicating that the most probable configuration for dijets is to be highly imbalanced in p_T . Measurements of absolutely normalized x_J distributions show that this comes

from the suppression of balanced dijets, as opposed to an enhancement of imbalanced jets, in comparison with pp collisions. This suppression of balanced dijets evolves smoothly as a function of the event centrality, with peripheral Pb+Pb collisions demonstrating only slight modification from pp collisions. The measurements of the pair nuclear modification factor, $R_{AA}^{\text{pair}}(p_{T,1})$ and $R_{AA}^{\text{pair}}(p_{T,2})$, show that subleading jets are more suppressed than leading jets. This is observed to be largely independent of jet p_T and this behavior is seen in all centralities. In central collisions, subleading jets are observed to be 20% more suppressed than the leading jets. In peripheral collisions, the suppression of subleading jets relative to leading jets is reduced, but the stronger suppression of subleading jets remains significant. These measurements provide new information about the role of path-length dependence and fluctuations in jet energy loss which will help constrain models of parton energy loss in the quark-gluon plasma.

ACKNOWLEDGMENTS

We thank CERN for the very successful operation of the LHC, as well as the support staff from our institutions without whom ATLAS could not be operated efficiently. We acknowledge the support of ANPCyT, Argentina; YerPhI, Armenia; ARC, Australia; BMWFW and FWF, Austria; ANAS, Azerbaijan; CNPq and FAPESP, Brazil; NSERC, NRC, and CFI, Canada; CERN; ANID, Chile; CAS, MOST, and NSFC, China; Minciencias, Colombia; MEYS CR, Czech Republic; DNRF and DNSRC, Denmark; IN2P3-CNRS and CEA-DRF/IRFU, France; SRNSFG, Georgia; BMBF, HGF, and MPG, Germany; GSRI, Greece; RGC and Hong Kong SAR, China; ISF and Benoziyo Center, Israel; INFN, Italy; MEXT and JSPS, Japan; CNRST, Morocco; NWO, Netherlands; RCN, Norway; MEiN, Poland; FCT, Portugal; MNE/IFA, Romania; MESTD, Serbia; MSSR, Slovakia; ARRS and MIZŠ, Slovenia; DSi/NRF, South Africa; MICINN, Spain; SRC and Wallenberg Foundation, Sweden; SERI, SNSF, and Cantons of Bern and Geneva, Switzerland; MOST, Taiwan; TEN-MAK, Türkiye; STFC, United Kingdom; DOE and NSF, United States of America. In addition, individual groups and members have received support from BCKDF, CANARIE, Compute Canada, and CRC, Canada; PRIMUS 21/SCI/017 and UNCE SCI/013, Czech Republic; COST, ERC, ERDF, Horizon 2020, and Marie Skłodowska-Curie Actions, European Union; Investissements d’Avenir Labex, Investissements d’Avenir Idex, and ANR, France; DFG and AvH Foundation, Germany; Herakleitos, Thales, and Aristeia programs co-financed by EU-ESF and the Greek NSRF, Greece; BSF-NSF and MINERVA, Israel; Norwegian Financial Mechanism 2014-2021, Norway; NCN and NAWA, Poland; La Caixa Banking Foundation, CERCA Programme Generalitat de Catalunya, and PROMETEO and GenT Programmes Generalitat Valenciana, Spain; Göran Gustafssons Stiftelse, Sweden; The Royal Society and Leverhulme Trust, United Kingdom. The crucial computing support from all WLCG partners is acknowledged gratefully, in particular from CERN, the ATLAS Tier-1 facilities at TRIUMF (Canada), NDGF (Denmark, Norway, Sweden), CC-IN2P3 (France), KIT/GridKA (Germany), INFN-CNAF (Italy), NL-T1 (Netherlands), PIC

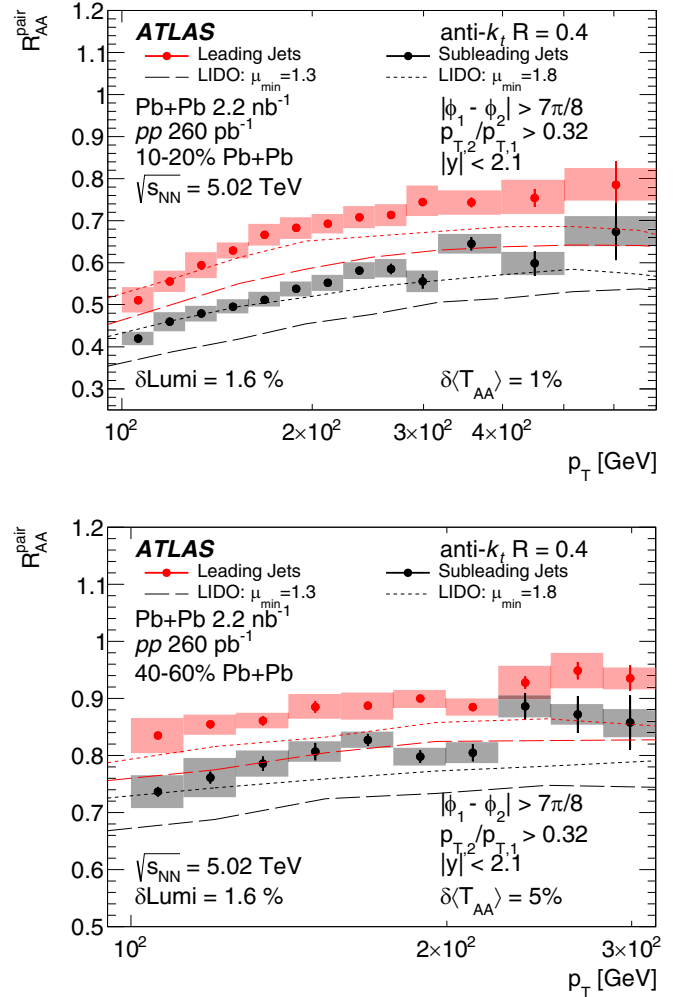


FIG. 18. The $R_{AA}^{\text{pair}}(p_{T,1})$ and $R_{AA}^{\text{pair}}(p_{T,2})$ distributions measured for Pb+Pb centrality selections compared with predictions from LIDO [42].

(Spain), ASGC (Taiwan), RAL (UK), and BNL (USA), the Tier-2 facilities worldwide, and large non-WLCG resource providers. Major contributors of computing resources are listed in Ref. [45].

APPENDIX

For completeness, the data including the full range of $p_{T,1}$ intervals and centrality selections in Pb+Pb collisions are included here. Figure 15 shows the dijet-yield-normalized distributions for pp collisions, compared to PYTHIA 8 calculations. Figure 16 shows unfolded $\frac{1}{N_{\text{pair}}} \frac{dN_{\text{pair}}}{dx_J}$ distributions for both Pb+Pb and pp collisions over twelve selections in $p_{T,1}$ between 100 and 562 GeV, for centrality intervals omitted previously. Figure 17 shows absolutely normalized x_J distributions for five centrality intervals for both Pb+Pb and pp collisions for twelve selections of $p_{T,1}$ between 100 and 562 GeV. Finally, Fig. 18 provides $R_{AA}^{\text{pair}}(p_{T,1})$ and $R_{AA}^{\text{pair}}(p_{T,2})$ distributions measured in two additional centrality intervals.

- [1] W. Busza, K. Rajagopal, and W. van der Schee, Heavy ion collisions: The big picture, and the big questions, *Annu. Rev. Nucl. Part. Sci.* **68**, 339 (2018).
- [2] M. L. Miller, K. Reygers, S. J. Sanders, and P. Steinberg, Glauber modeling in high energy nuclear collisions, *Annu. Rev. Nucl. Part. Sci.* **57**, 205 (2007).
- [3] M. Aaboud *et al.* (ATLAS Collaboration), Measurement of the nuclear modification factor for inclusive jets in Pb+Pb collisions at $\sqrt{s_{NN}} = 5.02$ TeV with the ATLAS detector, *Phys. Lett. B* **790**, 108 (2019).
- [4] A. M. Sirunyan, *et al.* (CMS Collaboration), First measurement of large area jet transverse momentum spectra in heavy-ion collisions, *J. High Energy Phys.* **05** (2021) 284.
- [5] S. Acharya *et al.* (ALICE Collaboration), Measurements of inclusive jet spectra in pp and central Pb-Pb collisions at $\sqrt{s_{NN}} = 5.02$ TeV, *Phys. Rev. C* **101**, 034911 (2020).
- [6] S. Cao and X.-N. Wang, Jet quenching and medium response in high-energy heavy-ion collisions: a review, *Rep. Prog. Phys.* **84**, 024301 (2021).
- [7] L. Cunqueiro and A. M. Sickles, Studying the QGP with Jets at the LHC and RHIC, *Prog. Part. Nucl. Phys.* **124**, 103940 (2022).
- [8] G.-Y. Qin and B. Müller, Explanation of Dijet Asymmetry in Pb+Pb Collisions at the Large Hadron Collider, *Phys. Rev. Lett.* **106**, 162302 (2011); **108**, 189904(E) (2012).
- [9] G. Aad *et al.* (ATLAS Collaboration), Measurements of azimuthal anisotropies of jet production in Pb+Pb collisions at $\sqrt{s_{NN}} = 5.02$ TeV with the ATLAS detector, *Phys. Rev. C* **105**, 064903 (2022).
- [10] J. G. Milhano and K. C. Zapp, Origins of the di-jet asymmetry in heavy ion collisions, *Eur. Phys. J. C* **76**, 288 (2016).
- [11] M. Aaboud *et al.* (ATLAS Collaboration), Measurement of jet p_T correlations in Pb+Pb and pp collisions at $\sqrt{s_{NN}} = 2.76$ TeV with the ATLAS detector, *Phys. Lett. B* **774**, 379 (2017).
- [12] G. Aad *et al.* (ATLAS Collaboration), Observation of a Centrality-Dependent Dijet Asymmetry in Lead-Lead Collisions at $\sqrt{s_{NN}} = 2.77$ TeV with the ATLAS Detector at the LHC, *Phys. Rev. Lett.* **105**, 252303 (2010).
- [13] S. Chatrchyan *et al.* (CMS Collaboration), Observation and studies of jet quenching in PbPb collisions at $\sqrt{s_{NN}} = 2.76$ TeV, *Phys. Rev. C* **84**, 024906 (2011).
- [14] G. Aad *et al.* (ATLAS Collaboration), The ATLAS experiment at the CERN Large Hadron Collider, *J. Instrum.* **3**, S08003 (2008).
- [15] M. Cacciari, G. P. Salam, and G. Soyez, The anti- k_t jet clustering algorithm, *J. High Energy Phys.* **04** (2008) 063.
- [16] ATLAS Collaboration, Luminosity determination in pp collisions at $\sqrt{s} = 13$ TeV using the ATLAS detector at the LHC, CERN Report No. ATLAS-CONF-2019-021, 2019 (unpublished), <https://cds.cern.ch/record/2677054>
- [17] G. Aad *et al.* (ATLAS Collaboration), Operation of the ATLAS trigger system in Run 2, *J. Instrum.* **15**, P10004 (2020).
- [18] ATLAS Collaboration, The ATLAS Collaboration software and firmware, CERN Report No. ATL-SOFT-PUB-2021-001, 2021 (unpublished), <https://cds.cern.ch/record/2767187>
- [19] M. Aaboud *et al.* (ATLAS Collaboration), Measurement of longitudinal flow decorrelations in Pb+Pb collisions at $\sqrt{s_{NN}} = 2.76$ and 5.02 TeV with the ATLAS detector, *Eur. Phys. J. C* **78**, 142 (2018).
- [20] C. Loizides, J. Kamin, and D. d'Enterria, Improved Monte Carlo Glauber predictions at present and future nuclear colliders, *Phys. Rev. C* **97**, 054910 (2018); **99**, 019901(E) (2019).
- [21] G. Aad *et al.* (ATLAS Collaboration), Measurement of W^\pm boson production in Pb+Pb collisions at $\sqrt{s_{NN}} = 5.02$ TeV with the ATLAS detector, *Eur. Phys. J. C* **79**, 935 (2019).
- [22] T. Sjöstrand *et al.*, An introduction to PYTHIA 8.2, *Comput. Phys. Commun.* **191**, 159 (2015).
- [23] ATLAS Collaboration, ATLAS Pythia 8 tunes to 7 TeV data, CERN Report No. ATL-PHYS-PUB-2014-021, 2014 (unpublished), <https://cds.cern.ch/record/1966419>
- [24] R. D. Ball *et al.*, Parton distributions with LHC data, *Nucl. Phys. B* **867**, 244 (2013).
- [25] ATLAS Collaboration, The Pythia 8 A3 tune description of ATLAS minimum bias and inelastic measurements incorporating the Donnachie–Landshoff diffractive model, CERN Report No. ATL-PHYS-PUB-2016-017, 2016 (unpublished), <https://cds.cern.ch/record/2206965>
- [26] S. Agostinelli *et al.*, GEANT4—a simulation toolkit, *Nucl. Instrum. Meth. A* **506**, 250 (2003).
- [27] G. Aad *et al.* (ATLAS Collaboration), The ATLAS Simulation Infrastructure, *Eur. Phys. J. C* **70**, 823 (2010).
- [28] M. Bähr *et al.*, Herwig++ physics and manual, *Eur. Phys. J. C* **58**, 639 (2008).
- [29] S. Gieseke, C. Röhr, and A. Siódtek, Colour reconnections in Herwig++, *Eur. Phys. J. C* **72**, 2225 (2012).
- [30] J. Pumplin *et al.*, New generation of Parton Distributions with Uncertainties from Global QCD Analysis, *J. High Energy Phys.* **07** (2002) 012.
- [31] M. Cacciari, G. P. Salam, and G. Soyez, FastJet User Manual, *Eur. Phys. J. C* **72**, 1896 (2012).
- [32] G. Aad *et al.* (ATLAS Collaboration), Jet energy measurement with the ATLAS detector in proton–proton collisions at $\sqrt{s} = 7$ TeV, *Eur. Phys. J. C* **73**, 2304 (2013).
- [33] M. Aaboud *et al.* (ATLAS Collaboration), Measurement of the azimuthal anisotropy of charged particles produced in $\sqrt{s_{NN}} = 5.02$ TeV Pb+Pb collisions with the ATLAS detector, *Eur. Phys. J. C* **78**, 997 (2018).
- [34] G. Aad *et al.* (ATLAS Collaboration), Jet energy measurement and its systematic uncertainty in proton-proton collisions at $\sqrt{s} = 7$ TeV with the ATLAS detector, *Eur. Phys. J. C* **75**, 17 (2015).
- [35] ATLAS Collaboration, Jet energy scale and its uncertainty for jets reconstructed using the ATLAS heavy ion jet algorithm, CERN Report No. ATLAS-CONF-2015-016, 2015 (unpublished), <https://cds.cern.ch/record/2008677>
- [36] M. Aaboud *et al.* (ATLAS Collaboration), Measurement of photon-jet transverse momentum correlations in 5.02 TeV Pb+Pb and pp collisions with ATLAS, *Phys. Lett. B* **789**, 167 (2019).
- [37] G. D'Agostini, A Multidimensional unfolding method based on Bayes' theorem, *Nucl. Instrum. Meth. A* **362**, 487 (1995).
- [38] T. Adye, Unfolding algorithms and tests using RooUnfold, [arXiv:1105.1160](https://arxiv.org/abs/1105.1160).
- [39] M. Aaboud *et al.* (ATLAS Collaboration), Jet energy scale measurements and their systematic uncertainties in proton-proton collisions at $\sqrt{s} = 13$ TeV with the ATLAS detector, *Phys. Rev. D* **96**, 072002 (2017).
- [40] M. Aaboud *et al.* (ATLAS Collaboration), Measurement of jet fragmentation in Pb+Pb and pp collisions at $\sqrt{s_{NN}} = 5.02$ TeV with the ATLAS detector, *Phys. Rev. C* **98**, 024908 (2018).

- [41] G. Aad *et al.* (ATLAS Collaboration), Jet energy scale and resolution measured in proton-proton collisions at $\sqrt{s} = 13$ TeV with the ATLAS detector, *Eur. Phys. J. C* **81**, 689 (2021).
- [42] W. Ke and X.-N. Wang, QGP modification to single inclusive jets in a calibrated transport model, *J. High Energy Phys.* **05** (2021) 041.
- [43] G. Aad *et al.* (ATLAS Collaboration), Measurements of the Nuclear Modification Factor for Jets in Pb+Pb Collisions at $\sqrt{s_{NN}} = 2.76$ TeV with the ATLAS Detector, *Phys. Rev. Lett.* **114**, 072302 (2015).
- [44] A. M. Sirunyan *et al.* (CMS Collaboration), In-medium modification of dijets in PbPb collisions at $\sqrt{s_{NN}} = 5.02$ TeV, *J. High Energy Phys.* **05** (2021) 116.
- [45] ATLAS Collaboration, ATLAS Computing Acknowledgements, CERN Report No. ATL-SOFT-PUB-2021-003, 2021 (unpublished), <https://cds.cern.ch/record/2776662>

-
- G. Aad ¹⁰¹ B. Abbott ¹¹⁹ D. C. Abbott ¹⁰² K. Abeling ⁵⁵ S. H. Abidi ²⁹ A. Aboulhorma ^{35e} H. Abramowicz ¹⁵⁰
 H. Abreu ¹⁴⁹ Y. Abulaiti ¹¹⁶ A. C. Abusleme Hoffman ^{136a} B. S. Acharya ^{68a,68b,a} B. Achkar ⁵⁵ L. Adam ⁹⁹
 C. Adam Bourdarios ⁴ L. Adamczyk ^{84a} L. Adamek ¹⁵⁴ S. V. Addepalli ²⁶ J. Adelman ¹¹⁴ A. Adiguzel ^{21c}
 S. Adorni ⁵⁶ T. Adye ¹³³ A. A. Affolder ¹³⁵ Y. Afik ³⁶ M. N. Agaras ¹³ J. Agarwala ^{72a,72b} A. Aggarwal ⁹⁹
 C. Agheorghiesei ^{27c} J. A. Aguilar-Saavedra ^{129f} A. Ahmad ³⁶ F. Ahmadov ^{38,b} W. S. Ahmed ¹⁰³ X. Ai ⁴⁸
 G. Aielli ^{75a,75b} I. Aizenberg ¹⁶⁷ M. Akbiyik ⁹⁹ T. P. A. Åkesson ⁹⁷ A. V. Akimov ³⁷ K. Al Khoury ⁴¹
 G. L. Alberghi ^{23b} J. Albert ¹⁶³ P. Albicocco ⁵³ M. J. Alconada Verzini ⁸⁹ S. Alderweireldt ⁵² M. Aleksa ³⁶
 I. N. Aleksandrov ³⁸ C. Alexa ^{27b} T. Alexopoulos ¹⁰ A. Alfonsi ¹¹³ F. Alfonsi ^{23b} M. Alhroob ¹¹⁹ B. Ali ¹³¹
 S. Ali ¹⁴⁷ M. Aliev ³⁷ G. Alimonti ^{70a} C. Allaire ³⁶ B. M. M. Allbrooke ¹⁴⁵ P. P. Alport ²⁰ A. Aloisio ^{71a,71b}
 F. Alonso ⁸⁹ C. Alpigiani ¹³⁷ E. Alunno Camelia ^{75a,75b} M. Alvarez Estevez ⁹⁸ M. G. Alvaggi ^{71a,71b}
 Y. Amaral Coutinho ^{81b} A. Ambler ¹⁰³ C. Amelung ³⁶ C. G. Ames ¹⁰⁸ D. Amidei ¹⁰⁵ S. P. Amor Dos Santos ^{129a}
 S. Amoroso ⁴⁸ K. R. Amos ¹⁶¹ C. S. Amrouche ⁵⁶ V. Ananiev ¹²⁴ C. Anastopoulos ¹³⁸ N. Andari ¹³⁴ T. Andeen ¹¹
 J. K. Anders ¹⁹ S. Y. Andrean ^{47a,47b} A. Andreazza ^{70a,70b} S. Angelidakis ⁹ A. Angerami ^{41,c} A. V. Anisenkov ³⁷
 A. Annovi ^{73a} C. Antel ⁵⁶ M. T. Anthony ¹³⁸ E. Antipov ¹²⁰ M. Antonelli ⁵³ D. J. A. Antrim ^{17a} F. Anulli ^{74a}
 M. Aoki ⁸² J. A. Aparisi Pozo ¹⁶¹ M. A. Aparo ¹⁴⁵ L. Aperio Bella ⁴⁸ C. Appelt ¹⁸ N. Aranzabal ³⁶
 V. Araujo Ferraz ^{81a} C. Arcangeletti ⁵³ A. T. H. Arce ⁵¹ E. Arena ⁹¹ J.-F. Arguin ¹⁰⁷ S. Argyropoulos ⁵⁴
 J.-H. Arling ⁴⁸ A. J. Armbruster ³⁶ O. Arnaez ¹⁵⁴ H. Arnold ¹¹³ Z. P. Arrubarrena Tame ¹⁰⁸ G. Artoni ^{74a,74b}
 H. Asada ¹¹⁰ K. Asai ¹¹⁷ S. Asai ¹⁵² N. A. Asbah ⁶¹ E. M. Asimakopoulou ¹⁵⁹ J. Assahsah ^{35d} K. Assamagan ²⁹
 R. Astalos ^{28a} R. J. Atkin ^{33a} M. Atkinson ¹⁶⁰ N. B. Atlay ¹⁸ H. Atmani ^{62b} P. A. Atmasiddha ¹⁰⁵ K. Augsten ¹³¹
 S. Auricchio ^{71a,71b} A. D. Auriol ²⁰ V. A. Aastrup ¹⁶⁹ G. Avner ¹⁴⁹ G. Avolio ³⁶ K. Axiotis ⁵⁶ M. K. Ayoub ^{14c}
 G. Azuelos ^{107,d} D. Babal ^{28a} H. Bachacou ¹³⁴ K. Bachas ^{151,e} A. Bachiu ³⁴ F. Backman ^{47a,47b} A. Badea ⁶¹
 P. Bagnaia ^{74a,74b} M. Bahmani ¹⁸ A. J. Bailey ¹⁶¹ V. R. Bailey ¹⁶⁰ J. T. Baines ¹³³ C. Bakalis ¹⁰ O. K. Baker ¹⁷⁰
 P. J. Bakker ¹¹³ E. Bakos ¹⁵ D. Bakshi Gupta ⁸ S. Balaji ¹⁴⁶ R. Balasubramanian ¹¹³ E. M. Baldwin ³⁷ P. Balek ¹³²
 E. Ballabene ^{70a,70b} F. Balli ¹³⁴ L. M. Baltes ^{63a} W. K. Balunas ³² J. Balz ⁹⁹ E. Banas ⁸⁵ M. Bandiermonte ¹²⁸
 A. Bandyopadhyay ²⁴ S. Bansal ²⁴ L. Barak ¹⁵⁰ E. L. Barberio ¹⁰⁴ D. Barberis ^{57b,57a} M. Barbero ¹⁰¹ G. Barbour ⁹⁵
 K. N. Barends ^{33a} T. Barillari ¹⁰⁹ M.-S. Barisits ³⁶ J. Barkeloo ¹²² T. Barklow ¹⁴² R. M. Barnett ^{17a} P. Baron ¹²¹
 D. A. Baron Moreno ¹⁰⁰ A. Baroncelli ^{62a} G. Barone ²⁹ A. J. Barr ¹²⁵ L. Barranco Navarro ^{47a,47b} F. Barreiro ⁹⁸
 J. Barreiro Guimarães da Costa ^{14a} U. Barron ¹⁵⁰ M. G. Barros Teixeira ^{129a} S. Barsov ³⁷ F. Bartels ^{63a}
 R. Bartoldus ¹⁴² A. E. Barton ⁹⁰ P. Bartos ^{28a} A. Basalaev ⁴⁸ A. Basan ⁹⁹ M. Baselga ⁴⁹ I. Bashta ^{76a,76b}
 A. Bassalat ^{66,f} M. J. Basso ¹⁵⁴ C. R. Basson ¹⁰⁰ R. L. Bates ⁵⁹ S. Batlamous ^{35e} J. R. Batley ³² B. Batool ¹⁴⁰
 M. Battaglia ¹³⁵ M. Bauce ^{74a,74b} P. Bauer ²⁴ A. Bayirli ^{21a} J. B. Beacham ⁵¹ T. Beau ¹²⁶ P. H. Beauchemin ¹⁵⁷
 F. Becherer ⁵⁴ P. Bechtle ²⁴ H. P. Beck ^{19,g} K. Becker ¹⁶⁵ C. Becot ⁴⁸ A. J. Beddall ^{21d} V. A. Bednyakov ³⁸
 C. P. Bee ¹⁴⁴ L. J. Beemster ¹⁵ T. A. Beermann ³⁶ M. Begalli ^{81b,81d} M. Begel ²⁹ A. Behera ¹⁴⁴ J. K. Behr ⁴⁸
 C. Beirao Da Cruz E Silva ³⁶ J. F. Beirer ²⁴ F. Beisiegel ²⁴ M. Belfkir ^{115b} G. Bella ¹⁵⁰ L. Bellagamba ^{23b}
 A. Bellerive ³⁴ P. Bellos ²⁰ K. Beloborodov ³⁷ K. Belotskiy ³⁷ N. L. Belyaev ³⁷ D. Benchekroun ^{35a}
 F. Bendebba ^{35a} Y. Benhammou ¹⁵⁰ D. P. Benjamin ²⁹ M. Benoit ²⁹ J. R. Bensinger ²⁶ S. Bentvelsen ¹¹³
 L. Beresford ³⁶ M. Beretta ⁵³ D. Berge ¹⁸ E. Bergeaas Kuutmann ¹⁵⁹ N. Berger ⁴ B. Bergmann ¹³¹ J. Beringer ^{17a}
 S. Berlendis ⁷ G. Bernardi ⁵ C. Bernius ¹⁴² F. U. Bernlochner ²⁴ T. Berry ⁹⁴ P. Berta ¹³² A. Berthold ⁵⁰
 I. A. Bertram ⁹⁰ O. Bessidskaia Bylund ¹⁶⁹ S. Bethke ¹⁰⁹ A. Betti ⁴⁴ A. J. Bevan ⁹³ M. Bhamjee ^{33c} S. Bhatta ¹⁴⁴
 D. S. Bhattacharya ¹⁶⁴ P. Bhattachari ²⁶ V. S. Bhopatkar ⁶ R. Bi ¹²⁸ R. Bi ^{29,h} R. M. Bianchi ¹²⁸ O. Biebel ¹⁰⁸
 R. Bielski ¹²² N. V. Biesuz ^{73a,73b} M. Biglietti ^{76a} T. R. V. Billoud ¹³¹ M. Bind ⁵⁵ A. Bingul ^{21b} C. Bini ^{74a,74b}
 S. Biondi ^{23b,23a} A. Biondini ⁹¹ C. J. Birch-sykes ¹⁰⁰ G. A. Bird ^{20,133} M. Birman ¹⁶⁷ T. Bisanz ³⁶ D. Biswas ^{168,i}
 A. Bitadze ¹⁰⁰ K. Bjørke ¹²⁴ I. Bloch ⁴⁸ C. Blocker ²⁶ A. Blue ⁵⁹ U. Blumenschein ⁹³ J. Blumenthal ⁹⁹
 G. J. Bobbink ¹¹³ V. S. Bobrovnikov ³⁷ M. Boehler ⁵⁴ D. Bogavac ³⁶ A. G. Bogdanchikov ³⁷ C. Bohm ^{47a}
 V. Boisvert ⁹⁴ P. Bokan ⁴⁸ T. Bold ^{84a} M. Bomben ⁵ M. Bona ⁹³ M. Boonekamp ¹³⁴ C. D. Booth ⁹⁴
 A. G. Borbely ⁵⁹ H. M. Borecka-Bielska ¹⁰⁷ L. S. Borgna ⁹⁵ G. Borissov ⁹⁰ D. Bortolotto ¹²⁵ D. Boscherini ^{23b}
 M. Bosman ¹³ J. D. Bossio Sola ³⁶ K. Bouaouda ^{35a} J. Boudreau ¹²⁸ E. V. Bouhova-Thacker ⁹⁰ D. Boumediene ⁴⁰

- R. Bouquet⁵ A. Boveia¹¹⁸ J. Boyd³⁶ D. Boye²⁹ I. R. Boyko³⁸ J. Bracinik²⁰ N. Brahimi^{62d,62c} G. Brandt¹⁶⁹ O. Brandt³² F. Braren⁴⁸ B. Brau¹⁰² J. E. Brau¹²² W. D. Breaden Madden⁵⁹ K. Brendlinger⁴⁸ R. Brener¹⁶⁷ L. Brenner³⁶ R. Brenner¹⁵⁹ S. Bressler¹⁶⁷ B. Brickwedde⁹⁹ D. Britton⁵⁹ D. Britzger¹⁰⁹ I. Brock²⁴ G. Brooijmans⁴¹ W. K. Brooks^{136f} E. Brost²⁹ P. A. Bruckman de Renstrom⁸⁵ B. Brüers⁴⁸ D. Bruncko^{28,j} A. Bruni^{23b} G. Bruni^{23b} M. Bruschi^{23b} N. Bruscino^{74a,74b} L. Bryngemark¹⁴² T. Buanes¹⁶ Q. Buat¹³⁷ P. Buchholz¹⁴⁰ A. G. Buckley⁵⁹ I. A. Budagov^{38,j} M. K. Bugge¹²⁴ O. Bulekov³⁷ B. A. Bullard⁶¹ S. Burdin⁹¹ C. D. Burgard⁴⁸ A. M. Burger⁴⁰ B. Burghgrave⁸ J. T. P. Burr³² C. D. Burton¹¹ J. C. Burzynski¹⁴¹ E. L. Busch⁴¹ V. Büscher⁹⁹ P. J. Bussey⁵⁹ J. M. Butler²⁵ C. M. Buttar⁵⁹ J. M. Butterworth⁹⁵ W. Buttlinger¹³³ C. J. Buxo Vazquez¹⁰⁶ A. R. Buzykaev³⁷ G. Cabras^{23b} S. Cabrera Urbán¹⁶¹ D. Caforio⁵⁸ H. Cai¹²⁸ Y. Cai^{14a,14d} V. M. M. Cairo³⁶ O. Cakir^{3a} N. Calace³⁶ P. Calafuria^{17a} G. Calderini¹²⁶ P. Calfayan⁶⁷ G. Callea⁵⁹ L. P. Caloba^{81b} D. Calvet⁴⁰ S. Calvet⁴⁰ T. P. Calvet¹⁰¹ M. Calvetti^{73a,73b} R. Camacho Toro¹²⁶ S. Camarda³⁶ D. Camarero Munoz⁹⁸ P. Camarri^{75a,75b} M. T. Camerlingo^{76a,76b} D. Cameron¹²⁴ C. Camincher¹⁶³ M. Campanelli⁹⁵ A. Camplani⁴² V. Canale^{71a,71b} A. Canesse¹⁰³ M. Cano Bret⁷⁹ J. Cantero¹⁶¹ Y. Cao¹⁶⁰ F. Capocasa²⁶ M. Capua^{43b,43a} A. Carbone^{70a,70b} R. Cardarelli^{75a} J. C. J. Cardenas⁸ F. Cardillo¹⁶¹ T. Carli³⁶ G. Carlino^{71a} B. T. Carlson^{128,k} E. M. Carlson^{163,155a} L. Carminati^{70a,70b} M. Carnesale^{74a,74b} S. Caron¹¹² E. Carquin^{136f} S. Carrá^{70a,70b} G. Carratta^{23b,23a} F. Carrio Argos^{33g} J. W. S. Carter¹⁵⁴ T. M. Carter⁵² M. P. Casado^{13,1} A. F. Casha¹⁵⁴ E. G. Castiglia¹⁷⁰ F. L. Castillo^{63a} L. Castillo Garcia¹³ V. Castillo Gimenez¹⁶¹ N. F. Castro^{129a,129e} A. Catinaccio³⁶ J. R. Catmore¹²⁴ V. Cavaliere²⁹ N. Cavalli^{23b,23a} V. Cavasinni^{73a,73b} E. Celebi^{21a} F. Celli¹²⁵ M. S. Centonze^{69a,69b} K. Cerny¹²¹ A. S. Cerqueira^{81a} A. Cerri¹⁴⁵ L. Cerrito^{75a,75b} F. Cerutti^{17a} A. Cervelli^{23b} S. A. Cetin^{21d} Z. Chadi^{35a} D. Chakraborty¹¹⁴ M. Chala^{129f} J. Chan¹⁶⁸ W. S. Chan¹¹³ W. Y. Chan¹⁵² J. D. Chapman³² B. Chargeishvili^{148b} D. G. Charlton²⁰ T. P. Charman⁹³ M. Chatterjee¹⁹ S. Chekanov⁶ S. V. Chekulaev^{155a} G. A. Chelkov^{38,m} A. Chen¹⁰⁵ B. Chen¹⁵⁰ B. Chen¹⁶³ C. Chen^{62a} H. Chen^{14c} H. Chen²⁹ J. Chen^{62c} J. Chen²⁶ S. Chen¹⁵² S. J. Chen^{14c} X. Chen^{62c} X. Chen^{14b,n} Y. Chen^{62a} C. L. Cheng¹⁶⁸ H. C. Cheng^{64a} A. Cheplakov³⁸ E. Cheremushkina⁴⁸ E. Cherepanova¹¹³ R. Cherkaoui El Moursli^{35e} E. Cheu⁷ K. Cheung⁶⁵ L. Chevalier¹³⁴ V. Chiarella⁵³ G. Chiarelli^{73a} G. Chiodini^{69a} A. S. Chisholm²⁰ A. Chitan^{27b} Y. H. Chiu¹⁶³ M. V. Chizhov³⁸ K. Choi¹¹ A. R. Chomont^{74a,74b} Y. Chou¹⁰² E. Y. S. Chow¹¹³ T. Chowdhury^{33g} L. D. Christopher^{33g} K. L. Chu^{64a} M. C. Chu^{64a} X. Chu^{14a,14d} J. Chudoba¹³⁰ J. J. Chwastowski⁸⁵ D. Cieri¹⁰⁹ K. M. Ciesla^{84a} V. Cindro⁹² A. Ciocio^{17a} F. Cirotto^{71a,71b} Z. H. Citron^{167,o} M. Citterio^{70a} D. A. Ciubotaru^{27b} B. M. Ciungu¹⁵⁴ A. Clark⁵⁶ P. J. Clark⁵² J. M. Clavijo Columbie⁴⁸ S. E. Clawson¹⁰⁰ C. Clement^{47a,47b} J. Clercx⁴⁸ L. Clissa^{23b,23a} Y. Coadou¹⁰¹ M. Cobal^{68a,68c} A. Coccaro^{57b} R. F. Coelho Barrue^{129a} R. Coelho Lopes De Sa¹⁰² S. Coelli^{70a} H. Cohen¹⁵⁰ A. E. C. Coimbra^{70a,70b} B. Cole⁴¹ J. Collot⁶⁰ P. Conde Muiño^{129a,129g} S. H. Connell^{33c} I. A. Connolly⁵⁹ E. I. Conroy¹²⁵ F. Conventi^{71a,p} H. G. Cooke²⁰ A. M. Cooper-Sarkar¹²⁵ F. Cormier¹⁶² L. D. Corpe³⁶ M. Corradi^{74a,74b} E. E. Corrigan⁹⁷ F. Corriveau^{103,q} A. Cortes-Gonzalez¹⁸ M. J. Costa¹⁶¹ F. Costanza⁴ D. Costanzo¹³⁸ B. M. Cote¹¹⁸ G. Cowan⁹⁴ J. W. Cowley³² K. Cranmer¹¹⁶ S. Crépé-Renaudin⁶⁰ F. Crescioli¹²⁶ M. Cristinziani¹⁴⁰ M. Cristoforetti^{77a,77b,r} V. Croft¹⁵⁷ G. Crosetti^{43b,43a} A. Cueto³⁶ T. Cuhadar Donszelmann¹⁵⁸ H. Cui^{14a,14d} Z. Cui⁷ A. R. Cukierman¹⁴² W. R. Cunningham⁵⁹ F. Curcio^{43b,43a} P. Czodrowski³⁶ M. M. Czurylo^{63b} M. J. Da Cunha Sargedas De Sousa^{62a} J. V. Da Fonseca Pinto^{81b} C. Da Via¹⁰⁰ W. Dabrowski^{84a} T. Dado⁴⁹ S. Dahbi^{33g} T. Dai¹⁰⁵ C. Dallapiccola¹⁰² M. Dam⁴² G. D'amen²⁹ V. D'Amico^{76a,76b} J. Damp⁹⁹ J. R. Dandoy¹²⁷ M. F. Daneri³⁰ M. Danninger¹⁴¹ V. Dao¹³⁶ G. Darbo^{57b} S. Darmora⁶ S. J. Das²⁹ A. Dattagupta¹²² S. D'Auria^{70a,70b} C. David^{155b} T. Davidek¹³² D. R. Davis⁵¹ B. Davis-Purcell³⁴ I. Dawson⁹³ K. De⁸ R. De Asmundis^{71a} M. De Beurs¹¹³ S. De Castro^{23b,23a} N. De Groot¹¹² P. de Jong¹¹³ H. De la Torre¹⁰⁶ A. De Maria^{14c} A. De Salvo^{74a} U. De Sanctis^{75a,75b} M. De Santis^{75a,75b} A. De Santo¹⁴⁵ J. B. De Vivie De Regie⁶⁰ D. V. Dedovich³⁸ J. Degens¹¹³ A. M. Deiana⁴⁴ F. Del Corso^{23b,23a} J. Del Peso⁹⁸ F. Del Rio^{63a} F. Deliot¹³⁴ C. M. Delitzsch⁴⁹ M. Della Pietra^{71a,71b} D. Della Volpe⁵⁶ A. Dell'Acqua³⁶ L. Dell'Asta^{70a,70b} M. Delmastro⁴ P. A. Delsart⁶⁰ S. Demers¹⁷⁰ M. Demichev³⁸ S. P. Denisov³⁷ L. D'Eramo¹¹⁴ D. Derendarz⁸⁵ F. Derue¹²⁶ P. Dervan⁹¹ K. Desch²⁴ K. Dette¹⁵⁴ C. Deutsch²⁴ P. O. Deviveiros³⁶ F. A. Di Bello^{74a,74b} A. Di Ciaccio^{75a,75b} L. Di Ciaccio⁴ A. Di Domenico^{74a,74b} C. Di Donato^{71a,71b} A. Di Girolamo³⁶ G. Di Gregorio^{73a,73b} A. Di Luca^{77a,77b} B. Di Micco^{76a,76b} R. Di Nardo^{76a,76b} C. Diaconu¹⁰¹ F. A. Dias¹¹³ T. Dias Do Vale¹⁴¹ M. A. Diaz^{136a,136b} F. G. Diaz Capriles²⁴ M. Didenko¹⁶¹ E. B. Diehl¹⁰⁵ L. Diehl⁵⁴ S. Díez Cornell⁴⁸ C. Diez Pardos¹⁴⁰ C. Dimitriadi^{24,159} A. Dimitrieva^{17a} W. Ding^{14b} J. Dingfelder²⁴ I-M. Dinu^{27b} S. J. Dittmeier^{63b} F. Dittus³⁶ F. Djama¹⁰¹ T. Djobava^{148b} J. I. Djupsland¹⁶ D. Dodsworth²⁶ C. Doglioni^{100,97} J. Dolejsi¹³² Z. Dolezal¹³² M. Donadelli^{81c} B. Dong^{62c} J. Donini⁴⁰ A. D'Onofrio^{14c} M. D'Onofrio⁹¹ J. Dopke¹³³ A. Doria^{71a} M. T. Dova⁸⁹ A. T. Doyle⁵⁹ M. A. Draguet¹²⁵ E. Drechsler¹⁴¹ E. Dreyer¹⁶⁷ I. Drivas-koulouris¹⁰ A. S. Drobac¹⁵⁷ D. Du^{62a} T. A. du Pree¹¹³ F. Dubinin³⁷ M. Dubovsky^{28a} E. Duchovni¹⁶⁷ G. Duckeck¹⁰⁸ O. A. Ducu³⁶ D. Duda¹⁰⁹ A. Dudarev³⁶ M. D'uffizi¹⁰⁰ L. Duflot⁶⁶ M. Dührssen³⁶ C. Dülsen¹⁶⁹ A. E. Dumitriu^{27b} M. Dunford^{63a} S. Dungs⁴⁹ K. Dunne^{47a,47b} A. Duperrin¹⁰¹ H. Duran Yildiz^{3a} M. Düren⁵⁸

- A. Durglishvili^{148b}, B. L. Dwyer¹¹⁴, G. I. Dyckes^{17a}, M. Dyndal^{84a}, S. Dysch¹⁰⁰, B. S. Dziedzic⁸⁵, Z. O. Earnshaw¹⁴⁵, B. Eckerova^{28a}, M. G. Eggleston⁵¹, E. Egidio Purcino De Souza^{81b}, L. F. Ehrke⁵⁶, G. Eigen¹⁶, K. Einsweiler^{17a}, T. Ekelof¹⁵⁹, P. A. Ekman⁹⁷, Y. El Ghazali^{35b}, H. El Jarrari^{35e,147}, A. El Moussaouy¹⁶, V. Ellajosyula¹⁵⁹, M. Ellert¹⁵⁹, F. Ellinghaus¹⁶⁹, A. A. Elliot⁹³, N. Ellis¹³, J. Elmsheuser²⁹, M. Elsing³⁶, D. Emeliyanov¹³³, A. Emerman⁴¹, Y. Enari¹⁵², I. Ene^{17a}, S. Epari¹³, J. Erdmann⁴⁹, A. Ereditato¹⁹, P. A. Erland⁸⁵, M. Errenst¹⁶⁹, M. Escalier⁶⁶, C. Escobar¹⁶¹, E. Etzion¹⁵⁰, G. Evans^{129a}, H. Evans⁶⁷, M. O. Evans¹⁴⁵, A. Ezhilov³⁷, S. Ezzarqouni^{35a}, F. Fabbri⁵⁹, L. Fabbri^{23b,23a}, G. Facini⁹⁵, V. Fadeyev¹³⁵, R. M. Fakhrutdinov³⁷, S. Falciano^{74a}, P. J. Falke²⁴, S. Falke³⁶, J. Faltova¹³², Y. Fan^{14a}, Y. Fang^{14a,14d}, G. Fanourakis⁴⁶, M. Fanti^{70a,70b}, M. Faraj^{68a,68b}, A. Farbin⁸, A. Farilla^{76a}, T. Farooque¹⁰⁶, S. M. Farrington⁵², F. Fassi^{35e}, D. Fassouliotis⁹, M. Faucci Giannelli^{75a,75b}, W. J. Fawcett³², L. Fayard⁶⁶, O. L. Fedin^{37,m}, G. Fedotov³⁷, M. Feickert¹⁶⁰, L. Feligioni¹⁰¹, A. Fell¹³⁸, D. E. Fellers¹²², C. Feng^{62b}, M. Feng^{14b}, M. J. Fenton¹⁵⁸, A. B. Fenyuk³⁷, L. Ferencz⁴⁸, S. W. Ferguson⁴⁵, J. A. Fernandez Pretel⁵⁴, J. Ferrando⁴⁸, A. Ferrari¹⁵⁹, P. Ferrari¹¹³, R. Ferrari^{72a}, D. Ferrere⁵⁶, C. Ferretti¹⁰⁵, F. Fiedler⁹⁹, A. Filipčič⁹², E. K. Filmer¹, F. Filthaut¹¹², M. C. N. Fiolhais^{129a,129c,s}, L. Fiorini¹⁶¹, F. Fischer¹⁴⁰, W. C. Fisher¹⁰⁶, T. Fitschen^{20,66}, I. Fleck¹⁴⁰, P. Fleischmann¹⁰⁵, T. Flick¹⁶⁹, L. Flores¹²⁷, M. Flores^{33d}, L. R. Flores Castillo^{64a}, F. M. Follega^{77a,77b}, N. Fomin¹⁶, J. H. Foo¹⁵⁴, B. C. Forland⁶⁷, A. Formica¹³⁴, A. C. Forti¹⁰⁰, E. Fortin¹⁰¹, A. W. Fortman⁶¹, M. Foti^{17a}, L. Fountas⁹, D. Fournier⁶⁶, H. Fox⁹⁰, P. Francavilla^{73a,73b}, S. Francescato⁶¹, M. Franchini^{23b,23a}, S. Franchino^{63a}, D. Francis³⁶, L. Franco¹¹², L. Franconi¹⁹, M. Franklin⁶¹, G. Frattari²⁶, A. C. Freegard⁹³, P. M. Freeman²⁰, W. S. Freund^{81b}, N. Fritzsche⁵⁰, A. Froch⁵⁴, D. Froidevaux³⁶, J. A. Frost¹²⁵, Y. Fu^{62a}, M. Fujimoto¹¹⁷, E. Fullana Torregrosa¹⁶¹, J. Fuster¹⁶¹, A. Gabrielli^{23b,23a}, A. Gabrielli³⁶, P. Gadow⁴⁸, G. Gagliardi^{57b,57a}, L. G. Gagnon^{17a}, G. E. Gallardo¹²⁵, E. J. Gallas¹²⁵, B. J. Gallop¹³³, R. Gamboa Goni⁹³, K. K. Gan¹¹⁸, S. Ganguly¹⁵², J. Gao^{62a}, Y. Gao⁵², F. M. Garay Walls^{136a,136b}, B. Garcia^{29,h}, C. García¹⁶¹, J. E. García Navarro¹⁶¹, J. A. García Pascual^{14a}, M. Garcia-Sciveres^{17a}, R. W. Gardner³⁹, D. Garg⁷⁹, R. B. Garg¹⁴², S. Gargiulo⁵⁴, C. A. Garner¹⁵⁴, V. Garonne²⁹, S. J. Gasiorowski¹³⁷, P. Gaspar^{81b}, G. Gaudio^{72a}, V. Gautam¹³, P. Gauzzi^{74a,74b}, I. L. Gavrilenco³⁷, A. Gavrilyuk³⁷, C. Gay¹⁶², G. Gaycken⁴⁸, E. N. Gazis¹⁰, A. A. Geanta^{27b}, C. M. Gee¹³⁵, J. Geisen⁹⁷, M. Geisen⁹⁹, C. Gemme^{57b}, M. H. Genest⁶⁰, S. Gentile^{74a,74b}, S. George⁹⁴, W. F. George²⁰, T. Geralis⁴⁶, L. O. Gerlach⁵⁵, P. Gessinger-Befurt³⁶, M. Ghasemi Bostanabad¹⁶³, M. Ghineimat¹⁴⁰, A. Ghosal¹⁴⁰, A. Ghosh⁷, B. Giacobbe^{23b}, S. Giagu^{74a,74b}, N. Giangiocomi¹⁵⁴, P. Giannetti^{73a}, A. Giannini^{62a}, S. M. Gibson⁹⁴, M. Gignac¹³⁵, D. T. Gil^{84b}, A. K. Gilbert^{84a}, B. J. Gilbert⁴¹, D. Gillberg³⁴, G. Gilles¹¹³, N. E. K. Gillwald⁴⁸, L. Ginabat¹²⁶, D. M. Gingrich^{2,d}, M. P. Giordani^{68a,68c}, P. F. Giraud¹³⁴, G. Giugliarelli^{68a,68c}, D. Giugni^{70a}, F. Giuli³⁶, I. Gkalias^{9,t}, L. K. Gladilin³⁷, C. Glasman⁹⁸, G. R. Gledhill¹²², M. Glisic¹²², I. Gnesi^{43b,u}, Y. Go^{29,h}, M. Goblirsch-Kolb²⁶, D. Godin¹⁰⁷, S. Goldfarb¹⁰⁴, T. Golling⁵⁶, M. G. D. Gololo^{33g}, D. Golubkov³⁷, J. P. Gombas¹⁰⁶, A. Gomes^{129a,129b}, G. Gomes Da Silva¹⁴⁰, A. J. Gomez Delegido¹⁶¹, R. Goncalves Gama⁵⁵, R. Gonçalo^{129a,129c}, G. Gonella¹²², L. Gonella¹²⁰, A. Gongadze³⁸, F. Gonnella²⁰, J. L. Gonski⁴¹, R. Y. González Andana⁵², S. González de la Hoz¹⁶¹, S. Gonzalez Fernandez¹³, R. Gonzalez Lopez⁹¹, C. Gonzalez Renteria^{17a}, R. Gonzalez Suarez¹⁵⁹, S. Gonzalez-Sevilla⁵⁶, G. R. Gonzalvo Rodriguez¹⁶¹, L. Goossens³⁶, N. A. Gorasia²⁰, P. A. Gorbounov³⁷, B. Gorini³⁶, E. Gorini^{69a,69b}, A. Gorišek⁹², A. T. Goshaw⁵¹, M. I. Gostkin³⁸, C. A. Gottardo¹¹², M. Gouighri^{35b}, V. Goumarre⁴⁸, A. Goussiou¹³⁷, N. Govender^{33c}, C. Goy⁴, I. Grabowska-Bold^{84a}, K. Graham³⁴, E. Gramstad¹²⁴, S. Grancagnolo¹⁸, M. Grandi¹⁴⁵, V. Gratchev^{37,j}, P. M. Gravila^{27f}, F. G. Gravili^{69a,69b}, H. M. Gray^{17a}, M. Greco^{69a,69b}, C. Grefe²⁴, I. M. Gregor⁴⁸, P. Grenier¹⁴², C. Grieco¹³, A. A. Grillo¹³⁵, K. Grimm^{31,v}, S. Grinstein^{13,w}, J.-F. Grivaz⁶⁶, E. Gross¹⁶⁷, J. Grosse-Knetter⁵⁵, C. Grud¹⁰⁵, A. Grummer¹¹¹, J. C. Grundy¹²⁵, L. Guan¹⁰⁵, W. Guan¹⁶⁸, C. Gubbels¹⁶², J. G. R. Guerrero Rojas¹⁶¹, G. Guerrieri^{68a,68c}, F. Guescini¹⁰⁹, R. Gugel⁹⁹, J. A. M. Guhit¹⁰⁵, A. Guida⁴⁸, T. Guillemin⁴, E. Guilloton^{165,133}, S. Guindon³⁶, F. Guo^{14a,14d}, J. Guo^{62c}, L. Guo⁶⁶, Y. Guo¹⁰⁵, R. Gupta⁴⁸, S. Gurbuz²⁴, S. S. Gurdasani⁵⁴, G. Gustavino³⁶, M. Guth⁵⁶, P. Gutierrez¹¹⁹, L. F. Gutierrez Zagazeta¹²⁷, C. Gutschow⁹⁵, C. Guyot¹³⁴, C. Gwenlan¹²⁵, C. B. Gwilliam⁹¹, E. S. Haaland¹²⁴, A. Haas¹¹⁶, M. Habedank⁴⁸, C. Haber^{17a}, H. K. Hadavand⁸, A. Hadef⁹⁹, S. Hadzic¹⁰⁹, M. Haleem¹⁶⁴, J. Haley¹²⁰, J. J. Hall¹³⁸, G. D. Hallewell¹⁰¹, L. Halser¹⁹, K. Hamano¹⁶³, H. Hamdaoui^{35e}, M. Hamer²⁴, G. N. Hamity⁵², J. Han^{62b}, K. Han^{62a}, L. Han^{14c}, L. Han^{62a}, S. Han^{17a}, Y. F. Han¹⁵⁴, K. Hanagaki⁸², M. Hance¹³⁵, D. A. Hangal^{41,c}, M. D. Hank³⁹, R. Hankache¹⁰⁰, J. B. Hansen⁴², J. D. Hansen⁴², P. H. Hansen⁴², K. Hara¹⁵⁶, D. Harada⁵⁶, T. Harenberg¹⁶⁹, S. Harkusha³⁷, Y. T. Harris¹²⁵, P. F. Harrison¹⁶⁵, N. M. Hartman¹⁴², N. M. Hartmann¹⁰⁸, Y. Hasegawa¹³⁹, A. Hasib⁵², S. Haug¹⁹, R. Hauser¹⁰⁶, M. Havranek¹³¹, C. M. Hawkes²⁰, R. J. Hawkings³⁶, S. Hayashida¹¹⁰, D. Hayden¹⁰⁶, C. Hayes¹⁰⁵, R. L. Hayes¹⁶², C. P. Hays¹²⁵, J. M. Hays⁹³, H. S. Hayward⁹¹, F. He^{62a}, Y. He¹⁵³, Y. He¹²⁶, M. P. Heath⁵², V. Hedberg⁹⁷, A. L. Heggelund¹²⁴, N. D. Hehir⁹³, C. Heidegger⁵⁴, K. K. Heidegger⁵⁴, W. D. Heidorn⁸⁰, J. Heilman³⁴, S. Heim⁴⁸, T. Heim^{17a}, J. G. Heinlein¹²⁷, J. J. Heinrich¹²², L. Heinrich³⁶, J. Hejbal¹³⁰, L. Helary⁴⁸, A. Held¹¹⁶, S. Hellesund¹²⁴, C. M. Helling¹⁶², S. Hellman^{47a,47b}, C. Helsens³⁶, R. C. W. Henderson⁹⁰, L. Henkelmann³², A. M. Henriques Correia³⁶, H. Herde¹⁴², Y. Hernández Jiménez¹⁴⁴, H. Herr⁹⁹, M. G. Herrmann¹⁰⁸, T. Herrmann⁵⁰, G. Herten⁵⁴

- R. Hertenberger¹⁰⁸ L. Hervas³⁶ N. P. Hessey^{155a} H. Hibi⁸³ E. Higón-Rodriguez¹⁶¹ S. J. Hillier²⁰
I. Hinchliffe^{17a} F. Hinterkeuser²⁴ M. Hirose¹²³ S. Hirose¹⁵⁶ D. Hirschbuehl¹⁶⁹ T. G. Hitchings¹⁰⁰ B. Hiti⁹²
J. Hobbs¹⁴⁴ R. Hobincu^{27e} N. Hod¹⁶⁷ M. C. Hodgkinson¹³⁸ B. H. Hodgkinson³² A. Hoecker³⁶ J. Hofer⁴⁸
D. Hohn⁵⁴ T. Holm²⁴ M. Holzbock¹⁰⁹ L. B. A. H. Hommels³² B. P. Honan¹⁰⁰ J. Hong^{62c} T. M. Hong¹²⁸
Y. Hong⁵⁵ J. C. Honig⁵⁴ A. Hönle¹⁰⁹ B. H. Hooberman¹⁶⁰ W. H. Hopkins⁶ Y. Horii¹¹⁰ S. Hou¹⁴⁷
A. S. Howard⁹² J. Howarth⁵⁹ J. Hoya⁸⁹ M. Hrabovsky¹²¹ A. Hrynevich³⁷ T. Hrynyova⁴ P. J. Hsu⁶⁵
S.-C. Hsu¹³⁷ Q. Hu^{41,c} Y. F. Hu^{14a,14d,x} D. P. Huang⁹⁵ S. Huang^{64b} X. Huang^{14c} Y. Huang^{62a} Y. Huang^{14a}
Z. Huang¹⁰⁰ Z. Hubacek¹³¹ M. Huebner²⁴ F. Huegging²⁴ T. B. Huffman¹²⁵ M. Huhtinen³⁶ S. K. Huiberts¹⁶
R. Hulskens¹⁰³ N. Huseynov^{12,m} J. Huston¹⁰⁶ J. Huth⁶¹ R. Hyneman¹⁴² S. Hyrych^{28a} G. Iacobucci⁵⁶
G. Iakovidis²⁹ I. Ibragimov¹⁴⁰ L. Iconomidou-Fayard⁶⁶ P. Iengo^{71a,71b} R. Iguchi¹⁵² T. Iizawa⁵⁶ Y. Ikegami⁸²
A. Ilg¹⁹ N. Ilic¹⁵⁴ H. Imam^{35a} T. Ingebretsen Carlson^{47a,47b} G. Introzzi^{72a,72b} M. Iodice^{76a} V. Ippolito^{74a,74b}
M. Ishino¹⁵² W. Islam¹⁶⁸ C. Issever^{18,48} S. Istin^{21a,y} H. Ito¹⁶⁶ J. M. Iturbe Ponce^{64a} R. Iuppa^{77a,77b}
A. Ivina¹⁶⁷ J. M. Izen⁴⁵ V. Izzo^{71a} P. Jacka^{130,131} P. Jackson¹ R. M. Jacobs⁴⁸ B. P. Jaeger¹⁴¹
C. S. Jagfeld¹⁰⁸ G. Jäkel¹⁶⁹ K. Jakobs⁵⁴ T. Jakoubek¹⁶⁷ J. Jamieson⁵⁹ K. W. Janas^{84a} G. Jarlskog⁹⁷
A. E. Jaspan⁹¹ T. Javůrek³⁶ M. Javurkova¹⁰² F. Jeanneau¹³⁴ L. Jeanty¹²² J. Jejelava^{148a,z} P. Jenni^{54,aa}
C. E. Jessiman³⁴ S. Jézéquel⁴ J. Jia¹⁴⁴ X. Jia⁶¹ X. Jia^{14a,14d} Z. Jia^{14c} Y. Jiang^{62a} S. Jiggins⁵²
J. Jimenez Pena¹⁰⁹ S. Jin^{14c} A. Jinaru^{27b} O. Jinnouchi¹⁵³ H. Jivan^{33g} P. Johansson¹³⁸ K. A. Johns⁷
C. A. Johnson⁶⁷ D. M. Jones³² E. Jones¹⁶⁵ P. Jones³² R. W. L. Jones⁹⁰ T. J. Jones⁹¹ J. Jovicevic¹⁵ X. Ju^{17a}
J. J. Junggeburth³⁶ A. Juste Rozas^{13,w} S. Kabana^{136e} A. Kaczmarska⁸⁵ M. Kado^{74a,74b} H. Kagan¹¹⁸
M. Kagan¹⁴² A. Kahn⁴¹ A. Kahn¹²⁷ C. Kahra⁹⁹ T. Kaji¹⁶⁶ E. Kajomovitz¹⁴⁹ N. Kakati¹⁶⁷ C. W. Kalderon²⁹
A. Kamenshchikov¹⁵⁴ N. J. Kang¹³⁵ Y. Kano¹¹⁰ D. Kar^{33g} K. Karava¹²⁵ M. J. Kareem^{155b} E. Karentzos⁵⁴
I. Karkanas¹⁵¹ S. N. Karpov³⁸ Z. M. Karpova³⁸ V. Kartvelishvili⁹⁰ A. N. Karyukhin³⁷ E. Kasimi¹⁵¹
C. Kato^{62d} J. Katzy⁴⁸ S. Kaur³⁴ K. Kawade¹³⁹ K. Kawagoe⁸⁸ T. Kawaguchi¹¹⁰ T. Kawamoto¹³⁴
G. Kawamura⁵⁵ E. F. Kay¹⁶³ F. I. Kaya¹⁵⁷ S. Kazakos¹³ V. F. Kazanin³⁷ Y. Ke¹⁴⁴ J. M. Keaveney^{33a}
R. Keeler¹⁶³ G. V. Kehris⁶¹ J. S. Keller³⁴ A. S. Kelly⁹⁵ D. Kelsey¹⁴⁵ J. J. Kempster²⁰ J. Kendrick²⁰
K. E. Kennedy⁴¹ O. Kepka¹³⁰ B. P. Kerridge¹⁶⁵ S. Kersten¹⁶⁹ B. P. Kerševan⁹² L. Keszeghova^{28a}
S. Katabchi Haghighat¹⁵⁴ M. Khandoga¹²⁶ A. Khanov¹²⁰ A. G. Kharlamov³⁷ T. Kharlamova³⁷ E. E. Khoda¹³⁷
T. J. Khoo¹⁸ G. Khoriauli¹⁶⁴ J. Khubua^{148b} Y. A. R. Khwaira⁶⁶ M. Kiehn³⁶ A. Kilgallon¹²² D. W. Kim^{47a,47b}
E. Kim¹⁵³ Y. K. Kim³⁹ N. Kimura⁹⁵ A. Kirchhoff⁵⁵ D. Kirchmeier⁵⁰ C. Kirfel²⁴ J. Kirk¹³³
A. E. Kiryunin¹⁰⁹ T. Kishimoto¹⁵² D. P. Kisliuk¹⁵⁴ C. Kitsaki¹⁰ O. Kivernyk²⁴ M. Klassen^{63a} C. Klein³⁴
L. Klein¹⁶⁴ M. H. Klein¹⁰⁵ M. Klein⁹¹ U. Klein⁹¹ P. Klimek³⁶ A. Klimentov²⁹ F. Klimpel¹⁰⁹ T. Klingl²⁴
T. Klioutchnikova³⁶ F. F. Klitzner¹⁰⁸ P. Kluit¹¹³ S. Kluth¹⁰⁹ E. Knerner⁷⁸ T. M. Knight¹⁵⁴ A. Knue⁵⁴
D. Kobayashi⁸⁸ R. Kobayashi⁸⁶ M. Kocian¹⁴² T. Kodama¹⁵² P. Kodyš¹³² D. M. Koeck¹⁴⁵ P. T. Koenig²⁴
T. Koffas³⁴ N. M. Köhler³⁶ M. Kolb¹³⁴ I. Koletsou⁴ T. Komarek¹²¹ K. Köneke⁵⁴ A. X. Y. Kong¹
T. Kono¹¹⁷ N. Konstantinidis⁹⁵ B. Konya⁹⁷ R. Kopeliansky⁶⁷ S. Koperny^{84a} K. Korcyl⁸⁵ K. Kordas¹⁵¹
G. Koren¹⁵⁰ A. Korn⁹⁵ S. Korn⁵⁵ I. Korolkov¹³ N. Korotkova³⁷ B. Kortman¹¹³ O. Kortner¹⁰⁹ S. Kortner¹⁰⁹
W. H. Kostecka¹¹⁴ V. V. Kostyukhin¹⁴⁰ A. Kotsokechagia⁶⁶ A. Kotwal⁵¹ A. Koulouris³⁶
A. Kourkoumelis-Charalampidi^{72a,72b} C. Kourkoumelis⁹ E. Kourlitis⁶ O. Kovanda¹⁴⁵ R. Kowalewski¹⁶³
W. Kozanecki¹³⁴ A. S. Kozhin³⁷ V. A. Kramarenko³⁷ G. Kramberger⁹² P. Kramer⁹⁹ M. W. Krasny¹²⁶
A. Krasznahorkay³⁶ J. A. Kremer⁹⁹ T. Kresse⁵⁰ J. Kretzschmar⁹¹ K. Kreul¹⁸ P. Krieger¹⁵⁴ F. Krieter¹⁰⁸
S. Krishnamurthy¹⁰² A. Krishnan^{63b} M. Krivos¹³² K. Krizka^{17a} K. Kroeninger⁴⁹ H. Kroha¹⁰⁹ J. Kroll¹³⁰
J. Kroll¹²⁷ K. S. Krowpmann¹⁰⁶ U. Kruchonak³⁸ H. Krüger²⁴ N. Krumnack⁸⁰ M. C. Kruse⁵¹ J. A. Krzysiak⁸⁵
A. Kubota¹⁵³ O. Kuchinskaia³⁷ S. Kuday^{3a} D. Kuechler⁴⁸ J. T. Kuechler⁴⁸ S. Kuehn³⁶ T. Kuhl⁴⁸
V. Kukhtin³⁸ Y. Kulchitsky^{37,m} S. Kuleshov^{136d,136b} M. Kumar^{33g} N. Kumari¹⁰¹ M. Kuna⁶⁰ A. Kupco¹³⁰
T. Kupfer⁴⁹ A. Kupich³⁷ O. Kuprash⁵⁴ H. Kurashige⁸³ L. L. Kurchaninov^{155a} Y. A. Kurochkin³⁷ A. Kurova³⁷
E. S. Kuwertz³⁶ M. Kuze¹⁵³ A. K. Kvam¹⁰² J. Kvita¹²¹ T. Kwan¹⁰³ K. W. Kwok^{64a} C. Lacasta¹⁶¹
F. Lacava^{74a,74b} H. Lacker¹⁸ D. Lacour¹²⁶ N. N. Lad⁹⁵ E. Ladygin³⁸ B. Laforge¹²⁶ T. Lagouri^{136e} S. Lai⁵⁵
I. K. Lakomiec^{84a} N. Lalloue⁶⁰ J. E. Lambert¹¹⁹ S. Lammers⁶⁷ W. Lampl⁷ C. Lampoudis¹⁵¹
A. N. Lancaster¹¹⁴ E. Lançon²⁹ U. Landgraf⁵⁴ M. P. J. Landon⁹³ V. S. Lang⁵⁴ R. J. Langenberg¹⁰²
A. J. Lankford¹⁵⁸ F. Lanni²⁹ K. Lantzsch²⁴ A. Lanza^{72a} A. Lapertosa^{57b,57a} J. F. Laporte¹³⁴ T. Lari^{70a}
F. Lasagni Manghi^{23b} M. Lassnig³⁶ V. Latonova¹³⁰ T. S. Lau^{64a} A. Laudrain⁹⁹ A. Laurier³⁴ S. D. Lawlor⁹⁴
Z. Lawrence¹⁰⁰ M. Lazzaroni^{70a,70b} B. Le¹⁰⁰ B. Leban⁹² A. Lebedev⁸⁰ M. LeBlanc³⁶ T. LeCompte⁶
F. Ledroit-Guillon⁶⁰ A. C. A. Lee⁹⁵ G. R. Lee¹⁶ L. Lee⁶¹ S. C. Lee¹⁴⁷ S. Lee^{47a,47b} L. L. Leeuw^{33c}
H. P. Lefebvre⁹⁴ M. Lefebvre¹⁶³ C. Leggett^{17a} K. Lehmann¹⁴¹ G. Lehmann Miotto³⁶ W. A. Leight¹⁰²
A. Leisos^{151,ab} M. A. L. Leite^{81c} C. E. Leitgeb⁴⁸ R. Leitner¹³² K. J. C. Leney⁴⁴ T. Lenz²⁴ S. Leone^{73a}
C. Leonidopoulos⁵² A. Leopold¹⁴³ C. Leroy¹⁰⁷ R. Les¹⁰⁶ C. G. Lester³² M. Levchenko³⁷ J. Levêque⁴
D. Levin¹⁰⁵ L. J. Levinson¹⁶⁷ D. J. Lewis²⁰ B. Li^{14b} B. Li^{62b} C. Li^{62a} C.-Q. Li^{62c,62d} H. Li^{62a} H. Li^{62b}
H. Li^{14c} H. Li^{62b} J. Li^{62c} K. Li¹³⁷ L. Li^{62c} M. Li^{14a,14d} Q. Y. Li^{62a} S. Li^{62d,62c,ac} T. Li^{62b} X. Li¹⁰³

- Z. Li^{62b} Z. Li¹²⁵ Z. Li¹⁰³ Z. Li⁹¹ Z. Liang^{14a} M. Liberatore⁴⁸ B. Liberti^{75a} K. Lie^{64c} J. Lieber Marin^{81b}
 K. Lin¹⁰⁶ R. A. Linck⁶⁷ R. E. Lindley⁷ J. H. Lindon² A. Linss⁴⁸ E. Lipeles¹²⁷ A. Lipniacka¹⁶
 T. M. Liss^{160,ad} A. Lister¹⁶² J. D. Little⁴ B. Liu^{14a} X. Liu¹⁴¹ D. Liu^{62d,62c} J. B. Liu^{62a} J. K. K. Liu³²
 K. Liu^{62d,62c} M. Liu^{62a} M. Y. Liu^{62a}
- P. Liu^{14a} Q. Liu^{62d,137,62c} X. Liu^{62a} Y. Liu⁴⁸ Y. Liu^{14c,14d} Y. L. Liu¹⁰⁵ Y. W. Liu^{62a} M. Livan^{72a,72b}
 J. Llorente Merino¹⁴¹ S. L. Lloyd⁹³ E. M. Lobodzinska⁴⁸ P. Loch⁷ S. Loffredo^{75a,75b} T. Lohse¹⁸
 K. Lohwasser¹³⁸ M. Lokajicek¹³⁰ J. D. Long¹⁶⁰ I. Longarini^{74a,74b} L. Longo^{69a,69b} R. Longo¹⁶⁰
- I. Lopez Paz³⁶ A. Lopez Solis⁴⁸ J. Lorenz¹⁰⁸ N. Lorenzo Martinez⁴ A. M. Lory¹⁰⁸ A. Losle⁵⁴ X. Lou^{47a,47b}
 X. Lou^{14a,14d} A. Lounis⁶⁶ J. Love⁶ P. A. Love⁹⁰ J. J. Lozano Bahilo¹⁶¹ G. Lu^{14a,14d} M. Lu⁷⁹ S. Lu¹²⁷
 Y. J. Lu⁶⁵ H. J. Lubatti¹³⁷ C. Luci^{74a,74b} F. L. Lucio Alves^{14c} A. Lucotte⁶⁰ F. Luehring⁶⁷ I. Luise¹⁴⁴
- O. Lukianchuk⁶⁶ O. Lundberg¹⁴³ B. Lund-Jensen¹⁴³ N. A. Luongo¹²² M. S. Lutz¹⁵⁰ D. Lynn²⁹ H. Lyons⁹¹
 R. Lysak¹³⁰ E. Lytken⁹⁷ F. Lyu^{14a} V. Lyubushkin³⁸ T. Lyubushkina³⁸ H. Ma²⁹ L. L. Ma^{62b} Y. Ma⁹⁵
 D. M. Mac Donell¹⁶³ G. Maccarrone⁵³ J. C. MacDonald¹³⁸ R. Madar⁴⁰ W. F. Mader⁵⁰ J. Maeda⁸³
- T. Maeno²⁹ M. Maerker⁵⁰ V. Magerl⁵⁴ J. Magro^{68a,68c} H. Maguire¹³⁸ D. J. Mahon⁴¹ C. Maidantchik^{81b}
 A. Maio^{129a,129b,129d} K. Maj^{84a} O. Majersky^{28a} S. Majewski¹²² N. Makovec⁶⁶ V. Maksimovic¹⁵
 B. Malaescu¹²⁶ Pa. Malecki⁸⁵ V. P. Maleev³⁷ F. Malek⁶⁰ D. Malito^{43b,43a} U. Mallik⁷⁹ C. Malone³²
 S. Maltezos¹⁰ S. Malyukov³⁸ J. Mamuzic¹³ G. Mancini⁵³ G. Manco^{72a,72b} J. P. Mandalia⁹³ I. Mandić⁹²
 L. Manhaes de Andrade Filho^{81a} I. M. Maniatis¹⁵¹ M. Manisha¹³⁴ J. Manjarres Ramos⁵⁰ D. C. Mankad¹⁶⁷
- K. H. Mankinen⁹⁷ A. Mann¹⁰⁸ A. Manousos⁷⁸ B. Mansoulie¹³⁴ S. Manzoni³⁶ A. Marantis¹⁵¹ G. Marchiori⁵
 M. Marcisovsky¹³⁰ L. Marcoccia^{75a,75b} C. Marcon⁹⁷ M. Marinescu²⁰ M. Marjanovic¹¹⁹ Z. Marshall^{17a}
- S. Marti-Garcia¹⁶¹ T. A. Martin¹⁶⁵ V. J. Martin⁵² B. Martin dit Latour¹⁶ L. Martinelli^{74a,74b} M. Martinez^{13,w}
 P. Martinez Agullo¹⁶¹ V. I. Martinez Outschoorn¹⁰² P. Martinez Suarez¹³ S. Martin-Haugh¹³³ V. S. Martoiu^{27b}
 A. C. Martyniuk⁹⁵ A. Marzin³⁶ S. R. Maschek¹⁰⁹ L. Masetti⁹⁹ T. Mashimo¹⁵² J. Masik¹⁰⁰
 A. L. Maslennikov³⁷ L. Massa^{23b} P. Massarotti^{71a,71b} P. Mastrandrea^{73a,73b} A. Mastroberardino^{43b,43a}
- T. Masubuchi¹⁵² T. Mathisen¹⁵⁹ A. Matic¹⁰⁸ N. Matsuzawa¹⁵² J. Maurer^{27b} B. Maček⁹² D. A. Maximov³⁷
 R. Mazini¹⁴⁷ I. Maznas¹⁵¹ M. Mazza¹⁰⁶ S. M. Mazza¹³⁵ C. Mc Ginn^{29,h} J. P. Mc Gowen¹⁰³ S. P. Mc Kee¹⁰⁵
 T. G. McCarthy¹⁰⁹ W. P. McCormack^{17a} E. F. McDonald¹⁰⁴ A. E. McDougall¹¹³ J. A. McFayden¹⁴⁵
- G. Mchedlidze^{148b} R. P. Mckenzie^{33g} T. C. Mclachlan⁴⁸ D. J. McLaughlin⁹⁵ K. D. McLean¹⁶³ S. J. McMahon¹³³
 P. C. McNamara¹⁰⁴ R. A. McPherson^{163,q} J. E. Mdhluli^{33g} S. Meehan³⁶ T. Megy⁴⁰ S. Mehlhase¹⁰⁸
 A. Mehta⁹¹ B. Meirose⁴⁵ D. Melini¹⁴⁹ B. R. Mellado Garcia^{33g} A. H. Melo⁵⁵ F. Meloni⁴⁸
 E. D. Mendes Gouveia^{129a} A. M. Mendes Jacques Da Costa²⁰ H. Y. Meng¹⁵⁴ L. Meng⁹⁰ S. Menke¹⁰⁹
 M. Mentink³⁶ E. Meoni^{43b,43a} C. Merlassino¹²⁵ L. Merola^{71a,71b} C. Meroni^{70a} G. Merz¹⁰⁵ O. Meshkov³⁷
 J. K. R. Meshreki¹⁴⁰ J. Metcalfe⁶ A. S. Mete⁶ C. Meyer⁶⁷ J.-P. Meyer¹³⁴ M. Michetti¹⁸ R. P. Middleton¹³³
 L. Mijović⁵² G. Mikenberg¹⁶⁷ M. Mikestikova¹³⁰ M. Mikuž⁹² H. Mildner¹³⁸ A. Milic¹⁵⁴ C. D. Milke⁴⁴
 D. W. Miller³⁹ L. S. Miller³⁴ A. Milov¹⁶⁷ D. A. Milstead^{47a,47b} T. Min^{14c} A. A. Minaenko³⁷ I. A. Minashvili^{148b}
 L. Mince⁵⁹ A. I. Mincer¹¹⁶ B. Mindur^{84a} M. Mineev³⁸ Y. Minegishi¹⁵² Y. Mino⁸⁶ L. M. Mir¹³
 M. Miralles Lopez¹⁶¹ M. Mironova¹²⁵ T. Mitani¹⁶⁶ A. Mitra¹⁶⁵ V. A. Mitsou¹⁶¹ O. Miura¹⁵⁴ P. S. Miyagawa⁹³
 Y. Miyazaki⁸⁸ A. Mizukami⁸² J. U. Mjörnmark⁹⁷ T. Mkrtchyan^{63a} M. Mlynarikova¹¹⁴ T. Moa^{47a,47b}
 S. Mobius⁵⁵ K. Mochizuki¹⁰⁷ P. Moder⁴⁸ P. Mogg¹⁰⁸ A. F. Mohammed^{14a,14d} S. Mohapatra⁴¹
 G. Mokgatitswane^{33g} B. Mondal¹⁴⁰ S. Mondal¹³¹ K. Mönig⁴⁸ E. Monnier¹⁰¹ L. Monsonis Romero,
 J. Montejoe Berlingen³⁶ M. Montella¹¹⁸ F. Monticelli⁸⁹ N. Morange⁶⁶ A. L. Moreira De Carvalho^{129a}
 M. Moreno Llácer¹⁶¹ C. Moreno Martinez¹³ P. Morettini^{57b} S. Morgenstern¹⁶⁵ M. Morii⁶¹ M. Morinaga¹⁵²
 V. Morisbak¹²⁴ A. K. Morley³⁶ F. Morodei^{74a,74b} L. Morvaj³⁶ P. Moschovakos³⁶ B. Moser³⁶ M. Mosidze,
 T. Moskalets⁵⁴ P. Moskvitina¹¹² J. Moss^{31,ae} E. J. W. Moyse¹⁰² S. Muanza¹⁰¹ J. Mueller¹²⁸
 D. Muenstermann⁹⁰ R. Müller¹⁹ G. A. Mullier⁹⁷ J. J. Mullin¹²⁷ D. P. Mungo^{70a,70b} J. L. Munoz Martinez¹³
 D. Munoz Perez¹⁶¹ F. J. Munoz Sanchez¹⁰⁰ M. Murin¹⁰⁰ W. J. Murray^{165,133} A. Murrone^{70a,70b} J. M. Muse¹¹⁹
 M. Muškinja^{17a} C. Mwewa²⁹ A. G. Myagkov^{37,m} A. J. Myers⁸ A. A. Myers¹²⁸ G. Myers⁶⁷ M. Myska¹³¹
 B. P. Nachman^{17a} O. Nackenhorst⁴⁹ A. Nag⁵⁰ K. Nagai¹²⁵ K. Nagano⁸² J. L. Nagle^{29,h} E. Nagy¹⁰¹
 A. M. Nairz³⁶ Y. Nakahama⁸² K. Nakamura⁸² H. Nanjo¹²³ R. Narayan⁴⁴ E. A. Narayanan¹¹¹ I. Naryshkin³⁷
 M. Naseri³⁴ C. Nass²⁴ G. Navarro^{22a} J. Navarro-Gonzalez¹⁶¹ R. Nayak¹⁵⁰ P. Y. Nechaeva³⁷ F. Nechansky⁴⁸
 T. J. Neep²⁰ A. Negri^{72a,72b} M. Negrini^{23b} C. Nellist¹¹² C. Nelson¹⁰³ K. Nelson¹⁰⁵ S. Nemecek¹³⁰
 M. Nessi^{36,af} M. S. Neubauer¹⁶⁰ F. Neuhaus⁹⁹ J. Neundorf⁴⁸ R. Newhouse¹⁶² P. R. Newman²⁰ C. W. Ng¹²⁸
 Y. S. Ng¹⁸ Y. W. Y. Ng¹⁵⁸ B. Ngair^{35e} H. D. N. Nguyen¹⁰⁷ R. B. Nickerson¹²⁵ R. Nicolaidou¹³⁴ J. Nielsen¹³⁵
 M. Niemeyer⁵⁵ N. Nikiforou³⁶ V. Nikolaenko^{37,m} I. Nikolic-Audit¹²⁶ K. Nikolopoulos²⁰ P. Nilsson²⁹
 H. R. Nindhito⁵⁶ A. Nisati^{74a} N. Nishu² R. Nisius¹⁰⁹ J.-E. Nitschke⁵⁰ E. K. Nkadimeng^{33g}
 S. J. Noacco Rosende⁸⁹ T. Nobe¹⁵² D. L. Noel³² Y. Noguchi⁸⁶ T. Nommensen¹⁴⁶ M. A. Nomura,
 M. B. Norfolk¹³⁸ R. R. B. Norisam⁹⁵ B. J. Norman³⁴ J. Novak⁹² T. Novak⁴⁸ O. Novgorodova⁵⁰
 L. Novotny¹³¹ R. Novotny¹¹¹ L. Nozka¹²¹ K. Ntekas¹⁵⁸ E. Nurse⁹⁵ F. G. Oakham^{34,d} J. Ocariz¹²⁶ A. Ochi⁸³

- I. Ochoa ^{129a}, S. Oda ⁸⁸, S. Oerderk ¹⁵⁹, A. Ogrodnik ^{84a}, A. Oh ¹⁰⁰, C. C. Ohm ¹⁴³, H. Oide ¹⁵³, R. Oishi ¹⁵², M. L. Ojeda ⁴⁸, Y. Okazaki ⁸⁶, M. W. O'Keefe ⁹¹, Y. Okumura ¹⁵², A. Olariu ^{27b}, L. F. Oleiro Seabra ^{129a}, S. A. Olivares Pino ^{136e}, D. Oliveira Damazio ²⁹, D. Oliveira Goncalves ^{81a}, J. L. Oliver ¹⁵⁸, M. J. R. Olsson ¹⁵⁸, A. Olszewski ⁸⁵, J. Olszowska ^{85,j}, Ö.O. Öncel ⁵⁴, D. C. O'Neil ¹⁴¹, A. P. O'Neill ¹⁹, A. Onofre ^{129a,129e}, P. U. E. Onyisi ¹¹, M. J. Oreglia ³⁹, G. E. Orellana ⁸⁹, D. Orestano ^{76a,76b}, N. Orlando ¹³, R. S. Orr ¹⁵⁴, V. O'Shea ⁵⁹, R. Ospanov ^{62a}, G. Otero y Garzon ³⁰, H. Otono ⁸⁸, P. S. Ott ^{63a}, G. J. Ottino ^{17a}, M. Ouchrif ^{35d}, J. Ouellette ^{29,h}, F. Ould-Saada ¹²⁴, M. Owen ⁵⁹, R. E. Owen ¹³³, K. Y. Oyulmaz ^{21a}, V. E. Ozcan ^{21a}, N. Ozturk ⁸, S. Ozturk ^{21d}, J. Pacalt ¹²¹, H. A. Pacey ³², K. Pachal ⁵¹, A. Pacheco Pages ¹³, C. Padilla Aranda ¹³, G. Padovano ^{74a,74b}, S. Pagan Griso ^{17a}, G. Palacino ⁶⁷, A. Palazzo ^{69a,69b}, S. Palazzo ⁵², S. Palestini ³⁶, M. Palka ^{84b}, J. Pan ¹⁷⁰, T. Pan ^{64a}, D. K. Panchal ¹¹, C. E. Pandini ¹¹³, J. G. Panduro Vazquez ⁹⁴, P. Pani ⁴⁸, G. Panizzo ^{68a,68c}, L. Paolozzi ⁵⁶, C. Papadatos ¹⁰⁷, S. Parajuli ⁴⁴, A. Paramonov ⁶, C. Paraskevopoulos ¹⁰, D. Paredes Hernandez ^{64b}, T. H. Park ¹⁵⁴, M. A. Parker ³², F. Parodi ^{57b,57a}, E. W. Parrish ¹¹⁴, V. A. Parrish ⁵², J. A. Parsons ⁴¹, U. Parzefall ⁵⁴, B. Pascual Dias ¹⁰⁷, L. Pascual Dominguez ¹⁵⁰, V. R. Pascuzzi ^{17a}, F. Pasquali ¹¹³, E. Pasqualucci ^{74a}, S. Passaggio ^{57b}, F. Pastore ⁹⁴, P. Paswan ^{47a,47b}, J. R. Pater ¹⁰⁰, J. Patton ⁹¹, T. Pauly ³⁶, J. Pearkes ¹⁴², M. Pedersen ¹²⁴, R. Pedro ^{129a}, S. V. Peleganchuk ³⁷, O. Penc ¹³⁰, C. Peng ^{64b}, H. Peng ^{62a}, M. Penzin ³⁷, B. S. Peralva ^{81a,81d}, A. P. Pereira Peixoto ⁶⁰, L. Pereira Sanchez ^{147a,47b}, D. V. Perepelitsa ^{29,h}, E. Perez Codina ^{155a}, M. Perganti ¹⁰, L. Perini ^{70a,70b,j}, H. Pernegger ³⁶, S. Perrella ³⁶, A. Perrevoort ¹¹², O. Perrin ⁴⁰, K. Peters ⁴⁸, R. F. Y. Peters ¹⁰⁰, B. A. Petersen ³⁶, T. C. Petersen ⁴², E. Petit ¹⁰¹, V. Petousis ¹³¹, C. Petridou ¹⁵¹, A. Petrukhin ¹⁴⁰, M. Pettee ^{17a}, N. E. Pettersson ³⁶, A. Petukhov ³⁷, K. Petukhova ¹³², A. Peyaud ¹³⁴, R. Pezoa ^{136f}, L. Pezzotti ³⁶, G. Pezzullo ¹⁷⁰, T. Pham ¹⁰⁴, P. W. Phillips ¹³³, M. W. Phipps ¹⁶⁰, G. Piacquadio ¹⁴⁴, E. Pianori ^{17a}, F. Piazza ^{70a,70b}, R. Piegaia ³⁰, D. Pietreanu ^{27b}, A. D. Pilkington ¹⁰⁰, M. Pinamonti ^{68a,68c}, J. L. Pinfold ², B. C. Pinheiro Pereira ^{129a}, C. Pitman Donaldson ⁹⁵, D. A. Pizzi ³⁴, L. Pizzimento ^{75a,75b}, A. Pizzini ¹¹³, M.-A. Pleier ²⁹, V. Plesanovs ⁵⁴, V. Pleskot ¹³², E. Plotnikova ³⁸, G. Poddar ⁴, R. Poettgen ⁹⁷, R. Poggi ⁵⁶, L. Poggiali ¹²⁶, I. Pogrebnyak ¹⁰⁶, D. Pohl ²⁴, I. Pokharel ⁵⁵, S. Polacek ¹³², G. Polesello ^{72a}, A. Poley ^{141,155a}, R. Polifka ¹³¹, A. Polini ^{23b}, C. S. Pollard ¹²⁵, Z. B. Pollock ¹¹⁸, V. Polychronakos ²⁹, D. Ponomarenko ³⁷, L. Pontecorvo ³⁶, S. Popa ^{27a}, G. A. Popeneciu ^{27d}, D. M. Portillo Quintero ^{155a}, S. Pospisil ¹³¹, P. Postolache ^{27c}, K. Potamianos ¹²⁵, I. N. Potrap ³⁸, C. J. Potter ³², H. Potti ¹, T. Poulsen ⁴⁸, J. Poveda ¹⁶¹, G. Pownall ⁴⁸, M. E. Pozo Astigarraga ³⁶, A. Prades Ibanez ¹⁶¹, M. M. Prapa ⁴⁶, D. Price ¹⁰⁰, M. Primavera ^{69a}, M. A. Principe Martin ⁹⁸, M. L. Proffitt ¹³⁷, N. Proklova ³⁷, K. Prokofiev ^{64c}, G. Proto ^{75a,75b}, S. Protopopescu ²⁹, J. Proudfoot ⁶, M. Przybycien ^{84a}, J. E. Puddefoot ¹³⁸, D. Pudzha ³⁷, P. Puzo ⁶⁶, D. Pyatiizbyantseva ³⁷, J. Qian ¹⁰⁵, Y. Qin ¹⁰⁰, T. Qiu ⁹³, A. Quadt ⁵⁵, M. Queitsch-Maitland ²⁴, G. Rabanal Bolanos ⁶¹, D. Rafanoharanra ⁵⁴, F. Ragusa ^{70a,70b}, J. L. Rainbolt ³⁹, J. A. Raine ⁵⁶, S. Rajagopalan ²⁹, E. Ramakoti ³⁷, K. Ran ^{14a,14d}, V. Raskina ¹²⁶, D. F. Rassloff ^{63a}, S. Rave ⁹⁹, B. Ravina ⁵⁹, I. Ravinovich ¹⁶⁷, M. Raymond ³⁶, A. L. Read ¹²⁴, N. P. Readioff ¹³⁸, D. M. Rebuzzi ^{72a,72b}, G. Redlinger ²⁹, K. Reeves ⁴⁵, J. A. Reidelsturz ¹⁶⁹, D. Reikher ¹⁵⁰, A. Reiss ⁹⁹, A. Rej ¹⁴⁰, C. Rembsler ³⁶, A. Renardi ⁴⁸, M. Renda ^{27b}, M. B. Rendel ¹⁰⁹, A. G. Rennie ⁵⁹, S. Resconi ^{70a}, M. Ressegotti ^{57b,57a}, E. D. Ressegue ^{17a}, S. Rettie ⁹⁵, B. Reynolds ¹¹⁸, E. Reynolds ^{17a}, M. Rezaei Estabragh ¹⁶⁹, O. L. Rezanova ³⁷, P. Reznicek ¹³², E. Ricci ^{77a,77b}, R. Richter ¹⁰⁹, S. Richter ^{47a,47b}, E. Richter-Was ^{84b}, M. Ridel ¹²⁶, P. Rieck ¹¹⁶, P. Riedler ³⁶, M. Rijssenbeek ¹⁴⁴, A. Rimoldi ^{72a,72b}, M. Rimoldi ⁴⁸, L. Rinaldi ^{23b,23a}, T. T. Rinn ²⁹, M. P. Rinnagel ¹⁰⁸, G. Ripellino ¹⁴³, I. Riu ¹³, P. Rivadeneira ⁴⁸, J. C. Rivera Vergara ¹⁶³, F. Rizatdinova ¹²⁰, E. Rizvi ⁹³, C. Rizzi ⁵⁶, B. A. Roberts ¹⁶⁵, B. R. Roberts ^{17a}, S. H. Robertson ^{103,q}, M. Robin ⁴⁸, D. Robinson ³², C. M. Robles Gajardo ^{136f}, M. Robles Manzano ⁹⁹, A. Robson ⁵⁹, A. Rocchi ^{75a,75b}, C. Roda ^{73a,73b}, S. Rodriguez Bosca ^{63a}, Y. Rodriguez Garcia ^{22a}, A. Rodriguez Rodriguez ⁵⁴, A. M. Rodríguez Vera ^{155b}, S. Roe ³⁶, J. T. Roemer ¹⁵⁸, A. R. Roepe-Gier ¹¹⁹, J. Roggel ¹⁶⁹, O. Röhne ¹²⁴, R. A. Rojas ¹⁶³, B. Roland ⁵⁴, C. P. A. Roland ⁶⁷, J. Roloff ²⁹, A. Romaniouk ³⁷, E. Romano ^{72a,72b}, M. Romano ^{23b}, A. C. Romero Hernandez ¹⁶⁰, N. Rompotis ⁹¹, L. Roos ¹²⁶, S. Rosati ^{74a}, B. J. Rosser ³⁹, E. Rossi ⁴, E. Rossi ^{71a,71b}, L. P. Rossi ^{57b}, L. Rossini ⁴⁸, R. Rosten ¹¹⁸, M. Rotaru ^{27b}, B. Rottler ⁵⁴, D. Rousseau ⁶⁶, D. Roussel ³², G. Rovelli ^{72a,72b}, A. Roy ¹⁶⁰, A. Rozanov ¹⁰¹, Y. Rozen ¹⁴⁹, X. Ruan ^{33g}, A. Rubio Jimenez ¹⁶¹, A. J. Ruby ⁹¹, T. A. Ruggeri ¹, F. Rühr ⁵⁴, A. Ruiz-Martinez ¹⁶¹, A. Rummler ³⁶, Z. Rurikova ⁵⁴, N. A. Rusakovitch ³⁸, H. L. Russell ¹⁶³, J. P. Rutherford ⁷, E. M. Rüttinger ¹³⁸, K. Rybacki ⁹⁰, M. Rybar ¹³², E. B. Rye ¹²⁴, A. Ryzhov ³⁷, J. A. Sabater Iglesias ⁵⁶, P. Sabatini ¹⁶¹, L. Sabetta ^{74a,74b}, H.-F.-W. Sadrozinski ¹³⁵, F. Safai Tehrani ^{74a}, B. Safarzadeh Samani ¹⁴⁵, M. Safdari ¹⁴², S. Saha ¹⁰³, M. Sahinsoy ¹⁰⁹, M. Saimpert ¹³⁴, M. Saito ¹⁵², T. Saito ¹⁵², D. Salamani ³⁶, G. Salamanna ^{76a,76b}, A. Salnikov ¹⁴², J. Salt ¹⁶¹, A. Salvador Salas ¹³, D. Salvatore ^{43b,43a}, F. Salvatore ¹⁴⁵, A. Salzburger ³⁶, D. Sammel ⁵⁴, D. Sampsonidis ¹⁵¹, D. Sampsonidou ^{62d,62c}, J. Sánchez ¹⁶¹, A. Sanchez Pineda ⁴, V. Sanchez Sebastian ¹⁶¹, H. Sandaker ¹²⁴, C. O. Sander ⁴⁸, J. A. Sandesara ¹⁰², M. Sandhoff ¹⁶⁹, C. Sandoval ^{22b}, D. P. C. Sankey ¹³³, A. Sansoni ⁵³, L. Santi ^{74a,74b}, C. Santoni ⁴⁰, H. Santos ^{129a,129b}, S. N. Santpur ^{17a}, A. Santra ¹⁶⁷, K. A. Saoucha ¹³⁸, J. G. Saraiva ^{129a,129d}, J. Sardain ¹⁰¹, O. Sasaki ⁸², K. Sato ¹⁵⁶, C. Sauer ^{63b}, F. Sauerburger ⁵⁴, E. Sauvan ⁴, P. Savard ^{154,d}, R. Sawada ¹⁵², C. Sawyer ¹³³, L. Sawyer ⁹⁶, I. Sayago Galvan ¹⁶¹, C. Sbarra ^{23b}, A. Sbrizzi ^{23b,23a}, T. Scanlon ⁹⁵, J. Schaarschmidt ¹³⁷, P. Schacht ¹⁰⁹, D. Schaefer ³⁹, U. Schäfer ⁹⁹, A. C. Schaffer ⁶⁶, D. Schaile ¹⁰⁸

- R. D. Schamberger¹⁴⁴ E. Schanet¹⁰⁸ C. Scharf¹⁸ V. A. Schegelsky³⁷ D. Scheirich¹³² F. Schenck¹⁸
M. Schernau¹⁵⁸ C. Scheulen⁵⁵ C. Schiavi^{57b,57a} Z. M. Schillaci²⁶ E. J. Schioppa^{69a,69b} M. Schioppa^{43b,43a}
B. Schlag⁹⁹ K. E. Schleicher⁵⁴ S. Schlenker³⁶ K. Schmieden⁹⁹ C. Schmitt⁹⁹ S. Schmitt⁴⁸ L. Schoeffel¹³⁴
A. Schoening^{63b} P. G. Scholer⁵⁴ E. Schopf¹²⁵ M. Schott⁹⁹ J. Schovancova³⁶ S. Schramm⁵⁶ F. Schroeder¹⁶⁹
H-C. Schultz-Coulon^{63a} M. Schumacher⁵⁴ B. A. Schumm¹³⁵ Ph. Schune¹³⁴ A. Schwartzman¹⁴²
T. A. Schwarz¹⁰⁵ Ph. Schwemling¹³⁴ R. Schwienhorst¹⁰⁶ A. Sciaudra¹³⁵ G. Sciolla²⁶ F. Scuri^{73a} F. Scutti¹⁰⁴
C. D. Sebastiani⁹¹ K. Sedlaczek⁴⁹ P. Seema¹⁸ S. C. Seidel¹¹¹ A. Seiden¹³⁵ B. D. Seidlitz⁴¹ T. Seiss³⁹
C. Seitz⁴⁸ J. M. Seixas^{81b} G. Sekhniaidze^{71a} S. J. Sekula⁴⁴ L. Selen⁴ N. Semprini-Cesari^{23b,23a} S. Sen⁵¹
D. Sengupta⁵⁶ V. Senthilkumar¹⁶¹ L. Serin⁶⁶ L. Serkin^{68a,68b} M. Sessa^{76a,76b} H. Severini¹¹⁹ S. Sevova¹⁴²
F. Sforza^{57b,57a} A. Sfyrla⁵⁶ E. Shabalina⁵⁵ R. Shaheen¹⁴³ J. D. Shahinian¹²⁷ N. W. Shaikh^{47a,47b}
D. Shaked Renous¹⁶⁷ L. Y. Shan^{14a} M. Shapiro^{17a} A. Sharma³⁶ A. S. Sharma¹⁶² P. Sharma⁷⁹ S. Sharma⁴⁸
P. B. Shatalov³⁷ K. Shaw¹⁴⁵ S. M. Shaw¹⁰⁰ Q. Shen^{62c} P. Sherwood⁹⁵ L. Shi⁹⁵ C. O. Shimmin¹⁷⁰
Y. Shimogama¹⁶⁶ J. D. Shinner⁹⁴ I. P. J. Shipsey¹²⁵ S. Shirabe⁶⁰ M. Shiyakova³⁸ J. Shlomi¹⁶⁷
M. J. Shochet³⁹ J. Shojaii¹⁰⁴ D. R. Shope¹⁴³ S. Shrestha¹¹⁸ E. M. Shrif^{33g} M. J. Shroff¹⁶³ P. Sicho¹³⁰
A. M. Sickles¹⁶⁰ E. Sideras Haddad^{33g} O. Sidiropoulou³⁶ A. Sidoti^{23b} F. Siegert⁵⁰ Dj. Sijacki¹⁵ R. Sikora^{84a}
F. Sili⁸⁹ J. M. Silva²⁰ M. V. Silva Oliveira³⁶ S. B. Silverstein^{47a} S. Simion⁶⁶ R. Simoniello³⁶ E. L. Simpson⁵⁹
N. D. Simpson⁹⁷ S. Simsek^{21d} S. Sindhu⁵⁵ P. Sinervo¹⁵⁴ V. Sinetckii³⁷ S. Singh¹⁴¹ S. Singh¹⁵⁴ S. Sinha⁴⁸
S. Sinha^{33g} M. Sioli^{23b,23a} I. Siral¹²² S. Yu. Sivoklokov^{37j} J. Sjölin^{47a,47b} A. Skaf⁵⁵ E. Skorda⁹⁷
P. Skubic¹¹⁹ M. Slawinska⁸⁵ V. Smakhtin¹⁶⁷ B. H. Smart¹³³ J. Smiesko¹³² S. Yu. Smirnov³⁷ Y. Smirnov³⁷
L. N. Smirnova^{37,m} O. Smirnova⁹⁷ E. A. Smith³⁹ H. A. Smith¹²⁵ J. L. Smith⁹¹ R. Smith¹⁴² M. Smizanska⁹⁰
K. Smolek¹³¹ A. Smykiewicz⁸⁵ A. A. Snesarev³⁷ H. L. Snoek¹¹³ S. Snyder²⁹ R. Sobie^{163,q} A. Soffer¹⁵⁰
C. A. Solans Sanchez³⁶ E. Yu. Soldatov³⁷ U. Soldevila¹⁶¹ A. A. Solodkov³⁷ S. Solomon⁵⁴ A. Soloshenko³⁸
K. Solovieva⁵⁴ O. V. Solovyanov³⁷ V. Solov'yev³⁷ P. Sommer³⁶ A. Sonay¹³ W. Y. Song^{155b} A. Sopczak¹³¹
A. L. Sopio⁹⁵ F. Sopkova^{28b} V. Sothilingam^{63a} S. Sottocornola^{72a,72b} R. Soualah^{115c} Z. Soumaimi^{35e} D. South⁴⁸
S. Spagnolo^{69a,69b} M. Spalla¹⁰⁹ F. Spanò⁹⁴ D. Sperlich⁵⁴ G. Spigo³⁶ M. Spina¹⁴⁵ S. Spinali⁹⁰
D. P. Spiteri⁵⁹ M. Spousta¹³² E. J. Staats³⁴ A. Stabile^{70a,70b} R. Stamen^{63a} M. Stamenkovic¹¹³ A. Stampekkis²⁰
M. Standke²⁴ E. Stanecka⁸⁵ B. Stanislaus^{17a} M. M. Stanitzki⁴⁸ M. Stankaityte¹²⁵ B. Stapf⁴⁸
E. A. Starchenko³⁷ G. H. Stark¹³⁵ J. Stark¹⁰¹ D. M. Starko^{155b} P. Staroba¹³⁰ P. Starovoitov^{63a} S. Stärz¹⁰³
R. Staszewski⁸⁵ G. Stavropoulos⁴⁶ J. Steentoft¹⁵⁹ P. Steinberg²⁹ A. L. Steinhebel¹²² B. Stelzer^{141,155a}
H. J. Stelzer¹²⁸ O. Stelzer-Chilton^{155a} H. Stenzel⁵⁸ T. J. Stevenson¹⁴⁵ G. A. Stewart³⁶ M. C. Stockton³⁶
G. Stoicea^{27b} M. Stolarski^{129a} S. Stonjek¹⁰⁹ A. Straessner⁵⁰ J. Strandberg¹⁴³ S. Strandberg^{47a,47b}
M. Strauss¹¹⁹ T. Strebler¹⁰¹ P. Strizenec^{28b} R. Ströhmer¹⁶⁴ D. M. Strom¹²² L. R. Strom⁴⁸ R. Stroynowski⁴⁴
A. Strubig^{47a,47b} S. A. Stucci²⁹ B. Stugu¹⁶ J. Stupak¹¹⁹ N. A. Styles⁴⁸ D. Su¹⁴² S. Su^{62a} W. Su^{62d,137,62c}
X. Su^{62a,66} K. Sugizaki¹⁵² V. V. Sulin³⁷ M. J. Sullivan⁹¹ D. M. S. Sultan^{77a,77b} L. Sultanaliyeva³⁷
S. Sultansoy^{3b} T. Sumida⁸⁶ S. Sun¹⁰⁵ S. Sun¹⁶⁸ O. Sunneborn Gudnadottir¹⁵⁹ M. R. Sutton¹⁴⁵ M. Svatos¹³⁰
M. Swiatlowski^{155a} T. Swirski¹⁶⁴ I. Sykora^{28a} M. Sykora¹³² T. Sykora¹³² D. Ta⁹⁹ K. Tackmann^{48,ag}
A. Taffard¹⁵⁸ R. Tafifour^{155a} J. S. Tafoya Vargas⁶⁶ R. H. M. Taibah¹²⁶ R. Takashima⁸⁷ K. Takeda⁸³
E. P. Takeva⁵² Y. Takubo⁸² M. Talby¹⁰¹ A. A. Talyshев³⁷ K. C. Tam^{64b} N. M. Tamir¹⁵⁰ A. Tanaka¹⁵²
J. Tanaka¹⁵² R. Tanaka⁶⁶ M. Tanasini^{57b,57a} J. Tang^{62c} Z. Tao¹⁶² S. Tapia Araya⁸⁰ S. Tapprogge⁹⁹
A. Tarek Abouelfadl Mohamed¹⁰⁶ S. Tarem¹⁴⁹ K. Tariq^{62b} G. Tarna^{27b} G. F. Tartarelli^{70a} P. Tas¹³²
M. Tasevsky¹³⁰ E. Tassi^{43b,43a} A. C. Tate¹⁶⁰ G. Tateno¹⁵² Y. Tayalati^{35e} G. N. Taylor¹⁰⁴ W. Taylor^{155b}
H. Teagle⁹¹ A. S. Tee¹⁶⁸ R. Teixeira De Lima¹⁴² P. Teixeira-Dias⁹⁴ J. J. Teoh¹⁵⁴ K. Terashi¹⁵² J. Terron⁹⁸
S. Terzo¹³ M. Testa⁵³ R. J. Teuscher^{154,q} N. Themistokleous⁵² T. Theveneaux-Pelzer¹⁸ O. Thielmann¹⁶⁹
D. W. Thomas⁹⁴ J. P. Thomas²⁰ E. A. Thompson⁴⁸ P. D. Thompson²⁰ E. Thomson¹²⁷ E. J. Thorpe⁹³ Y. Tian⁵⁵
V. Tikhomirov^{37,m} Yu. A. Tikhonov³⁷ S. Timoshenko³⁷ E. X. L. Ting¹ P. Tipton¹⁷⁰ S. Tisserant¹⁰¹
S. H. Tlou^{33g} A. Tnourji⁴⁰ K. Todome^{23b,23a} S. Todorova-Nova¹³² S. Todt⁵⁰ M. Togawa⁸² J. Tojo⁸⁸
S. Tokár^{28a} K. Tokushuku⁸² R. Tombs³² M. Tomoto^{82,110} L. Tompkins¹⁴² P. Tornambe¹⁰² E. Torrence¹²²
H. Torres⁵⁰ E. Torró Pastor¹⁶¹ M. Toscani³⁰ C. Tosciri³⁹ D. R. Tovey¹³⁸ A. Traeet¹⁶ I. S. Trandafir^{27b}
T. Trefzger¹⁶⁴ A. Tricoli²⁹ I. M. Trigger^{155a} S. Trincaz-Duvoid¹²⁶ D. A. Trischuk¹⁶² B. Trocmé⁶⁰
A. Trofymov⁶⁶ C. Troncon^{70a} L. Truong^{33c} M. Trzebinski⁸⁵ A. Trzupek⁸⁵ F. Tsai¹⁴⁴ M. Tsai¹⁰⁵
A. Tsiamis¹⁵¹ P. V. Tsiareshka³⁷ S. Tsigaridas^{155a} A. Tsirigotis^{151,ab} V. Tsiskaridze¹⁴⁴ E. G. Tskhadadze^{148a}
M. Tsopoulou¹⁵¹ Y. Tsujikawa⁸⁶ I. I. Tsukerman³⁷ V. Tsulaia^{17a} S. Tsuno⁸² O. Tsur¹⁴⁹ D. Tsybychev¹⁴⁴
Y. Tu^{64b} A. Tudorache^{27b} V. Tudorache^{27b} A. N. Tuna³⁶ S. Turchikhin³⁸ I. Turk Cakir^{3a} R. Turra^{70a}
T. Turtuvshin³⁸ P. M. Tuts⁴¹ S. Tzamarias¹⁵¹ P. Tzanis¹⁰ E. Tzovara⁹⁹ K. Uchida¹⁵² F. Ukegawa¹⁵⁶
P. A. Ulloa Poblete^{136c} G. Unal³⁶ M. Unal¹¹ A. Undrus²⁹ G. Unel¹⁵⁸ K. Uno¹⁵² J. Urban^{28b} P. Urquijo¹⁰⁴
G. Usai⁸ R. Ushioda¹⁵³ M. Usman¹⁰⁷ Z. Uysal^{21b} V. Vacek¹³¹ B. Vachon¹⁰³ K. O. H. Vadla¹²⁴
T. Vafeiadis³⁶ C. Valderanis¹⁰⁸ E. Valdes Santurio^{47a,47b} M. Valente^{155a} S. Valentinetto^{23b,23a} A. Valero¹⁶¹
A. Vallier¹⁰¹ J. A. Valls Ferrer¹⁶¹ T. R. Van Daalen¹³⁷ P. Van Gemmeren⁶ S. Van Stroud⁹⁵ I. Van Vulpen¹¹³

- M. Vanadia ^{75a, 75b} W. Vandelli ³⁶ M. Vandenbroucke ¹³⁴ E. R. Vandewall ¹²⁰ D. Vannicola ¹⁵⁰ L. Vannoli ^{57b, 57a}
 R. Vari ^{74a} E. W. Varnes ⁷ C. Varni ^{17a} T. Varol ¹⁴⁷ D. Varouchas ⁶⁶ L. Varriale ¹⁶¹ K. E. Varvell ¹⁴⁶
 M. E. Vasile ^{27b} L. Vaslin ⁴⁰ G. A. Vasquez ¹⁶³ F. Vazeille ⁴⁰ T. Vazquez Schroeder ³⁶ J. Veatch ³¹ V. Vecchio ¹⁰⁰
 M. J. Veen ¹¹³ I. Veliscek ¹²⁵ L. M. Veloce ¹⁵⁴ F. Veloso ^{129a, 129c} S. Veneziano ^{74a} A. Ventura ^{69a, 69b}
 A. Verbytskyi ¹⁰⁹ M. Verducci ^{73a, 73b} C. Vergis ²⁴ M. Verissimo De Araujo ^{81b} W. Verkerke ¹¹³ J. C. Vermeulen ¹¹³
 C. Vernieri ¹⁴² P. J. Verschuuren ⁹⁴ M. Vessella ¹⁰² M. L. Vesterbacka ¹¹⁶ M. C. Vetterli ^{141,d} A. Vgenopoulos ¹⁵¹
 N. Viaux Maira ^{136f} T. Vickey ¹³⁸ O. E. Vickey Boeriu ¹³⁸ G. H. A. Viehhauser ¹²⁵ L. Vigani ^{63b} M. Villa ^{23b, 23a}
 M. Villaplana Perez ¹⁶¹ E. M. Villhauer ⁵² E. Vilucchi ⁵³ M. G. Vincter ³⁴ G. S. Virdee ²⁰ A. Vishwakarma ⁵²
 C. Vittori ^{23b, 23a} I. Vivarelli ¹⁴⁵ V. Vladimirov ¹⁶⁵ E. Voevodina ¹⁰⁹ F. Vogel ¹⁰⁸ P. Vokac ¹³¹ J. Von Ahnen ⁴⁸
 E. Von Toerne ²⁴ B. Vormwald ³⁶ V. Vorobel ¹³² K. Vorobev ³⁷ M. Vos ¹⁶¹ J. H. Vossebeld ⁹¹ M. Vozak ¹¹³
 L. Vozdecky ⁹³ N. Vranjes ¹⁵ M. Vranjes Milosavljevic ¹⁵ M. Vreeswijk ¹¹³ R. Vuillermet ³⁶ O. Vujinovic ⁹⁹
 I. Vukotic ³⁹ S. Wada ¹⁵⁶ C. Wagner ¹⁰² W. Wagner ¹⁶⁹ S. Wahdan ¹⁶⁹ H. Wahlberg ⁸⁹ R. Wakasa ¹⁵⁶
 M. Wakida ¹¹⁰ V. M. Walbrecht ¹⁰⁹ J. Walder ¹³³ R. Walker ¹⁰⁸ W. Walkowiak ¹⁴⁰ A. M. Wang ⁶¹ A. Z. Wang ¹⁶⁸
 C. Wang ^{62a} C. Wang ^{62c} H. Wang ^{17a} J. Wang ^{64a} P. Wang ⁴⁴ R.-J. Wang ⁹⁹ R. Wang ⁶¹ R. Wang ⁶
 S. M. Wang ¹⁴⁷ S. Wang ^{62b} T. Wang ^{62a} W. T. Wang ⁷⁹ W. X. Wang ^{62a} X. Wang ^{14c} X. Wang ¹⁶⁰ X. Wang ^{62c}
 Y. Wang ^{62d} Y. Wang ^{14c} Z. Wang ¹⁰⁵ Z. Wang ^{62d, 51, 62c} Z. Wang ¹⁰⁵ A. Warburton ¹⁰³ R. J. Ward ²⁰
 N. Warrack ⁵⁹ A. T. Watson ²⁰ M. F. Watson ²⁰ G. Watts ¹³⁷ B. M. Waugh ⁹⁵ A. F. Webb ¹¹ C. Weber ²⁹
 M. S. Weber ¹⁹ S. A. Weber ³⁴ S. M. Weber ^{63a} C. Wei ^{62a} Y. Wei ¹²⁵ A. R. Weidberg ¹²⁵ J. Weingarten ⁴⁹
 M. Weirich ⁹⁹ C. Weiser ⁵⁴ C. J. Wells ⁴⁸ T. Wenaus ²⁹ B. Wendland ⁴⁹ T. Wengler ³⁶ N. S. Wenke ¹⁰⁹
 N. Wermes ²⁴ M. Wessels ^{63a} K. Whalen ¹²² A. M. Wharton ⁹⁰ A. S. White ⁶¹ A. White ⁸ M. J. White ¹
 D. Whiteson ¹⁵⁸ L. Wickremasinghe ¹²³ W. Wiedenmann ¹⁶⁸ C. Wiel ⁵⁰ M. Wieters ¹³³ N. Wieseotte ⁹⁹
 C. Wiglesworth ⁴² L. A. M. Wiik-Fuchs ⁵⁴ D. J. Wilbern ¹¹⁹ H. G. Wilkens ³⁶ D. M. Williams ⁴¹ H. H. Williams ¹²⁷
 S. Williams ³² S. Willocq ¹⁰² P. J. Windischhofer ¹²⁵ F. Winklmeier ¹²² B. T. Winter ⁵⁴ M. Wittgen ¹⁴²
 M. Wobisch ⁹⁶ A. Wolf ⁹⁹ R. Wölker ¹²⁵ J. Wollrath ¹⁵⁸ M. W. Wolter ⁸⁵ H. Wolters ^{129a, 129c} V. W. S. Wong ¹⁶²
 A. F. Wongel ⁴⁸ S. D. Worm ⁴⁸ B. K. Wosiek ⁸⁵ K. W. Woźniak ⁸⁵ K. Wright ⁵⁹ J. Wu ^{14a, 14d} M. Wu ^{64a}
 S. L. Wu ¹⁶⁸ X. Wu ⁵⁶ Y. Wu ^{62a} Z. Wu ^{134, 62a} J. Wuerzinger ¹²⁵ T. R. Wyatt ¹⁰⁰ B. M. Wynne ⁵² S. Xella ⁴²
 L. Xia ^{14c} M. Xia ^{14b} J. Xiang ^{64c} X. Xiao ¹⁰⁵ M. Xie ^{62a} X. Xie ^{14a} J. Xiong ¹⁴⁵ D. Xu ^{14a} H. Xu ^{62a}
 H. Xu ^{62a} L. Xu ^{62a} R. Xu ¹²⁷ T. Xu ¹⁰⁵ W. Xu ¹⁰⁵ Y. Xu ^{14b} Z. Xu ^{62b} Z. Xu ¹⁴² B. Yabsley ¹⁴⁶
 S. Yacoob ^{33a} N. Yamaguchi ⁸⁸ Y. Yamaguchi ¹⁵³ H. Yamauchi ¹⁵⁶ T. Yamazaki ^{17a} Y. Yamazaki ⁸³ J. Yan ^{62c}
 S. Yan ¹²⁵ Z. Yan ²⁵ H. J. Yang ^{62c, 62d} H. T. Yang ^{17a} S. Yang ^{62a} T. Yang ^{64c} X. Yang ^{62a} X. Yang ^{14a}
 Y. Yang ⁴⁴ Z. Yang ^{62a, 105} W.-M. Yao ^{17a} Y. C. Yap ⁴⁸ H. Ye ^{14c} J. Ye ⁴⁴ S. Ye ²⁹ X. Ye ^{62a} I. Yeletskikh ³⁸
 M. R. Yexley ⁹⁰ P. Yin ⁴¹ K. Yorita ¹⁶⁶ C. J. S. Young ⁵⁴ C. Young ¹⁴² M. Yuan ¹⁰⁵ R. Yuan ^{62b, ah} L. Yue ⁹⁵
 X. Yue ^{63a} M. Zaazoua ^{35e} B. Zabinski ⁸⁵ E. Zaid ⁵² T. Zakareishvili ^{148b} N. Zakharchuk ³⁴ S. Zambito ⁵⁶
 J. Zang ¹⁵² D. Zanzi ⁵⁴ O. Zaplatilek ¹³¹ S. V. Zeißner ⁴⁹ C. Zeitnitz ¹⁶⁹ J. C. Zeng ¹⁶⁰ D. T. Zenger, Jr. ²⁶
 O. Zenin ³⁷ T. Ženiš ^{28a} S. Zenz ⁹³ S. Zerradi ^{35a} D. Zerwas ⁶⁶ B. Zhang ^{14c} D. F. Zhang ¹³⁸ G. Zhang ^{14b}
 J. Zhang ⁶ K. Zhang ^{14a, 14d} L. Zhang ^{14c} R. Zhang ¹⁶⁸ S. Zhang ¹⁰⁵ T. Zhang ¹⁵² X. Zhang ^{62c} X. Zhang ^{62b}
 Z. Zhang ^{17a} Z. Zhang ⁶⁶ H. Zhao ¹³⁷ P. Zhao ⁵¹ T. Zhao ^{62b} Y. Zhao ¹³⁵ Z. Zhao ^{62a} A. Zhemchugov ³⁸
 Z. Zheng ¹⁴² D. Zhong ¹⁶⁰ B. Zhou ¹⁰⁵ C. Zhou ¹⁶⁸ H. Zhou ⁷ N. Zhou ^{62c} Y. Zhou ⁷ C. G. Zhu ^{62b} C. Zhu ^{14a, 14d}
 H. L. Zhu ^{62a} H. Zhu ^{14a} J. Zhu ¹⁰⁵ Y. Zhu ^{62a} X. Zhuang ^{14a} K. Zhukov ³⁷ V. Zhulanov ³⁷ N. I. Zimine ³⁸
 J. Zinsser ^{63b} M. Ziolkowski ¹⁴⁰ L. Živković ¹⁵ A. Zoccoli ^{23b, 23a} K. Zoch ⁵⁶ T. G. Zorbas ¹³⁸ O. Zormpa ⁴⁶
 W. Zou ⁴¹ and L. Zwalski ³⁶

(ATLAS Collaboration)

¹Department of Physics, University of Adelaide, Adelaide, Australia²Department of Physics, University of Alberta, Edmonton, Alberta, Canada^{3a}Department of Physics, Ankara University, Ankara, Türkiye^{3b}Division of Physics, TOBB University of Economics and Technology, Ankara, Türkiye⁴LAPP, Univ. Savoie Mont Blanc, CNRS/IN2P3, Annecy, France⁵APC, Université Paris Cité, CNRS/IN2P3, Paris, France⁶High Energy Physics Division, Argonne National Laboratory, Argonne, Illinois, USA⁷Department of Physics, University of Arizona, Tucson, Arizona, USA⁸Department of Physics, University of Texas at Arlington, Arlington, Texas, USA⁹Physics Department, National and Kapodistrian University of Athens, Athens, Greece¹⁰Physics Department, National Technical University of Athens, Zografou, Greece¹¹Department of Physics, University of Texas at Austin, Austin, Texas, USA¹²Institute of Physics, Azerbaijan Academy of Sciences, Baku, Azerbaijan¹³Institut de Física d'Altes Energies (IFAE), Barcelona Institute of Science and Technology, Barcelona, Spain

^{14a}*Institute of High Energy Physics, Chinese Academy of Sciences, Beijing, China*^{14b}*Physics Department, Tsinghua University, Beijing, China*^{14c}*Department of Physics, Nanjing University, Nanjing, China*^{14d}*University of Chinese Academy of Science (UCAS), Beijing, China*¹⁵*Institute of Physics, University of Belgrade, Belgrade, Serbia*¹⁶*Department for Physics and Technology, University of Bergen, Bergen, Norway*^{17a}*Physics Division, Lawrence Berkeley National Laboratory, Berkeley, California, USA*^{17b}*University of California, Berkeley, California, USA*¹⁸*Institut für Physik, Humboldt Universität zu Berlin, Berlin, Germany*¹⁹*Albert Einstein Center for Fundamental Physics and Laboratory for High Energy Physics, University of Bern, Bern, Switzerland*²⁰*School of Physics and Astronomy, University of Birmingham, Birmingham, United Kingdom*^{21a}*Department of Physics, Bogazici University, Istanbul, Türkiye*^{21b}*Department of Physics Engineering, Gaziantep University, Gaziantep, Türkiye*^{21c}*Department of Physics, Istanbul University, Istanbul, Türkiye*^{21d}*Istinye University, Sarıyer, Istanbul, Türkiye*^{22a}*Facultad de Ciencias y Centro de Investigaciones, Universidad Antonio Nariño, Bogotá, Colombia*^{22b}*Departamento de Física, Universidad Nacional de Colombia, Bogotá, Colombia*^{23a}*Dipartimento di Fisica e Astronomia A. Righi, Università di Bologna, Bologna, Italy*^{23b}*INFN Sezione di Bologna, Italy*²⁴*Physikalisches Institut, Universität Bonn, Bonn, Germany*²⁵*Department of Physics, Boston University, Boston, Massachusetts, USA*²⁶*Department of Physics, Brandeis University, Waltham, Massachusetts, USA*^{27a}*Transilvania University of Brasov, Brasov, Romania*^{27b}*Horia Hulubei National Institute of Physics and Nuclear Engineering, Bucharest, Romania*^{27c}*Department of Physics, Alexandru Ioan Cuza University of Iasi, Iasi, Romania*^{27d}*Physics Department, National Institute for Research and Development of Isotopic and Molecular Technologies, Cluj-Napoca, Romania*^{27e}*University Politehnica Bucharest, Bucharest, Romania*^{27f}*West University in Timisoara, Timisoara, Romania*^{28a}*Faculty of Mathematics, Physics and Informatics, Comenius University, Bratislava, Slovak Republic*^{28b}*Department of Subnuclear Physics, Institute of Experimental Physics of the Slovak Academy of Sciences, Kosice, Slovak Republic*²⁹*Physics Department, Brookhaven National Laboratory, Upton, New York, USA*³⁰*Facultad de Ciencias Exactas y Naturales, Departamento de Física, y CONICET, Instituto de Física de Buenos Aires (IFIBA), Universidad de Buenos Aires, Buenos Aires, Argentina*³¹*California State University, California, USA*³²*Cavendish Laboratory, University of Cambridge, Cambridge, United Kingdom*^{33a}*Department of Physics, University of Cape Town, Cape Town, South Africa*^{33b}*iThemba Labs, Western Cape, South Africa*^{33c}*Department of Mechanical Engineering Science, University of Johannesburg, Johannesburg, South Africa*^{33d}*National Institute of Physics, University of the Philippines Diliman (Philippines), South Africa*^{33e}*University of South Africa, Department of Physics, Pretoria, South Africa*^{33f}*University of Zululand, KwaDlangezwa, South Africa*^{33g}*School of Physics, University of the Witwatersrand, Johannesburg, South Africa*³⁴*Department of Physics, Carleton University, Ottawa, Ontario, Canada*^{35a}*Faculté des Sciences Ain Chock, Réseau Universitaire de Physique des Hautes Energies - Université Hassan II, Casablanca, Morocco*^{35b}*Faculté des Sciences, Université Ibn-Tofail, Kénitra, Morocco*^{35c}*Faculté des Sciences Semlalia, Université Cadi Ayyad, LPHEA-Marrakech, Morocco*^{35d}*LPMR, Faculté des Sciences, Université Mohamed Premier, Oujda, Morocco*^{35e}*Faculté des sciences, Université Mohammed V, Rabat, Morocco*^{35f}*Institute of Applied Physics, Mohammed VI Polytechnic University, Ben Guerir, Morocco*³⁶*CERN, Geneva, Switzerland*³⁷*Affiliated with an institute covered by a cooperation agreement with CERN*³⁸*Affiliated with an international laboratory covered by a cooperation agreement with CERN*³⁹*Enrico Fermi Institute, University of Chicago, Chicago, Illinois, USA*⁴⁰*LPC, Université Clermont Auvergne, CNRS/IN2P3, Clermont-Ferrand, France*⁴¹*Nevis Laboratory, Columbia University, Irvington, New York, USA*⁴²*Niels Bohr Institute, University of Copenhagen, Copenhagen, Denmark*^{43a}*Dipartimento di Fisica, Università della Calabria, Rende, Italy*^{43b}*INFN Gruppo Collegato di Cosenza, Laboratori Nazionali di Frascati, Italy*⁴⁴*Physics Department, Southern Methodist University, Dallas, Texas, USA*

⁴⁵Physics Department, University of Texas at Dallas, Richardson, Texas, USA
⁴⁶National Centre for Scientific Research “Demokritos”, Agia Paraskevi, Greece

^{47a}Department of Physics, Stockholm University, Sweden

^{47b}Oskar Klein Centre, Stockholm, Sweden

⁴⁸Deutsches Elektronen-Synchrotron DESY, Hamburg and Zeuthen, Germany

⁴⁹Fakultät Physik, Technische Universität Dortmund, Dortmund, Germany

⁵⁰Institut für Kern- und Teilchenphysik, Technische Universität Dresden, Dresden, Germany

⁵¹Department of Physics, Duke University, Durham, North Carolina, USA

⁵²SUPA - School of Physics and Astronomy, University of Edinburgh, Edinburgh, United Kingdom

⁵³INFN e Laboratori Nazionali di Frascati, Frascati, Italy

⁵⁴Physikalisches Institut, Albert-Ludwigs-Universität Freiburg, Freiburg, Germany

⁵⁵II. Physikalisches Institut, Georg-August-Universität Göttingen, Göttingen, Germany

⁵⁶Département de Physique Nucléaire et Corpusculaire, Université de Genève, Genève, Switzerland

^{57a}Dipartimento di Fisica, Università di Genova, Genova, Italy

^{57b}INFN Sezione di Genova, Genova, Italy

⁵⁸II. Physikalisches Institut, Justus-Liebig-Universität Giessen, Giessen, Germany

⁵⁹SUPA - School of Physics and Astronomy, University of Glasgow, Glasgow, United Kingdom

⁶⁰LPSC, Université Grenoble Alpes, CNRS/IN2P3, Grenoble INP, Grenoble, France

⁶¹Laboratory for Particle Physics and Cosmology, Harvard University, Cambridge, Massachusetts, USA

^{62a}Department of Modern Physics and State Key Laboratory of Particle Detection and Electronics,

University of Science and Technology of China, Hefei, China

^{62b}Institute of Frontier and Interdisciplinary Science and Key Laboratory of Particle Physics and Particle Irradiation (MOE), Shandong University, Qingdao, China

^{62c}School of Physics and Astronomy, Shanghai Jiao Tong University, Key Laboratory for Particle Astrophysics and Cosmology (MOE), SKLPPC, Shanghai, China

^{62d}Tsung-Dao Lee Institute, Shanghai, China

^{63a}Kirchhoff-Institut für Physik, Ruprecht-Karls-Universität Heidelberg, Heidelberg, Germany

^{63b}Physikalisches Institut, Ruprecht-Karls-Universität Heidelberg, Heidelberg, Germany

^{64a}Department of Physics, Chinese University of Hong Kong, Shatin, N. T., Hong Kong, China

^{64b}Department of Physics, University of Hong Kong, Hong Kong, China

^{64c}Department of Physics and Institute for Advanced Study, Hong Kong University of Science and Technology, Clear Water Bay, Kowloon, Hong Kong, China

⁶⁵Department of Physics, National Tsing Hua University, Hsinchu, Taiwan

⁶⁶IJCLab, Université Paris-Saclay, CNRS/IN2P3, 91405 Orsay, France

⁶⁷Department of Physics, Indiana University, Bloomington, Indiana, USA

^{68a}INFN Gruppo Collegato di Udine, Sezione di Trieste, Udine, Italy

^{68b}ICTP, Trieste, Italy

^{68c}Dipartimento Politecnico di Ingegneria e Architettura, Università di Udine, Udine, Italy

^{69a}INFN Sezione di Lecce, Italy

^{69b}Dipartimento di Matematica e Fisica, Università del Salento, Lecce, Italy

^{70a}INFN Sezione di Milano, Italy

^{70b}Dipartimento di Fisica, Università di Milano, Milano, Italy

^{71a}INFN Sezione di Napoli, Italy

^{71b}Dipartimento di Fisica, Università di Napoli, Napoli, Italy

^{72a}INFN Sezione di Pavia, Italy

^{72b}Dipartimento di Fisica, Università di Pavia, Pavia, Italy

^{73a}INFN Sezione di Pisa, Italy

^{73b}Dipartimento di Fisica E. Fermi, Università di Pisa, Pisa, Italy

^{74a}INFN Sezione di Roma, Italy

^{74b}Dipartimento di Fisica, Sapienza Università di Roma, Roma, Italy

^{75a}INFN Sezione di Roma Tor Vergata, Italy

^{75b}Dipartimento di Fisica, Università di Roma Tor Vergata, Roma, Italy

^{76a}INFN Sezione di Roma Tre, Italy

^{76b}Dipartimento di Matematica e Fisica, Università Roma Tre, Roma, Italy

^{77a}INFN-TIFPA, Italy

^{77b}Università degli Studi di Trento, Trento, Italy

⁷⁸Universität Innsbruck, Department of Astro and Particle Physics, Innsbruck, Austria

⁷⁹University of Iowa, Iowa City, Iowa, USA

⁸⁰Department of Physics and Astronomy, Iowa State University, Ames, Iowa, USA

- ^{81a}*Departamento de Engenharia Elétrica, Universidade Federal de Juiz de Fora (UFJF), Juiz de Fora, Brazil*
^{81b}*Universidade Federal do Rio De Janeiro COPPE/EE/IF, Rio de Janeiro, Brazil*
^{81c}*Instituto de Física, Universidade de São Paulo, São Paulo, Brazil*
^{81d}*Rio de Janeiro State University, Rio de Janeiro, Brazil*
⁸²*KEK, High Energy Accelerator Research Organization, Tsukuba, Japan*
⁸³*Graduate School of Science, Kobe University, Kobe, Japan*
^{84a}*Faculty of Physics and Applied Computer Science, AGH University of Science and Technology, Krakow, Poland*
^{84b}*Marian Smoluchowski Institute of Physics, Jagiellonian University, Krakow, Poland*
⁸⁵*Institute of Nuclear Physics Polish Academy of Sciences, Krakow, Poland*
⁸⁶*Faculty of Science, Kyoto University, Kyoto, Japan*
⁸⁷*Kyoto University of Education, Kyoto, Japan*
⁸⁸*Research Center for Advanced Particle Physics and Department of Physics, Kyushu University, Fukuoka, Japan*
⁸⁹*Instituto de Física La Plata, Universidad Nacional de La Plata and CONICET, La Plata, Argentina*
⁹⁰*Physics Department, Lancaster University, Lancaster, United Kingdom*
⁹¹*Oliver Lodge Laboratory, University of Liverpool, Liverpool, United Kingdom*
⁹²*Department of Experimental Particle Physics, Jožef Stefan Institute and Department of Physics, University of Ljubljana, Ljubljana, Slovenia*
⁹³*School of Physics and Astronomy, Queen Mary University of London, London, United Kingdom*
⁹⁴*Department of Physics, Royal Holloway University of London, Egham, United Kingdom*
⁹⁵*Department of Physics and Astronomy, University College London, London, United Kingdom*
⁹⁶*Louisiana Tech University, Ruston, Louisiana, USA*
⁹⁷*Fysiska institutionen, Lunds universitet, Lund, Sweden*
⁹⁸*Departamento de Física Teórica C-15 and CIAFF, Universidad Autónoma de Madrid, Madrid, Spain*
⁹⁹*Institut für Physik, Universität Mainz, Mainz, Germany*
¹⁰⁰*School of Physics and Astronomy, University of Manchester, Manchester, United Kingdom*
¹⁰¹*CPPM, Aix-Marseille Université, CNRS/IN2P3, Marseille, France*
¹⁰²*Department of Physics, University of Massachusetts, Amherst, Massachusetts, USA*
¹⁰³*Department of Physics, McGill University, Montreal, Quebec, Canada*
¹⁰⁴*School of Physics, University of Melbourne, Victoria, Australia*
¹⁰⁵*Department of Physics, University of Michigan, Ann Arbor, Michigan, USA*
¹⁰⁶*Department of Physics and Astronomy, Michigan State University, East Lansing, Michigan, USA*
¹⁰⁷*Group of Particle Physics, University of Montreal, Montreal, Quebec, Canada*
¹⁰⁸*Fakultät für Physik, Ludwig-Maximilians-Universität München, München, Germany*
¹⁰⁹*Max-Planck-Institut für Physik (Werner-Heisenberg-Institut), München, Germany*
¹¹⁰*Graduate School of Science and Kobayashi-Maskawa Institute, Nagoya University, Nagoya, Japan*
¹¹¹*Department of Physics and Astronomy, University of New Mexico, Albuquerque, New Mexico, USA*
¹¹²*Institute for Mathematics, Astrophysics and Particle Physics, Radboud University/Nikhef, Nijmegen, Netherlands*
¹¹³*Nikhef National Institute for Subatomic Physics and University of Amsterdam, Amsterdam, Netherlands*
¹¹⁴*Department of Physics, Northern Illinois University, DeKalb, Illinois, USA*
^{115a}*New York University Abu Dhabi, Abu Dhabi, United Arab Emirates*
^{115b}*United Arab Emirates University, Al Ain, United Arab Emirates*
^{115c}*University of Sharjah, Sharjah, United Arab Emirates*
¹¹⁶*Department of Physics, New York University, New York, New York, USA*
¹¹⁷*Ochanomizu University, Otsuka, Bunkyo-ku, Tokyo, Japan*
¹¹⁸*Ohio State University, Columbus, Ohio, USA*
¹¹⁹*Homer L. Dodge Department of Physics and Astronomy, University of Oklahoma, Norman, Oklahoma, USA*
¹²⁰*Department of Physics, Oklahoma State University, Stillwater, Oklahoma, USA*
¹²¹*Palacký University, Joint Laboratory of Optics, Olomouc, Czech Republic*
¹²²*Institute for Fundamental Science, University of Oregon, Eugene, Oregon, USA*
¹²³*Graduate School of Science, Osaka University, Osaka, Japan*
¹²⁴*Department of Physics, University of Oslo, Oslo, Norway*
¹²⁵*Department of Physics, Oxford University, Oxford, United Kingdom*
¹²⁶*LPNHE, Sorbonne Université, Université Paris Cité, CNRS/IN2P3, Paris, France*
¹²⁷*Department of Physics, University of Pennsylvania, Philadelphia, Pennsylvania, USA*
¹²⁸*Department of Physics and Astronomy, University of Pittsburgh, Pittsburgh, Pennsylvania, USA*
^{129a}*Laboratório de Instrumentação e Física Experimental de Partículas - LIP, Lisboa, Portugal*
^{129b}*Departamento de Física, Faculdade de Ciências, Universidade de Lisboa, Lisboa, Portugal*
^{129c}*Departamento de Física, Universidade de Coimbra, Coimbra, Portugal*
^{129d}*Centro de Física Nuclear da Universidade de Lisboa, Lisboa, Portugal*
^{129e}*Departamento de Física, Universidade do Minho, Braga, Portugal*

^{129f}Departamento de Física Teórica y del Cosmos, Universidad de Granada, Granada (Spain), Portugal

^{129g}Instituto Superior Técnico, Universidade de Lisboa, Lisboa, Portugal

¹³⁰Institute of Physics of the Czech Academy of Sciences, Prague, Czech Republic

¹³¹Czech Technical University in Prague, Prague, Czech Republic

¹³²Charles University, Faculty of Mathematics and Physics, Prague, Czech Republic

¹³³Particle Physics Department, Rutherford Appleton Laboratory, Didcot, United Kingdom

¹³⁴IRFU, CEA, Université Paris-Saclay, Gif-sur-Yvette, France

¹³⁵Santa Cruz Institute for Particle Physics, University of California Santa Cruz, Santa Cruz, California, USA

^{136a}Departamento de Física, Pontificia Universidad Católica de Chile, Santiago, Chile

^{136b}Millennium Institute for Subatomic Physics at High Energy Frontier (SAPHIR), Santiago, Chile

^{136c}Instituto de Investigación Multidisciplinario en Ciencia y Tecnología, y Departamento de Física, Universidad de La Serena, Chile

^{136d}Department of Physics, Universidad Andres Bello, Santiago, Chile

^{136e}Instituto de Alta Investigación, Universidad de Tarapacá, Arica, Chile

^{136f}Departamento de Física, Universidad Técnica Federico Santa María, Valparaíso, Chile

¹³⁷Department of Physics, University of Washington, Seattle, Washington, USA

¹³⁸Department of Physics and Astronomy, University of Sheffield, Sheffield, United Kingdom

¹³⁹Department of Physics, Shinshu University, Nagano, Japan

¹⁴⁰Department Physik, Universität Siegen, Siegen, Germany

¹⁴¹Department of Physics, Simon Fraser University, Burnaby BC, Canada

¹⁴²SLAC National Accelerator Laboratory, Stanford, California, USA

¹⁴³Department of Physics, Royal Institute of Technology, Stockholm, Sweden

¹⁴⁴Departments of Physics and Astronomy, Stony Brook University, Stony Brook, New York, USA

¹⁴⁵Department of Physics and Astronomy, University of Sussex, Brighton, United Kingdom

¹⁴⁶School of Physics, University of Sydney, Sydney, Australia

¹⁴⁷Institute of Physics, Academia Sinica, Taipei, Taiwan

^{148a}E. Andronikashvili Institute of Physics, Iv. Javakhishvili Tbilisi State University, Tbilisi, Georgia

^{148b}High Energy Physics Institute, Tbilisi State University, Tbilisi, Georgia

^{148c}University of Georgia, Tbilisi, Georgia

¹⁴⁹Department of Physics, Technion, Israel Institute of Technology, Haifa, Israel

¹⁵⁰Raymond and Beverly Sackler School of Physics and Astronomy, Tel Aviv University, Tel Aviv, Israel

¹⁵¹Department of Physics, Aristotle University of Thessaloniki, Thessaloniki, Greece

¹⁵²International Center for Elementary Particle Physics and Department of Physics, University of Tokyo, Tokyo, Japan

¹⁵³Department of Physics, Tokyo Institute of Technology, Tokyo, Japan

¹⁵⁴Department of Physics, University of Toronto, Toronto, Ontario, Canada

^{155a}TRIUMF, Vancouver, British Columbia, Canada

^{155b}Department of Physics and Astronomy, York University, Toronto, Ontario, Canada

¹⁵⁶Division of Physics and Tomonaga Center for the History of the Universe, Faculty of Pure and Applied Sciences,

University of Tsukuba, Tsukuba, Japan

¹⁵⁷Department of Physics and Astronomy, Tufts University, Medford, Massachusetts, USA

¹⁵⁸Department of Physics and Astronomy, University of California Irvine, Irvine California, USA

¹⁵⁹Department of Physics and Astronomy, University of Uppsala, Uppsala, Sweden

¹⁶⁰Department of Physics, University of Illinois, Urbana, Illinois, USA

¹⁶¹Instituto de Física Corpuscular (IFIC), Centro Mixto Universidad de Valencia - CSIC, Valencia, Spain

¹⁶²Department of Physics, University of British Columbia, Vancouver, British Columbia, Canada

¹⁶³Department of Physics and Astronomy, University of Victoria, Victoria, British Columbia, Canada

¹⁶⁴Fakultät für Physik und Astronomie, Julius-Maximilians-Universität Würzburg, Würzburg, Germany

¹⁶⁵Department of Physics, University of Warwick, Coventry, United Kingdom

¹⁶⁶Waseda University, Tokyo, Japan

¹⁶⁷Department of Particle Physics and Astrophysics, Weizmann Institute of Science, Rehovot, Israel

¹⁶⁸Department of Physics, University of Wisconsin, Madison, Wisconsin, USA

¹⁶⁹Fakultät für Mathematik und Naturwissenschaften, Fachgruppe Physik, Bergische Universität Wuppertal, Wuppertal, Germany

¹⁷⁰Department of Physics, Yale University, New Haven, Connecticut, USA

^aAlso at Department of Physics, King's College London, London, United Kingdom.

^bAlso at Institute of Physics, Azerbaijan Academy of Sciences, Baku, Azerbaijan.

^cAlso at Lawrence Livermore National Laboratory, Livermore, California, USA.

^dAlso at TRIUMF, Vancouver, British Columbia, Canada.

^eAlso at Department of Physics, University of Thessaly, Volos, Greece.

^fAlso at Physics Department, An-Najah National University, Nablus, Palestine.

^gAlso at Department of Physics, University of Fribourg, Fribourg, Switzerland.

^hAlso at Department of Physics, University of Colorado Boulder, Boulder, Colorado, USA.

ⁱAlso at Department of Physics and Astronomy, University of Louisville, Louisville, Kentucky, USA.

^jDeceased.

^kAlso at Department of Physics, Westmont College, Santa Barbara, California, USA.

^lAlso at Departament de Fisica de la Universitat Autonoma de Barcelona, Barcelona, Spain.

^mAlso affiliated with an institute covered by a cooperation agreement with CERN.

ⁿAlso at The Collaborative Innovation Center of Quantum Matter (CICQM), Beijing, China.

^oAlso at Department of Physics, Ben Gurion University of the Negev, Beer Sheva, Israel.

^pAlso at Università di Napoli Parthenope, Napoli, Italy.

^qAlso at Institute of Particle Physics (IPP), Victoria, British Columbia, Canada.

^rAlso at Bruno Kessler Foundation, Trento, Italy.

^sAlso at Borough of Manhattan Community College, City University of New York, New York, New York, USA.

^tAlso at Department of Financial and Management Engineering, University of the Aegean, Chios, Greece.

^uAlso at Centro Studi e Ricerche Enrico Fermi, Rome, Italy.

^vAlso at Department of Physics, California State University, East Bay, California, USA.

^wAlso at Institutio Catalana de Recerca i Estudis Avancats, ICREA, Barcelona, Spain.

^xAlso at University of Chinese Academy of Sciences (UCAS), Beijing, China.

^yAlso at Physics Department, Yeditepe University, Istanbul, Türkiye.

^zAlso at Institute of Theoretical Physics, Ilia State University, Tbilisi, Georgia.

^{aa}Also at CERN, Geneva, Switzerland.

^{ab}Also at Hellenic Open University, Patras, Greece.

^{ac}Also at Center for High Energy Physics, Peking University, Beijing, China.

^{ad}Also at The City College of New York, New York, New York, USA.

^{ae}Also at Department of Physics, California State University, Sacramento, California, USA.

^{af}Also at Département de Physique Nucléaire et Corpusculaire, Université de Genève, Geneva, Switzerland.

^{ag}Also at Institut für Experimentalphysik, Universität Hamburg, Hamburg, Germany.

^{ah}Also at Department of Physics and Astronomy, Michigan State University, East Lansing, Michigan, USA.